Elaboration et caractérisation de mélanges de polymères à base de polypropylène et de polycarbonate à propriétés optimisées

Shann-Shan Dai

Nancy-Université INPL

en co-tutelle avec Sichuan University

Ecole Nationale Supérieure des Industries Chimiques (ENSIC)

Ecole Doctorale : Ressources Procédés Produits Environnement (RP2E)

Laboratoire Réactions et Génie des Procédés (LRGP-CNRS UPR 3349)

Elaboration et caractérisation de mélanges de polymères à base de polypropylène et de polycarbonate à propriétés optimisées

THESE

présentée en vue de l'obtention du

DOCTORAT DE L'INSTITUT NATIONAL POLYTECHNIQUE DE LORRAINE

Spécialité : Génie des Procédés et des Produits

par

Shann-Shan DAI

Soutenance prévue le 31 mai 2010 à 9h

Composition du jury :

Rapporteurs :	Yvan CHALAMET	Maître de Conférences (HDR) à l'Université Jean Monnet de Saint-Etienne
	Yong JIN	Professeur à l'Académie des Sciences de Chine
Examinatreurs :	Guo-Hua HU	Professeur à Nancy-Université – INPL et membre de l'IUF
	Lin YE	Professeur à Sichuan Université, Chine
	Sandrine HOPPE	Chargée de recherche au CNRS
	He-Sheng XIA	Professeur à Sichuan Université, Chine

Abstract

Polypropylene (PP) is one of the most consumed polymers. However, it exhibits low impact strength, greatly limiting its application potential. Polymer blending provides a practical and economic way of preparing new materials with combinations of properties not available in a single polymer. The development of PP based blends is often aimed at obtaining a pocessable material with high impact strength and sufficient stiffness. Elastomer modification has been proved to be effective in toughening PP, even at low temperature, with an concomitant adverse effect on the strength and modulus of the material. In order to improve the toughness of PP while retaining its rigidity as much as possible, a new concept "rigid–rigid polymer toughening" was developed. Polycarbonate (PC) was selected to blend with PP in this study because of the advantages it provides over many other conventional engineering polymers in terms of high strength and toughness.

PP and PC are immiscible with each other and the viscosity ratio between PC and PP is very high, resulting in poor dispersion of PC in the PP matrix. Thus, the key to obtaining materials with high toughness and balanced rigidity relies on effectively compatibilizing this polymer pair and reducing the viscosity ratio. In this study, novel compatibilizers for the PP/PC blend were prepared or chosen to promote interactions between PP and PC and control the morphology of the blend. Some of the compatibilizers took the role of both compatibilizer and toughener. Through efficient compatibilization, synergy in toughening and favorable viscosity match, the resulting PP/PC blends showed significant improvement in impact toughness with a relatively good tensile strength. The performance of compatibilizers and toughening mechanism of blends were studied in detail. The morphology evolution of PP/PC blends and the relationship between the composition and microstructure were simulated based on molecular dynamics and mesodyn theories.

Keywords： polypropylene, polycarbonate, blending, compatibility, viscosity, balanced toughness and rigidity, toughening mechanism, molecular simulation

Résumé

Le polypropylène est un des polymères les plus utilisés. Son potentiel d'applications devrait être encore plus grand si sa résistance au choc était plus élevée. Le mélange de polymères offre une voie pratique et économique pour élaborer de nouveaux matériaux qui peuvent avoir des propriétés que chacun des polymères ne possède pas nécessairement. L'élaboration de mélanges de polymères à base de PP a souvent pour objet d'obtenir des matériaux avec une résistance au choc élevée, une rigidité suffisante et une processabilité adéquate. L'incorporation d'un élastomère dans le PP peut améliorer efficacement le PP, même en basse température, avec cependant un effet néfaste concomitant sur la rigidité du matériau. Un nouveau concept d'amélioration de la résistance au choc par l'ajout de particules rigides a été développé afin d'améliorer la résistance au choc du PP tout en maintenant autant que possible sa rigidité. Dans cette étude, le polycarbonate (PC) est mélangé avec le PP en raison de ses propriétés exceptionnelles (rigidité élevée et résistance au choc excellente) par rapport à d'autres polymères techniques.

Le PC se disperse mal dans le PP car ils sont immiscibles entre eux et leur rapport de viscosité très élevé. Ainsi, la clé pour obtenir des mélanges PP/PC avec une résistance au choc élevée et une rigidité suffisante consiste à les compatbiliser et à diminuer le rapport de viscosité de manière efficace. Dans cette étude, de nouveaux agents compatibilisants ont été développés afin de promouvoir les interactions entre le PC et le PP et de contrôler la morphologie des mélanges. Certains de ces agents compatibilisants jouent à la fois les rôles d'agent compatibilisant et agents d'amélioration de la résistance au choc. Les mélanges PP/PC obtenus montrent une amélioration significative au niveau de la résistance au choc avec une rigidité relativement bonne. La performance des agents compatibilisants ainsi que les mécanismes d'amélioration de la résistance au choc ont été étudiés. L'évolution de la morphologie des mélanges PP/PC ainsi que la relation entre la composition et la microstructure ont été simulées avec l'aide des théories de dynamiques à l'échelle moléculaire et mésoscopique.

Mots clés : polypropylène, polycarbonate, procédés d'élaboration de mélanges de polymères, compatibilité, viscosité, résistance au choc, rigidité, mécanismes d'amélioration de la résistance au choc, simulation moléculaire.

Table of content

Abstract II
Table of contents IV
Chapter 1 Introduction 1
1.1 Motivation and objectives 1
1.2 overview of thesis 1
Chapter 2 Experimental 3
2.1 Materials 3
2.2 Sample preparation 4
2.2.1 Preparation of chemically modified polypropylene 4
2.2.2 Polymer blending 4
2.3 Characterization 4
2.3.1 Degree of grafting 4
2.3.2 FTIR analysis 5
2.3.3 GPC analysis 5
2.3.4 Torque analysis 5
2.3.5 Mechanical properties 5
2.3.6 J-integral 6
2.3.7 PLM analysis 7
2.3.8 DSC analysis 7
2.3.9 WAXD analysis 7
2.3.10 Rheological analysis 8
2.3.11 DMA analysis 8
2.3.12 SEM analysis 8
2.3.13 Simulation strategies 8
Chapter 3 Preparation of chemically modified PP and its compatibilizing effect on PP/PC blends 10
3.1 Introduction 10
3.2 Preparation and characterization of chemically modified PP 10
3.2.1 Mechanism and preparation process 10
3.2.2 Characterization of chemically modified PP 13
3.3 Compatibilizing effect of chemically modified PP on the properties of PP/PC blends 17
3.3.1 Effect of chemically modified PP on mechanical properties of PP/PC blends 17
3.3.2 Effect of chemically modified PP on dynamic mechanical properties of PP/PC blends 20
3.3.3 Effect of chemically modified PP on crystalline properties of PP/PC blends 23
3.3.4 Effect of chemically modified PP on the morphology of PP/PC blends 25
3.4 Conclusion 27
Chapter 4 Preparation and study of structure and properties of PP/PC/SEBS blends 28
4.1 Introduction 28
4.2 Effect of SEBS on mechanical properties of PP/PC blends 28
4.3 Effect of SEBS on dynamic mechanical properties of PP/PC blends 30
4.4 Effect of SEBS on crystalline properties of PP/PC blends 33
4.4 Effect of SEBS on morphologies of PP/PC blends 34
4.5 Toughening mechanism of PP/PC/SEBS blends 36
4.5.1 Analysis of impact fracture surfaces 36

4.5.2 Analysis of fracture toughness....38
4.6 Conclusion....41
Chapter 5 Preparation and study of structure and properties of PP/PC/POE blend 43
5.1 Introduction....43
5.2 Study of structure and properties of PP/PC/POE/SEPS blend 44
5.2.1 Effect of SEPS on mechanical properties of PP/PC/POE blend....44
5.2.2 Effect of SEPS on dynamic mechanical properties of PP/PC/POE blend....47
5.2.3 Effect of SEPS on crystalline properties of PP/PC/POE blend 51
5.2.4 Effect of SEPS on morphologies of PP/PC/POE blend....55
5.2.5 Effect of viscosity ratio on structure and properties of PP/PC/POE blend....57
5.2.6 Toughening mechanism of PP/PC/POE/SEPS blend....61
5.3 Compatibilizing effect of EVA/SEPS on PP/PC blend....65
5.3.1 Effect of EVA/SEPS on mechanical properties of PP/PC blend....65
5.3.2 Effect of EVA/SEPS on morphologies of PP/PC blend....66
5.3.3 Effect of EVA/SEPS on impact feature surface of PP/PC blend 67
5.4 Conclusion....68
Chapter 6 Molecular simulation on relationship between composition and microscopic structure of PP/PC blend....70
6.1 Introduction....70
6.2 Molecular dynamic simulations of PP/PC blend....70
6.3 Mesoscopic dynamic simulations of PP/PC blend 74
6.4 Dynamic simulation of effect of SEBS on morphologies of PP/PC blend....79
6.5 Conclusion....84
Chapter 7 Conclusion....85
Acknowledgements....88
References....89

Chapter 1 Introduction

1.1 Motivation and objectives

Polypropylene (PP) is one of the most widely used polymers. However, it exhibits low impact strength which greatly limits its application potential. Polymer blending offers an important route to new materials with combination of properties not available in a single polymer. Extensive research has been carried out on blending PP with elastomers in order to improve its toughness. It is a very effective method, even at low temperature. However, it is often concomitant with an adverse effect of elastomer toughening is significant reduction in modulus of the material [1-11]. This study called upon a so-called "rigid–rigid polymer toughening" concept [12-17]. PP was blended with polycarbonate (PC) whose strength and toughness are high in order to improve its toughness while retaining as much as possible its rigidity. PC and PP are immiscible because of disparities in polarity and solubility parameters [18]. Furthermore, the PC/PP viscosity ratio is very high. These two factors result in poor dispersion of the PC in the PP matrix. Therefore, it is necessary to search for an additive that acts as an effective compatibilizer and is capable of effectively reducing the viscosity of PC.

Based on the above discussion, the design or choice of compatibilizer for PP/PC blends deserves special attention. Graft or block polymers are commonly used as compatibilizers in immiscible polymer blends. Their efficiencies are believed to depend on their composition, molecular structures, molecular weights, and so on, which can integrated into the interaction parameters between the homopolymers and the graft or block polymers [19-33]. However, it is difficult to prepare block polymers based on PC..

The objective of the work presented in this thesis is to develop novel compatibilizers for PP/PC blends. Through efficient compatibilization, synergy in toughening and favorable viscosity match, the resulting PP blends could show significant improvement in impact toughness with a relatively good tensile strength. The compatibilizing effect and toughening mechanism will be studied in detail. The morphology evolution of PP/PC blends and the relationship between the composition and microstructure will also be studied at a microscale based on molecular dynamics and mesodyn theories simulations.

1.2 overview of thesis

A brief overview of this thesis is as follows.

Chapter 2 describes the main experiments in this study.

In chapter 3, through molecular design, Chemically modified PPwith proper molecular structure were prepared. They were used as compatibilizers for PP/PC blends. The composition, structure of grafted polymers and the grafting reaction were studied in terms of FTIR, GPC, degree of grafting and torque analysis. The effects of compatibilizers on the properties of the blends were also studied.

In chapter 4, hydrogenated styrene-butylene-styrene block polymer (SEBS) with both compatibilizing and toughening effects was used to modify PP. The double effect of the SEBS was examined in terms of morphology and mechanical and thermal properties of the PP/PC and compatibilized PP based blends. The SEM images of impact fracture surfaces and the method of J-integral were used to study the mechanism of toughness modification.

In chapter 5, polyolefin (POE) was used to toughen PP/PC blends and a styrene-ethylene-propylene-styrene block polymer (SEPS) with 60wt% of PS block was used as a compatibilizer for PP/PC/POE blends. Different from SEBS, SEPS could not toughen PP but showed a remarkable compatibilizing effect, which was achieved the migration of PP and PC into SEPS during blending.

The method of two-step blending by pre-blending of PC and SEPS allowed reducing the apparent viscosity of PC, leading to better viscosity match between components involved in the blend and more encapsulated structure. As a result, mechanical properties of the blends were improved. The SEM images of impact fracture surfaces and the concept of interparticle distance were used to study the mechanism of toughness modification.

EVA was selected to compatibilize PP/PC blends. It contained ester groups similar to those of PC and an aliphatic chain similar to that of PP. EVA/SEPS compound compatibilizer improved the elongation at break of materials obviously. The morphologies and impact feature surfaces of PP/PC and compatibilized PP based blends were studied.

In chapter 6, simulations based on molecular dynamics and mesodyn theories were used to study the morphology evolution of PP/PC blends and the relationship between the composition and microstructure. In addition, the compatibilizing effect of SEBS was also investigated in a microscale. Microscopic structures obtained from simulations were compared with the results of mechanical properties.

Chapter 2 Experimental

2.1 Materials

The materials used in this thesis are as follows:

Product designation	Characteristics	Supplier
PP (T30S)	melt flow index (MFI) 2.5-3.5g/10min (230℃, 2.16kg)	Dushanzi Petrochemical Co. Ltd
Maleated polypropylene (PP-g-MA, Orevac CA100)	degree of grafting 1%	Arkema
PC (L1250Y) was supplied by., with	MFI 6.7g/10min (300℃, 1.2kg);	Teijin Co
2-tertbutyl-6-(3-tertbutyl-2-hydroxy-5-methylbenzyl)-4-methylphenyl acrylic ester (BPA)	white crystalline powder appearance and melting point ≥ 130℃	Chemical Engineering Institute of Shanxi Province
Glycidyl methacrylate (GMA)		Shanghai Jingchao Chemical Co.
Styrene (St)		Shantou Xipang Chemical Co. of Guangdong Province
2-allyl bisphenol A (2A)		Laizhou Laiyu Chemical Co
Dicumyl peroxide (DCP)		Chengdu Kelong Chemical Co. of Sichuan Province;
Hydrogenated styrene-butadiene-styrene (SEBS, YH501)	30wt% styrene	Baling Petrochemical Co.
Styrene-ethylene-propylene-styrene (SEPS, Septon 2104)	65 wt% of Styrene	Kuraray Co
Ethylene-octene copolymer (POE, Engage 8150)	39% octene	Dupont-Dow
Antioxidant tetrakis-[methylene-β-(3,5-di-tert-butyl-4-hydroxyphenyl)-propionate] methane (1010)		Ciba-Geigy Co. Ltd.
Copolymer of ethylene and vinyl acetate		BASF

(EVA)		

2.2 Sample preparation

2.2.1 Preparation of chemically modified polypropylene

PP-g-BPA, PP-g-GMA, PP-g-GMA-St and PP-g-2A were prepared in a Haake mixer at 190°C with a rotor speed of 60rpm for 5min. The concentrations of the monomer and the free radical initiator were 8 and 0.1 wt.% with respect to PP, respectively. PP-g-MA was dried at 100°C in a vacuum oven for 24h. A series of HEDA/PP-g-MA blends with different HEDA/MA molar ratios (0.5, 1, 1.5, 2) were compounded in the Haake mixer at 190°C with a rotor speed of 60rpm for 5min. The HEDA modified PP samples were purified by dissolution in dimethylbenzene and precipitation in acetone for 3 times.

2.2.2 Polymer blending

One step blending: Blending all the polymer components at one time by using a co-rotating twin-screw extruder of type TSSJ-25/03 at a rotational speed of 90 rpm. The barrel temperature was in the range of 220 to 270°C. PC was dried at 120°C in a vacuum oven for 5h before blending. The extrudates were quenched in a water bath prior to pelletization. Dried blends were moulded to form impact and tensile specimens by using a K-TEC40 injection moulding machine. The barrel temperature profile was 260°C (hopper) ~ 280°C (nozzle) and the mould temperature was maintained at 50°C.

Two step blending: for studying the effect of viscosity ratio match on the properties of blends, PC and SEBS were pre-blended and then blended with other polymer components.

2.3 Characterization

2.3.1 Degree of grafting

After PP-g-GMA was completely dissolved in dimethylbenzene, KOH/ethyl alcohol was added in the solution to react with the epoxy rings of GMA. HCl/ethyl alcohol was used for the titration of the residue of KOH. The degree of grafting of GMA onto PP was calculated using the following formula:

$$D.G. = \left[\left(V_1 - V_2 \right) \cdot N \cdot M / 1000W \right] \cdot 100\% \qquad (2.1)$$

where V_1, consumed volume of HCl for the blank sample (mL); V_2, consumed volume of

HCl for the grafting sample (mL); N, molar concentration of HCl (mol/L); M, molecular weight of GMA (142g/mol); W, weight of purified grafting polymer (g).

The degree of grafting of St, 2A and BPA on to PP can be calculated with the Lambert-Beer law:

$$\frac{A_1}{A_2} = \frac{C_1}{C_2} \tag{2.2}$$

where A_1 is the absorption intensity of the monomer; C_1 is the molar concentration of the monomer; A_2 is the absorption intensity of the grafting polymer; C_2 is the molar concentration of the grafting polymer.

The absorption intensity of the monomer was measured with Shimadzu UV-240 by using dimethylbenzene as a solvent. The wavelength was ranged from 400 to 190 nm.

2.3.2 FTIR analysis

A FTIR of type Nicolet 560 was used to characterize monomer modified PP. The latter was mixed with KBr powder. The scanning rate was 20 min^{-1} and the resolution was 4cm^{-1}。

2.3.3 GPC analysis

Room temperature: Molecular weight and its distribution of PC were performed with gel chromatograph of Agilent-HP1100 by using tetrahydrofuran as solvent at room temperature.

High temperature: Molecular weight and its distribution of PP and PP-g-BPA were performed with gel chromatograph of PL-220 by using 1,2,4-trichioro-benzene as solvent at 150°C.

2.3.4 Torque analysis

The evolution of torque during the preparation of PP-g-HEDA was followed by the Haake mixer of HC-90.

2.3.5 Mechanical properties

The tensile strength of the samples was measured with a 4302 material testing machine from Instron Co. (U.S.A.) according to ISO527/1-1993 (E). The test speed was 50 mm/min, and the sample length between bench marks was 50 ± 0.5 mm. The notched charpy impact

strength of the samples was measured with a ZBC-4B impact testing machine from Xinsansi Co. (Shenzhen of China) according to ISO179-1993 (E).

2.3.6 J-integral

The J-integral [34] test was done according to ASTM E812-87 using a multiple-specimen technique at room temperature. The schematic of the three-point bend test specimen is shown in Fig. 2.1. A material testing machine of type 4302 Instron was used to perform the measurements at a crosshead speed of 2 mm/min. During testing, a series of specimens were loaded to different prescribed deflections which led to different levels of crack growth. The load-deflection curve was recorded and monitored. The potential energy (area under the load-deflection diagram) was calculated. After unloading, each specimen was immersed in liquid nitrogen for 5 min and broken up immediately to cause brittle fracture. The extent of crack growth in the fracture surface was measured by SEM. The J-integral value was calculated by the following expression:

$$J = -\frac{2U}{B(W-a)} \tag{2.3}$$

where U is the input energy to the specimen given by the area under the load-deflection curve; B is the thickness of the specimen; W is the width of the specimen and a is the crack length.

The calculated J-integral values were then plotted against the crack length, Δa, to obtain a J-R curve. Using this method, the J_c values were determined at the point of intersection between the J-R curve and the blunting line:

$$J = 2\sigma_y \times \Delta a \tag{2.4}$$

where σ_y is the yield stress.

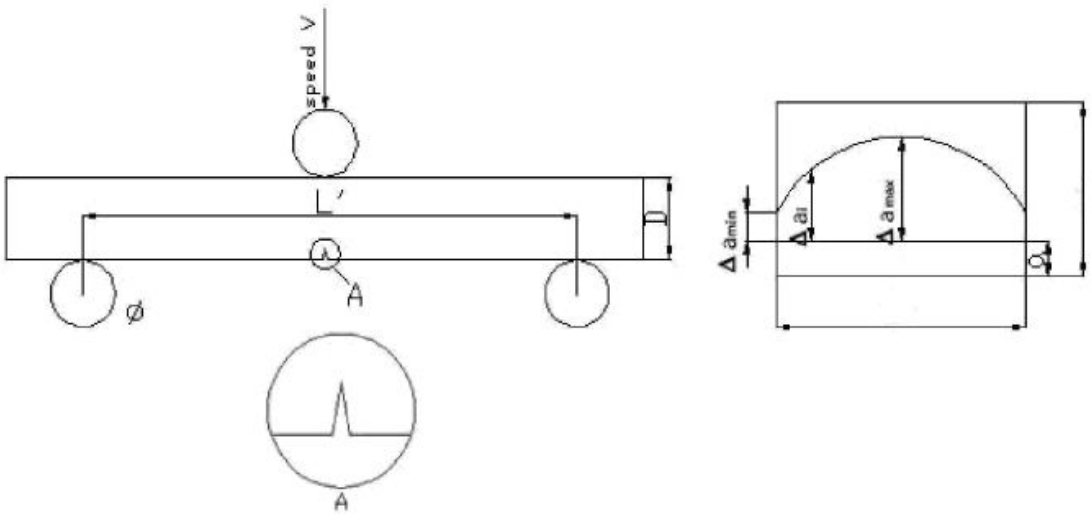

Fig. 2.1 Schematic diagram of J Integral test

2.3.7 PLM analysis

The crystal morphology measurement of PP was performed with Leitz Laborlux polarized light microscopy. The samples were heated and melt on a hot plate, pressed to a flake, and then crystallized at 150℃ for 3 hr.

2.3.8 DSC analysis

The non-isothermal crystallization was performed with a NETZSCHDSC 204. Samples of 5-10 mg in weight were heated quickly from ambient temperature to 280°C under nitrogen atmosphere, and were kept for 5 min before crystallization to eliminate the effect of the previous thermal history, then cooled to 30°C with a rate of 10°C/min. The crystallinity (X_c) can be evaluated from the heat evolved during crystallization (ΔH_c) using the following relation:

$$X_c = (\Delta H_c / \Delta H_m) \times 100\% \qquad (2.5)$$

where ΔH_m is the heat of fusion for 100% crystalline isotropic PP (ΔH_m=209J/g).

2.3.9 WAXD analysis

Wide-angle X-ray diffraction measurements were carried out with a Philip X'Pert Graphic & Identify instrument at room temperature to determine crystal parameters of samples. The materials were taken from the skin and core layer of the samples. The Cu Kα irradiation source was operated with a step size of 0.02° from 2θ=10° to 40°. The d-spacing

is calculated by substituting the scattering angles of the peak into the Bragg's equation [35]:

$$d = \frac{\lambda}{2\sin\theta} \tag{2.6}$$

where θ is the X-ray diffraction angle and wave length λ=0.153nm.

2.3.10 Rheological analysis

Rheological measurements were performed on the extruded materials by means of a capillary rheometer of type Rheograph 2002. A capillary die of long/diameter =30 was used. Over a shear rate range of 10-3000S^{-1} was used to study the effect of the shear rate on the rheological properties of the blend. The barrel temperature was operated at 270°C and piston velocity was 2.67-800mm/min. The viscosity obtained was the apparent viscosity, and the Bagley correction for entrance pressure loss was not applied, due to the relatively high L/D capillary used.

2.3.11 DMA analysis

The dynamic mechanical analysis was performed with DMA Q800 (U.S.A.) following the clamp single cantilever mode with a frequency of 1Hz. The temperature ranged from -80°C to 160°C with a heating rate of 3°C/min.

2.3.12 SEM analysis

Cryogenically fractured in liquid nitrogen, and etched with appropriate solvent, the fracture surfaces of the blends were sputter-coated with a thin gold layer in order to make samples electric conductive, avoiding the charge accumulated, and then observed by a JEOL JSM-5900LV SEM instrument, with an acceleration voltage of 20KV. To study the toughening mechanism, the impact-fractured surfaces of the blends were directly observed under the same condition without etching.

2.3.13 Simulation strategies

Molecular dynamics (MD) and mesoscopic dynamics (Mesodyn) simulations have been performed on the PP/PC and compatibilized blends at ambient temperature (298K) using the software packages of Mesodyn with Materials Studio Modeling (version 4.0) installed on Windows 2000. The overall methodology used in the simulation process is described in Fig. 2.2.

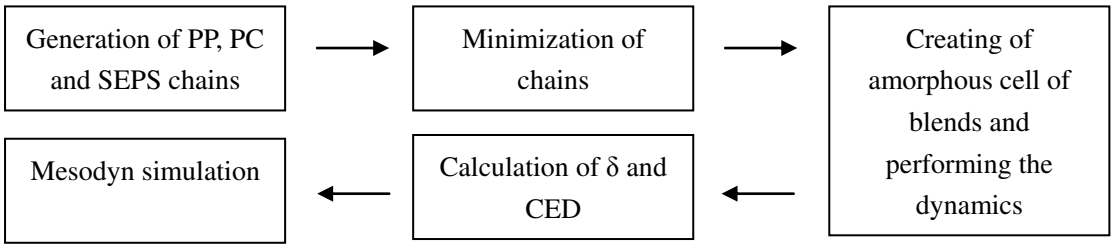

Fig. 2.2 Flowchart of the simulation procedure

Initially, the bulk phases were constructed with the Amorphous cell program, which utilizes the combined use of arc algorithm developed by Theodorou and Suter [36] and the scanning method of Meirovitch [37]. Minimization was done using the Conjugate Gradient Method (CGM), until the energy reached a minimum. The CGM used here worked on the Polak-Ribiere algorithm with a convergence level of 0.1kcal/mol/Å. The initial configurations were refined by the dynamics of 100 ps after the amorphous cell was generated. The COMPASS [38] (condensed-phase optimized molecular potentials for the atomistic simulation studies) force field was used for modeling inter-atomic interactions. This is indeed the widely used all-atom force field optimized to predict the structural, conformational, and thermophysical condensed phase properties for the most common molecules including polymers. As mentioned above, configurations were generated individually for each system to compute the cohesive energy density (CED). The MD simulations under constant temperature and density (NVT ensemble) were performed for each configuration using the Discover program. The energy of the system was monitored to ensure that it fluctuated around the average value, and this was considered as a criterion for having an “equilibrated” system. The phase separation dynamics of PP based blends at the mesoscopic level were investigated by Mesodyn program. This approach is base on the dynamic variant of the mean-field density functional theory [39] that is similar to the classical dynamic random phase approximation (RPA) [40]. Polymer chains are modeled as ideal Guassian chains consisting of beads, each representing the monomer chain (Kuhn statistical segments).

Chapter 3 Preparation of chemically modified PP and its compatibilizing effect on PP/PC blends

3.1 Introduction

Immiscible polymer pairs lead to phase separation and its corresponding blends often exhibit poor properties. To address this challenge, block or grafted polymers with proper molecular structure are usually used as compatibilizers which tend to locate between the two polymer components, promote the interfacial adhesion and reduce the interfacial tension [41-51].

PP and PC are immiscible with each other due to the evident differences in their polarity and solubility parameters ($\delta_{PP}\approx7.8(cal/cm^3)^{0.5}$, $\delta_{PC}\approx9.5(cal/cm^3)^{0.5}$)) [52]. Besides, terminal hydroxyl and carboxyl groups, there are also numbers of ester bonds in the PC chain.

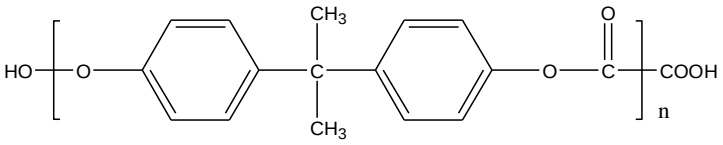

In this chapter, through molecular design, chemically modified PP with proper molecular structure were prepared as new compatibilizers for PP/PC blends. The preparation processes were optimized. The composition, structure of the chemically modified PP and the grafting reaction were studied in terms of FTIR, GPC, degree of grafting and torque analysis. The effects of compatibilizers on the mechanical properties, dynamic mechanical properties, crystalline properties and morphologies of blends were investigated in detail.

3.2 Preparation and characterization of chemically modified PP

3.2.1 Mechanism and preparation process

The chemical structural formulas of the monomers used in this study are shown in Fig 3.1. BPA, GMA, GMA-St, and 2A grafted onto PP were carried out by a free-radical mechanism. DCP is an effective and widely used initiator for the grafting reaction of PP, and Fig. 3.2 shows the process of decomposition of DCP. To limit the degradation of PP and homo-polymerization of monomer as much as possible, each monomer and initiator were mixed together firstly and then added into the Haake mixer full of completely melted

PP.

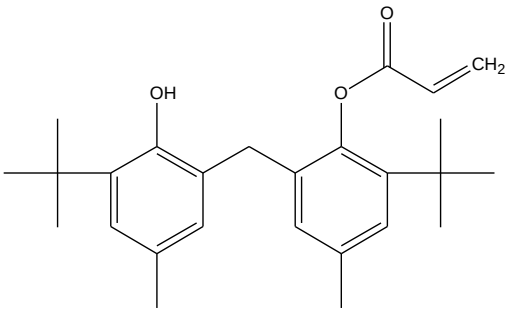

BPA

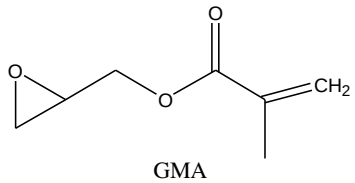

GMA

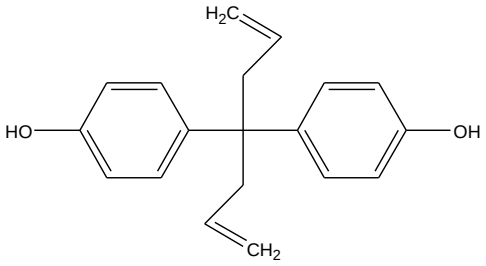

2A

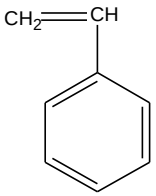

St

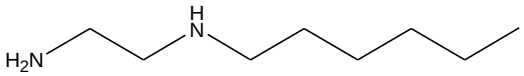

HEDA

Fig.3.1 Chemical structural formulas of grafting monomers

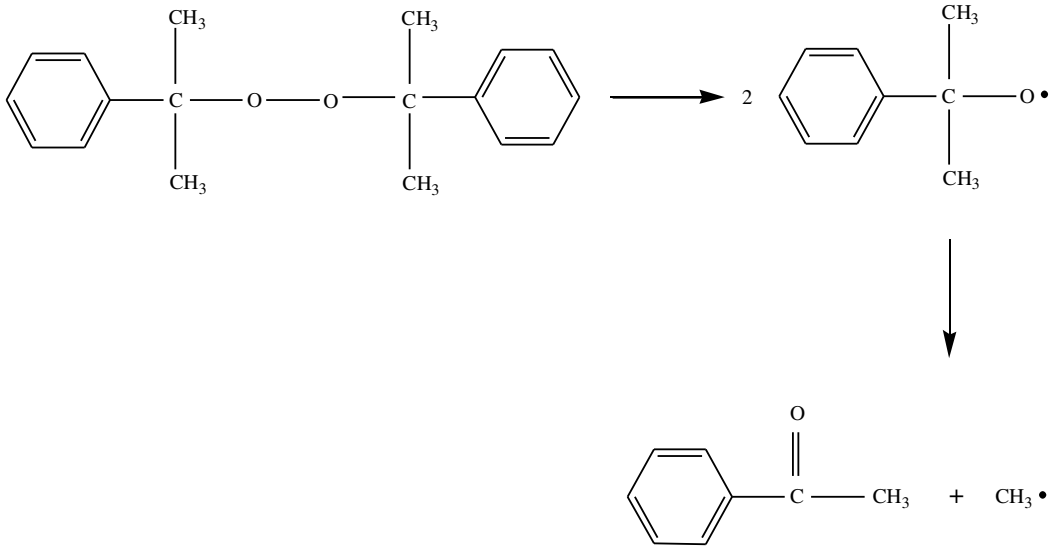

Fig.3.2 Decomposition reaction of DCP and the formation of free radicals

Inevitable degradation of PP occurs during the reaction of grafting, which reduces the

molecular weight and the properties of the PP. As shown in Table 3.1, the mechanical properties, including impact and tensile strength of PP/PP-g-GMA-St blends reduce slightly with an increase in concentration of DCP, a decrease in concentration of monomers and an increase in the amount of PP-g-GMA-St. Relatively good conditions for carrying out the free radical grafting of monomers onto PP were: 8 wt% of monomer, 0.1 wt% of initiator, 190°C, 60rpm and 5min.

Table 3.1 Mechanical properties of PP/PP-g-GMA-St blends

Processing parameters (wt %)	Impact strength (kJ/m2)	Tensile strength (MPa)	Elongation at break (%)
PP/PP-g-GMA-St=95/5 (0.1%DCP, 8%GMA,3%St,5min,190℃)	1.91	33.84	403.5
PP/PP-g-GMA-St=85/15 (0.1%DCP, 8%GMA,3%St,5min,190℃)	1.83	33.40	360.7
PP/PP-g-GMA-St=95/5 (0.3%DCP, 8%GMA,3%St,5min,190℃)	1.66	33.21	385.1
PP/PP-g-GMA-St=85/15 (0.3%DCP, 8%GMA,3%St,5min,190℃)	1.87	33.88	456.2
PP/PP-g-GMA-St=95/5 (0.5%DCP, 8%GMA,3%St,5min,190℃)	1.85	33.32	514.4
PP/PP-g-GMA-St=85/15 (0.5%DCP, 8%GMA,3%St,5min,190℃)	1.71	33.78	532.8
PP/PP-g-GMA-St=95/5 (0.3%DCP, 5%GMA,3%St,5min,190℃)	1.72	33.36	440.6
PP/PP-g-GMA-St=85/15 (0.3%DCP, 5%GMA,3%St,5min,190℃)	1.72	33.11	643.2
PP/PP-g-GMA-St=95/5 (0.3%DCP, 5%GMA,3%St,7min,190℃)	1.76	33.24	557.1
PP/PP-g-GMA-St=85/15 (0.3%DCP, 5%GMA,3%St,7min,190℃)	1.74	33.09	621.6

HEDA is a primary-secondary diamine, as shown in Fig. 3.1. Amine functional polymers are frequently used in the study of polymer-polymer reaction because of their high reactivity toward various functionalities (anhydride, isocyanate, oxazoline, epoxide and acid) and some types of linkages (carbamate and ester) [53-57]. As shown in Fig 3.3, there are four possible products due to the unequal reactivity of the primary and secondary amine. Reactions between small molecular analogues show that the primary amine is at least three times faster than the secondary amine [53-54]. The imide PP-g-HEDA (structure a) and amic acids (structure b and c) at equilibrium could be converted to each other by

rearrangement. Obviously, the structures like (b) and (c) are much less stable. In addition, the excess of PP-g-MA reacts with (a), leading to the formation of product (d) which is a branched structure. To maximize the amount of the desired PP-g-HEDA, the optimal HEDA/MA molar ratio was determined to be 1:1.

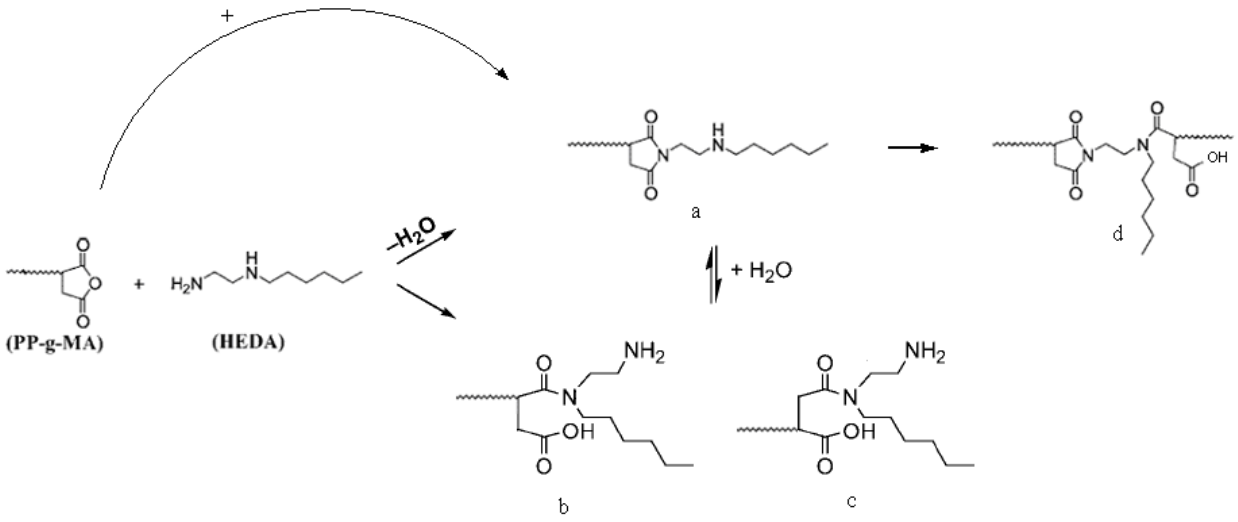

Fig.3.3 Main reactions occurring during the process of HEDA grafting

3.2.2 Characterization of chemically modified PP

3.2.2.1 FTIR analysis

As shown in Fig. 3.4, the FTIR spectrum of the neat PP has several absorption peaks at 2960-2920cm^{-1}, 2880-2840cm^{-1}, 1480-1430cm^{-1}, and 1380-1340cm^{-1} attributing to the stretching and bending vibration of C-C and C-H bonds. After grafting with BPA, GMA, GMA/st and 2A, respectively, new absorption peaks are observed at 1650cm^{-1} attributing to the benzene ring group. This indicates that the monomers are successfully grafted onto PP. In addition, the FTIR spectrum of PP-g-BPA also shows peaks characteristic of O-C=O (1750-1735cm^{-1}, 1300-1000cm^{-1}) and O-H (3700-3200cm^{-1}, 1300-1165cm^{-1}). PP-g-GMA and PP-g-GMA-St both have characteristic absorption of epoxy group (1210-1050cm^{-1}), O-C=O (1750-1735cm^{-1}, 1300-1000cm^{-1}) and O-H (3700-3200cm^{-1}, 1300-1165cm^{-1}). The FTIR spectrum of PP-g-2A also shows peaks related to O-H (3700-3200cm^{-1}, 1300-1165cm^{-1}).

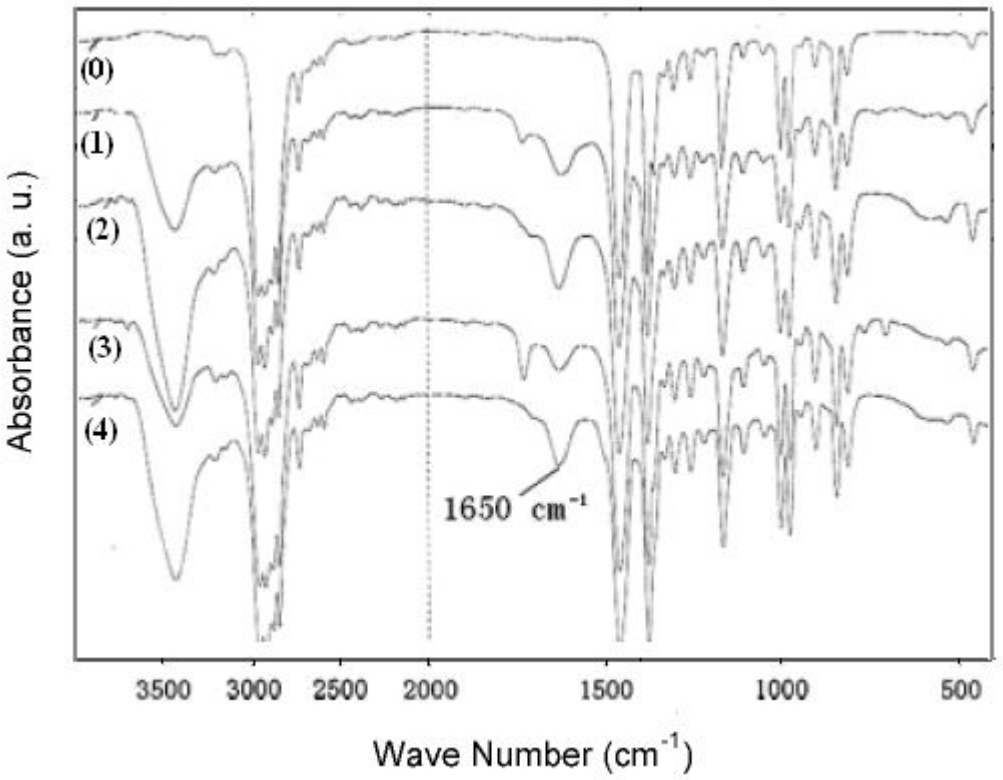

Fig.3.4 FTIR spectra of (0) PP; (1) PP-g-BPA; (2) PP-g-GMA; (3) PP-g-GMA-St; (4) PP-g-2A

Fig.3.5 shows the FTIR spectra of PP-g-MA and PP-g-HEDA prepared by different molar ratios of HEDA/MA. PP-g-MA usually has a characteristic absorption at about 1770-1790cm^{-1}, together with two small shoulders at 1710 and 1860cm^{-1}, which is assigned to the carbonyl group of the cyclic anhydride. The peak mentioned above rapidly reduces its intensity or even disappears with a high diamine concentration, accompanied by a new absorption band at 1705-1708cm^{-1} due to the formation of imide group, indicating PP-g-HEDA is successfully prepared. In addition, the spectrum of PP-g-HEDA shows peaks for N-H (3430cm^{-1}), –CO-N-CO- (1770-1700cm^{-1}, 900-850cm^{-1}) and $(CH_2)_n$ ($n \geq 4$, 720cm^{-1}).

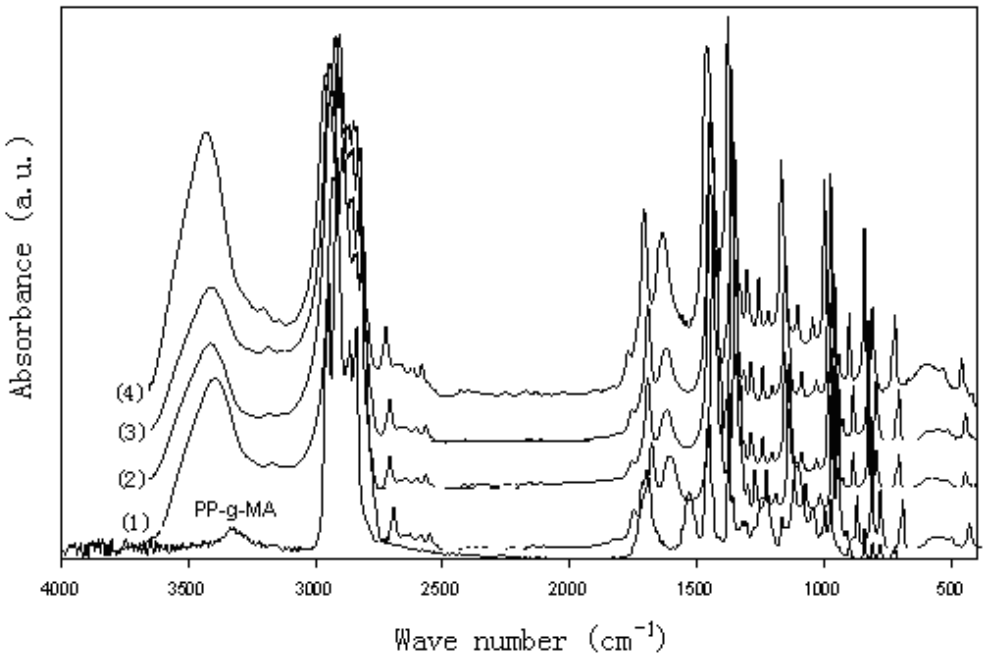

Fig.3.5 FTIR spectra of PP-g-MA and PP-g-HEDA
mol(HEDA)/mol(MA): (1) 0.5, (2) 1.0, (3) 1.5, (4) 2.0

The peak at 2720cm^{-1} is a characteristic absorption of the PP backbone that is not affected by the reaction between PP and HEDA. It was chosen to be an internal reference to calculate the anhydride conversion at each HEDA/MA ratio. When the HEDA/MA molar ratio is 0.5, the absorbance ratio between the peaks at 1709 and 2720cm^{-1} (I_{1709}/I_{2720}) is low, indicating that the excess of anhydride is responsible for its low conversion. An increase in the HEDA/MA molar ratio results in a higher I_{1709}/I_{2720} ratio, indicating an increased conversion of anhydride. When the HEDA/MA molar ratio is equal to or greater than 1, the I_{1709}/I_{2720} almost reaches the highest value. To increase the conversion of anhydride while reducing the amount of residual diamine as much as possible, the optimal HEDA/MA molar ratio is determined to be 1:1.

Table 3.2 Ratio of FTIR peak absorbance between 1709 and 2720cm^{-1}

mol(HEDA)/mol(MA)	I_{1709}/I_{2720}
0.5	2.56
1.0	2.73
1.5	2.78
2.0	2.79

3.2.2.2 Degree of grafting and molecular weight

The degrees of grafting of BPA, GMA, St, and 2A onto PP are calculated and listed in Table 3.3. They were relatively close to each other. The addition of St can improve the degree of grafting of GMA effectively, because St as an intermediate is grafted onto PP first, and then GMA is further grafted onto St.

Table 3.3 Degree of grafting of the compatibilizers

Sample	Degree of grafting (wt %)
PP-g-GMA	4.82 (GMA)
PP-g-GMA-St	6.88 (GMA) 2.5 (St)
PP-g-2A	4.73 (2A)
PP-g-BPA	5.59 (BPA)

The presence of a free radical initiator inevitably leads to the molecular degradation of PP during grafting under high temperature [58]. However, BPA is a sort of heat-resistant antioxidant and reduces this molecular degradation. The result of GPC analysis is listed in Table 3.4. Compared with neat PP, there is only a small amount of molecular degradation for PP-g-BPA and the molecular weight distribution becomes narrower at the same time. The loss of molecular weight of PP during grafting can be neglected.

Table 3.4 Molecular weight and distribution of PP and PP-g-BPA

Sample	M_w (g/mole)	M_w / M_n
PP	387 000	4.76
PP-g-BPA	342 000	3.54

3.2.2.3 Torque analysis

Blend viscosity can be estimated from torque and rotor speed through a model proposed by Lee and Pridon [59].

$$\eta = \frac{4.59n(1-0.924^{2/n})M}{a}(Pa \cdot s) \qquad (3.1)$$

where M is torque, n is power law index, a is an instrument constant. The instrument constant is a material specific parameter which changes with the molecular weight of the material. It is difficult to calculate the real viscosity from the mixer torque. Nevertheless

torques during mixing can still be qualitatively compared to reflect the evolution of viscosity of the blends. The melt viscosity is affected by the molecular weight and molecular structure of the product which is an indication of the reaction occurring in the mixer. As shown in Fig. 3.6, when the molar ratio of the HEDA/MA is 0.5, the excess of PP-g-MA reacts with imide PP-g-HEDA, leading to the formation of a branched product and an increase in torque during grafting.

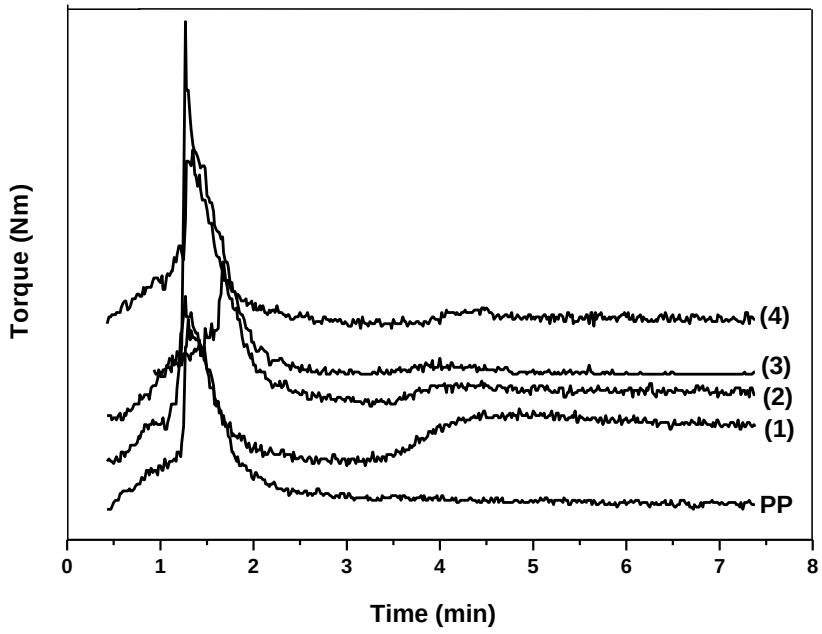

Fig.3.6 Torque value of grafted PP during the mixing process
mol (HEDA)/mol(MA)= (1): 0.5, (2):1, (3):1.5, (4):2

3.3 Compatibilizing effect of chemically modified PP on the properties of PP/PC blends

3.3.1 Effect of chemically modified PP on mechanical properties of PP/PC blends

As shown in Table 3.5, compared with the neat PP, Young's modulus of the PP/PC binary system increases while its notched charpy impact and tensile strength decrease due to the poor compatibility between PP and PC. The addition of a compatibilizer (PP-g-BPA, PP-g-GMA, PP-g-GMA-St, PP-g-2A or PP-g-HEDA) results in improvement in mechanical properties especially the tensile strength because of the promoted interfacial adhesion and reduced interfacial surface tension. With the same proportion, PP/PC/PP-g-BPA ternary blends represents the best balanced tensile and impact strength.

Table 3.5 Mechanical properties of PP and PP based blends

Sample	Notch impact strength (kJ/m^2)	Tensile strength (MPa)	Young's modulus (MPa)	Elongation at break (%)
PP	1.85	33.92	2543	>400
PP/PC (85/15)	1.52	33.50	2933	17.5
PP/PC/PP-g-BPA (80/15/5)	1.57	35.40	3492	14.2
PP/PC/PP-g-BPA (70/15/15)	1.88	37.00	2387	13.3
PP/PC/PP-g-GMA (70/15/15)	1.62	35.69	2940	16.1
PP/PC/PP-g-GMA-st (70/15/15)	1.45	34.57	2281	22.6
PP/PC/PP-g-2A (70/15/15)	1.78	35.17	3763	12.3
PP/PC/PP-g-HEDA (70/15/15)	1.58	34.30	3553	40.0

As far as the mechanism of compatibilizing is concerned, the epoxy group of GMA can react with –OH and –COOH groups at the end of PC molecular chain to form new covalent bonds across the interfaces [60], as equations shown in Fig. 3.7. 2A has a structure similar to bisphenol A, the latter being one of the monomers for the synthesis of PC [61]. BPA not only has benzene ring similar to PC, but also is a sort of heat-resistant antioxidant. It reduces the molecular degradation of PP during grafting and blending under high temperature, and the resulting blend PP/PC/PP-g-BPA represents best balanced mechanical properties.

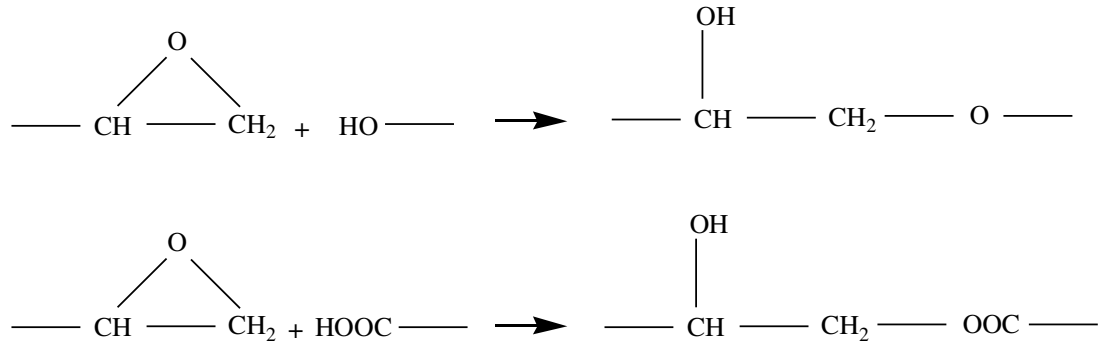

Fig.3.7 Reactions of the epoxy group of GMA with –OH and –COOH groups at the chain end of PC

The reaction between PC and PP-g-HEDA is shown in Fig. 3.8:

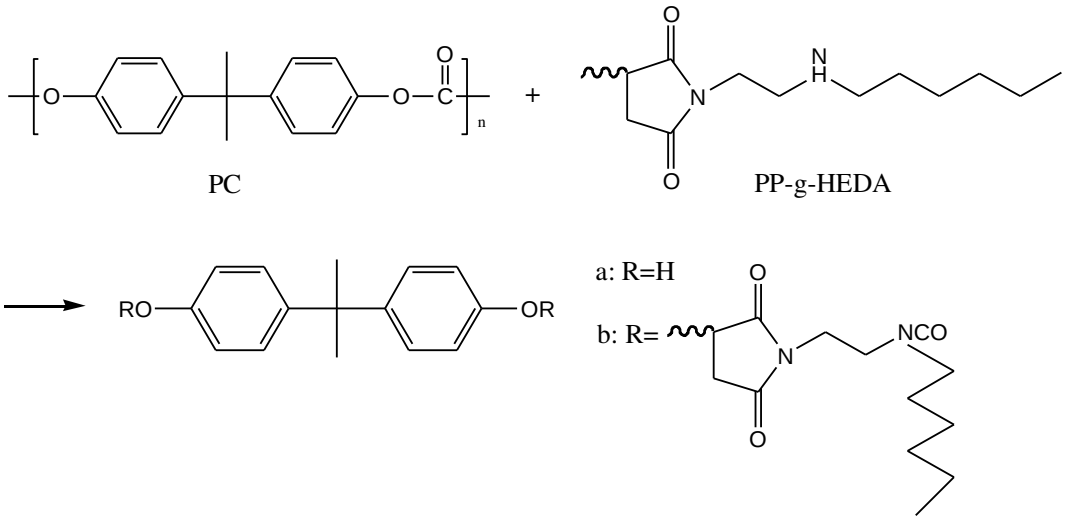

Fig 3.8 Reaction between PP-g-HEDA and PC

The FTIR analysis to prove the reaction mentioned above is shown in Fig. 3.9. The absorption of PP/PC binary system (1) and (3) shows a simply additive property of PP and PC. As discussed before, the spectrum of PP represents noticeable absorption peaks at 2960-2920cm^{-1}, 2880-2840cm^{-1}, 1480-1430cm^{-1}, and 1380-1340cm^{-1}, and 1300-650cm^{-1} (fingerprint region), assigning to the stretching and bending vibration of C-H and C-C bonds. For PC, the absorption peak at 1750-1735cm^{-1} is attributed to -COO- and those at 1510-1470 and 1465-1430cm^{-1} are attributed to the benzene ring with para-substitution. In the PP/PP-g-HEDA/PC blend (2), the appearance of new absorption peaks at 1710cm-1 and 1670-1630cm^{-1} is attributed to NCO, and the disappearance of absorption of NH further illustrates the reaction mentioned above. In the PP-g-HEDA/PC binary blend (4), the absorption of both NCO and NH is found because PP-g-NHEDA as matrix is in excess.

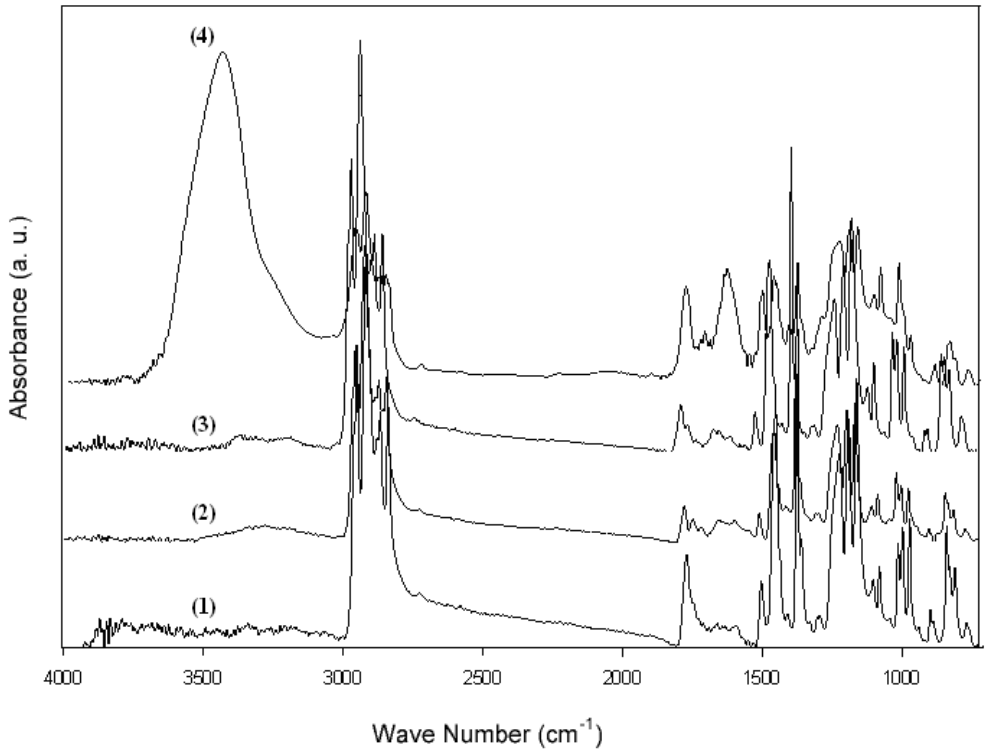

Fig. 3.9 The FTIR spectra of PP based blends

(1) PP/PC=85/15; (2) PP/PP-g-NHEDA/PC=70/15/15; (3) PP/PC=70/30; (4) PP-g-NHEDA/PC=70/30

To analyze the effect of PP-g-HEDA on the molecular weight of PC in the blends due to the reaction shown in Fig. 3.8, the results of GPC are listed in Table 3.6. There was little decrease in the molecular weight of PC. The molecular weight distribution of PC in PP-g-HEDA compatibilized blends became a bit broader. The effect of the degradation of PC on the mechanical properties of PP based blends and the size of PC particles in the corresponding blends can be neglected.

Table 3.6 GPC results of PC in the blends

Sample	PC in blend (1)	PC in blend (2)	PC in blend (3)	PC in blend (4)
M_n	2 500	2 300	3 700	3 900
M_p	20 900	20 400	30 800	29 700
I_p	8.3	8.8	8.2	7.5

(1)PP/PC=85/15; (2) PP/PP-g-HEDA/PC=70/15/15; (3)PP/PC=70/30; (4)PP-g-HEDA/PC=70/30

3.3.2 Effect of chemically modified PP on dynamic mechanical properties of PP/PC blends

The DMA curves of PP based blends are represented in Fig.3.10. For comparison purpose, the DMA curve of PP and PC are also plotted. Generally, glass transition shifts in

blends can be attributed to interactions between the components. The well separated T_g peaks of the neat PP and neat PC indicate the obvious phase separation between them. Invariable absorption peaks of PP and PC in the binary system indicate the bad compatibility between them. However, by addition of PP-g-BPA, the peaks of PP are shifted to higher temperatures while those of PC are shifted to lower temperatures. The shift is more obvious when the content of PP-g-BPA is higher. The DMA data clearly show that the addition of PP-g-BPA leads to the formation of new interphase domains, decreasing the interfacial tension and improving the compatibility of PP/PC blend.

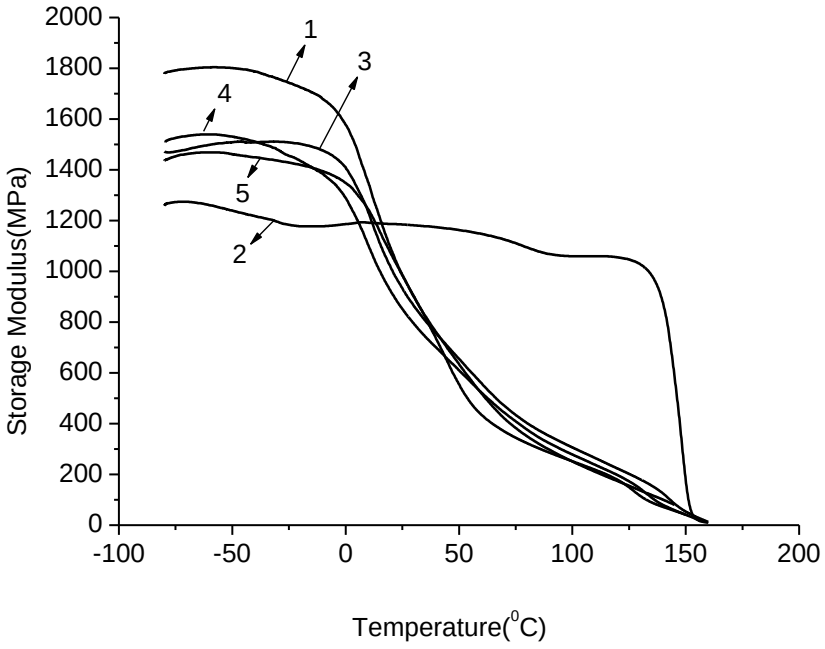

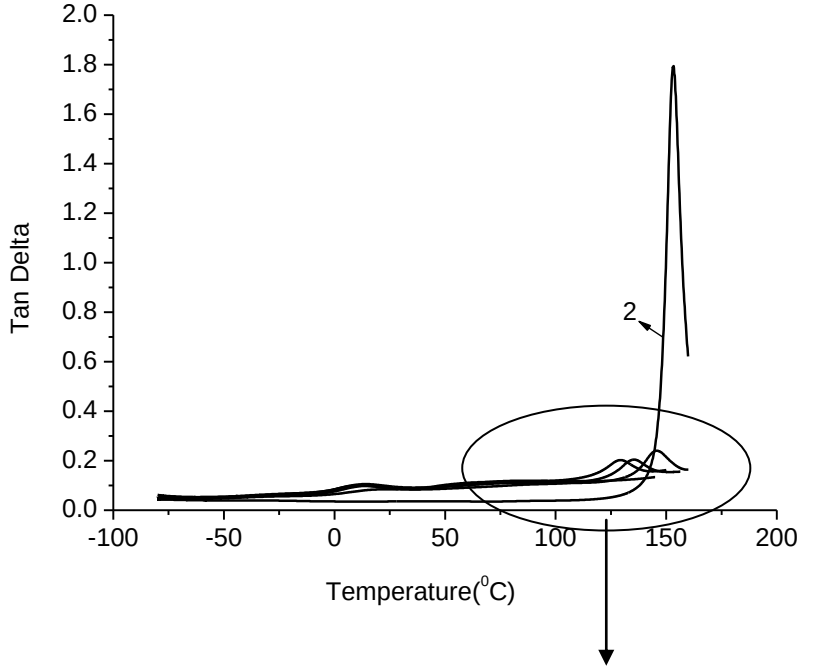
Tan Delta
Temperature(0C)
2

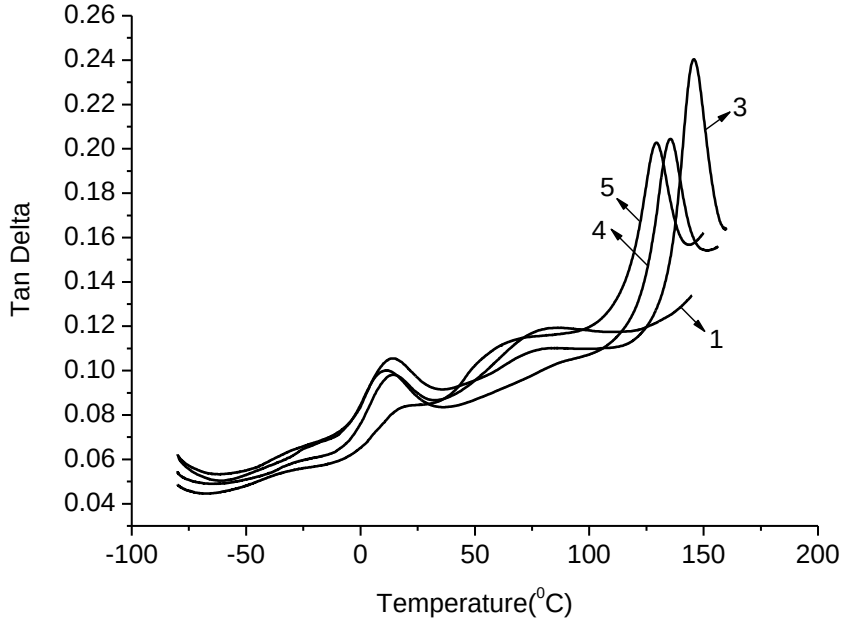
Tan Delta
Temperature(0C)
1
2
3
4
5

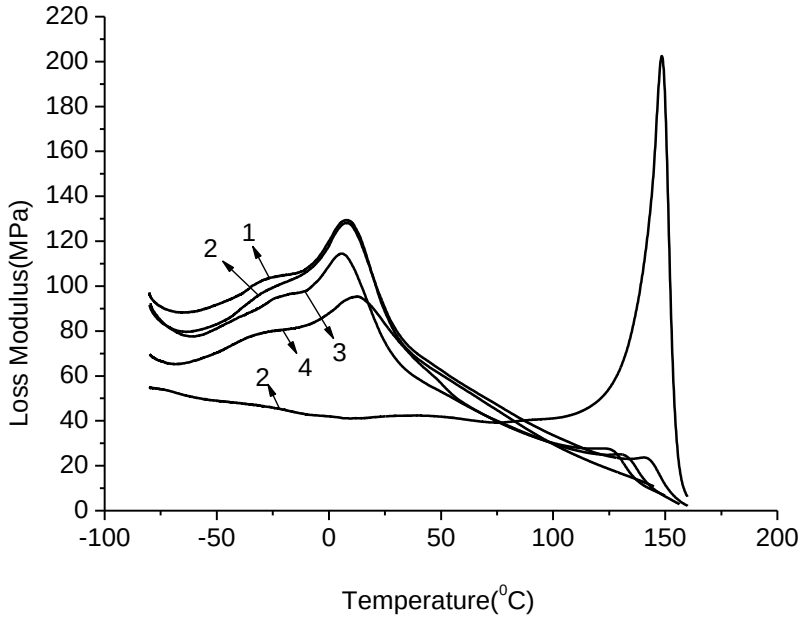

Fig.3.10 DMA curves of 1: PP; 2: PC; 3: PP/PC (85/15); 4: PP/PC/PP-g-BPA (80/15/5); 5: PP/PC/PP-g-BPA (70/15/15)

Table 3.7 DMA data of PP based blends.

Sample	PP	PC	PP/PC (85/15)	PP/PC/PP-g-BPA (80/15/5)	PP/PC/PP-g-BPA (70/15/15)
T_g °C (Loss modulus)	7.8	149.0	7.8/142.9	8.0/135.0	13.1/124.4
T_g °C (Tan delta)	13.5	152.7	13.6/146.3	13.5/131.1	16.1/129.0

3.3.3 Effect of chemically modified PP on crystalline properties of PP/PC blends

Fig.3.11 shows the PLM images of PP and PP based blends. Nucleation of PP is a homogeneous process. It can be seen that the spherulite size of the samples of the neat PP is relatively large, which brings about stress concentration during impact. In the PP/PC blend, the spherulite size becomes smaller, indicating PC can act as a heterogeneous nucleation site for PP to crystallize. Addition of PP-g-BPA further refines the crystal grains of PP. An increase in the compatibilizer content promotes the heterogeneous nucleation.

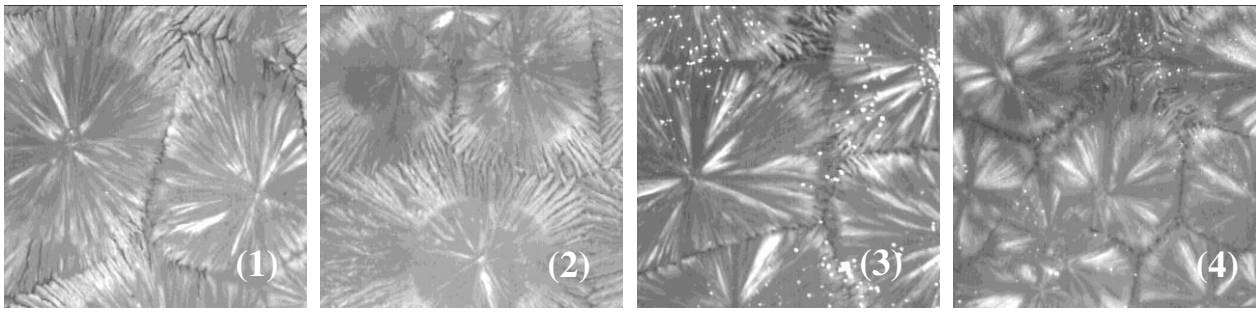

Fig.3.11 PLM images of PP and PP based blends (×200)

(1) PP; (2) PP/PC (85/15); (3) PP/PC/PP-g-BPA (80/15/5); (4) PP/PC/PP-g-BPA (70/15/15)

As shown in Fig. 3.12 and Table 3.8, compared with PP/PC binary blend, the compatibilized blends show a slight decrease in melting temperatures, which was probably ascribed to more imperfections in the crystalline structures resulting from the disruption of more uniformly, distributed PC in PP matrix.

The major differences in thermal behavior of the PP based blends occurred during the DSC cooling scan period as shown in Fig.3.12 and Table 3.8. In the PP/PC binary blend, the solidification of PC particles dispersed in the PP melt easily results in the heterogeneous nucleation of PP and consequently a significant increase in its crystallization temperature (T_{peak}). The T_{peak} of a binary PP/PC blend displayed 8°C higher than that of the neat PP. PP-g-BPA can improve the interfacial adhesion of PP/PC blend, and the nucleation effect of PC on PP becomes stronger during crystallization process of PP, which further increases the T_{peak} of PP.

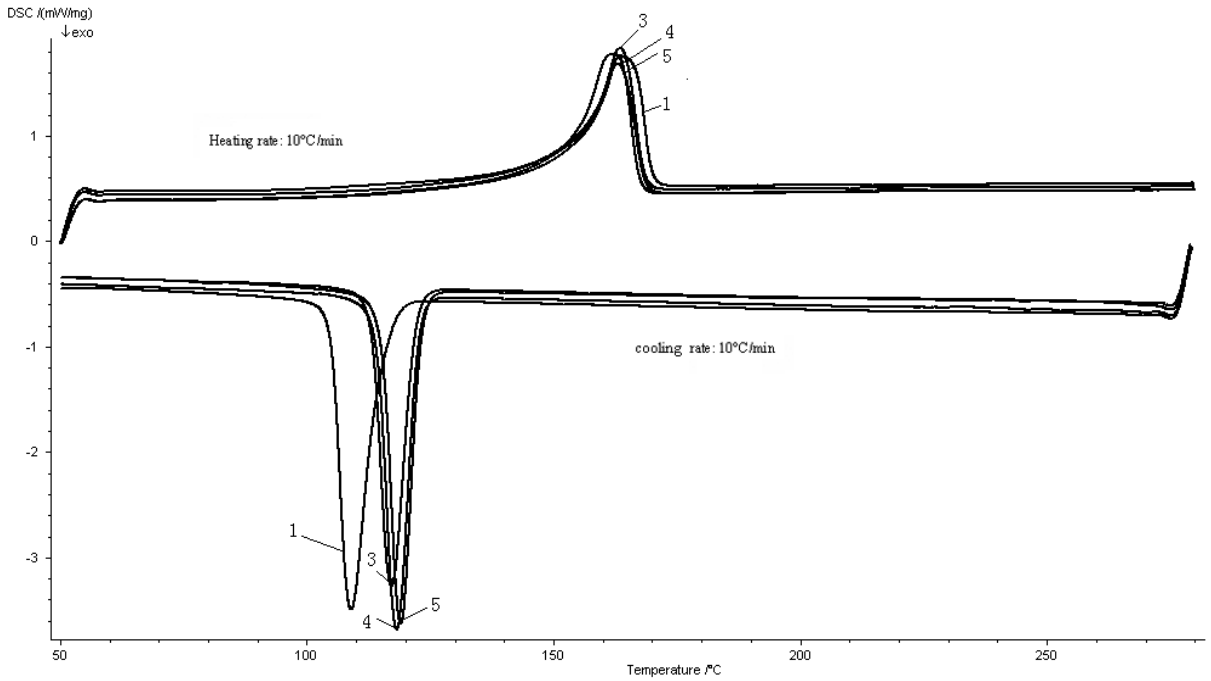

Fig.3.12 DSC curves of PP and PP based blends
1: PP; 3: PP/PC (85/15); 4: PP/PC/PP-g-BPA (80/15/5); 5: PP/PC/PP-g-BPA (70/15/15)

Table 3.8 DSC results for PP based blends.

Sample	T_m (℃)	T_{cOnset} (℃)	T_{cPeak} (℃)	T_{cEnd} (℃)	T_m-T_{cPeak} (℃)	$\triangle W_c$ (50%,℃)	$\triangle H_c$ (J/g)	X_c (%)
PP	163.6	103.9	109.6	115.5	54.0	6.6	120.8	57.8
PP/PC (85/15)	164.5	113.2	117.3	122.3	47.2	5.3	100.6	48.1
PP/PC/PP-g-BPA (80/15/5)	163.6	114.3	118.3	122.8	45.3	5.1	108.9	52.1
PP/PC/PP-g-BPA (70/15/15)	163.4	115.3	119.2	123.4	44.2	4.7	104.3	49.9

Notes: T_m: melting point. T_{cOnset}, onset crystallization temperature. T_{cPeak}, crystallization peak temperature. T_{cEnd}, end crystallization temperature. T_m-T_{cPeak}: degree of supercooling. $\triangle W_c$, crystalline half-peak width. X_c, degree of crystallinity. $\triangle H_c$, crystalline enthalpy.

3.3.4 Effect of chemically modified PP on the morphology of PP/PC blends

As shown in Fig.3.13, SEM images clearly reveal the morphologies of a series of PP

based blends. In the binary system, PC exists in big cylinder-shaped or spherical domains, and these particles are non-uniformly distributed throughout the whole system, resulting from the high interfacial tension and weak adhesion between PP and PC. Generally speaking, an effective compatibilizer endows polyblend with a finer phase domain size, a larger interfacial area and stronger interfacial adhesion [62]. As expected, the addition of PP-g-BPA results in spherical, smaller and more homogeneous PC particles. A higher PP-g-BPA content further decreases PC particle size.

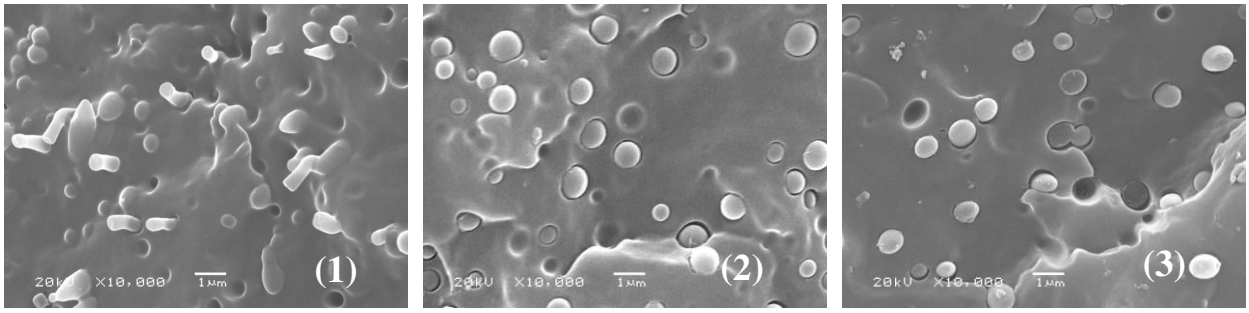

Fig.3.13 SEM images of PP and PP based blends (×10000)
(1) PP/PC (85/15); (2) PP/PC/PP-g-BPA (80/15/5); (3) PP/PC/PP-g-BPA (80/15/15)

SEM images of the PP/PC blend and PP-g-HEDA compatibilized system are shown in Fig. 3.14. The PC particle size and its distribution are also plotted. In the binary system, due to the high interfacial tension and weak adhesion between PP and PC, PC as the disperse phase has big particle size and inhomogeneity. The average diameter of the PC particles is about 0.64μm, and most particles are between 0.55 and 0.80 μm. The addition of PP-g-HEDA results in a significant decrease in size and improved homogeneity of PC particles. The average diameter of PC particles are reduced to 0.29μm and most particles are between 0.20 and 0.30μm.

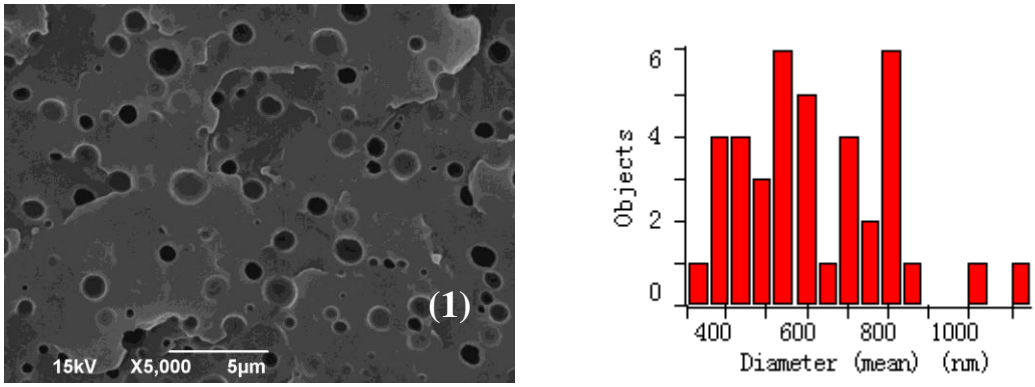

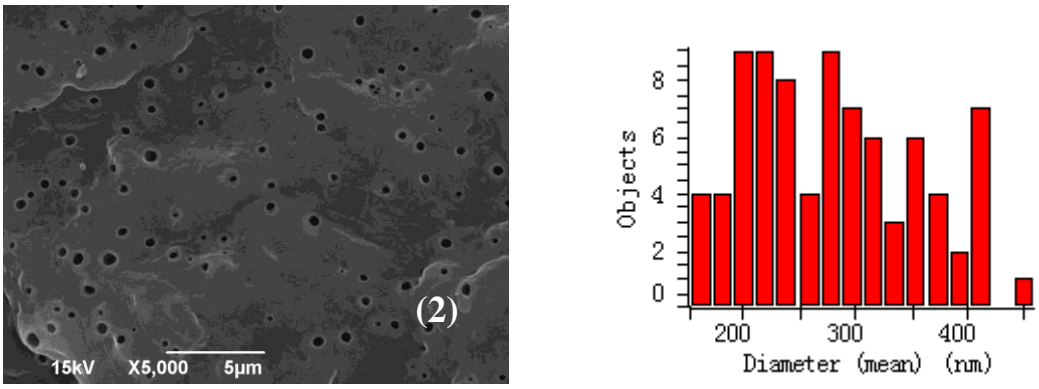

Fig.3.14 SEM images and the diameter distribution of PP and PP based blends (×5000)
(1) PP/PC (85/15); (2) PP/PC/PP-g-HEDA (80/15/15)

3.4 Conclusion

Through molecular designing, chemically modified PP with proper molecular structure were prepared as the new compatibilizers for PP/PC blends. PP-g-BPA, PP-g-GMA, PP-g-GMA-St, and PP-g-2A was prepared through free-radical reaction theory and the technique was optimized. Through the reaction between amide and anhydride, PP-g-HEDA with imide structure was obtained by controlling the ratio of amino group and acid anhydride. The composition, structure of grafted polymers and the grafting reaction were studied in terms of FTIR, GPC, degree of grafting and torque analysis. The mechanical properties, especially the tensile strength of PP based blends were improved with increasing grafted PP compatibilizer. PP/PC/PP-g-BPA ternary blend exhibited the best combination mechanical properties. The well separated T_g peaks of neat PP and PC are indicative of immiscibility of the component polymers. With increasing PP-g-BPA, the two T_gs shifting inside of their respective original T_g suggested partial miscibility of the two polymers. PC as the heterogeneous nucleator resulted in the reduction of nucleation potential barrier, increasing of crystallizing temperature, amount of crystals, and decreasing of crystallinity, crystal size and crystallization time. The heterogeneous nucleation effect of PC was enhanced by addition of PP-g-BPA. Spherical or stick shape of PC particles dispersed in the matrix in big size non-uniformly. The addition of PP-g-BPA or PP-g-HEDA resulted in decreasing and much more homogeneous size of the dispersed PC particles. The particle size was reduced to 289nm from 635nm by addition of PP-g-HEDA.

Chapter 4 Preparation and study of structure and properties of PP/PC/SEBS blends

4.1 Introduction

The molecular structure of hydrogenated styrene-butadiene-styrene (SEBS) is shown as follow:

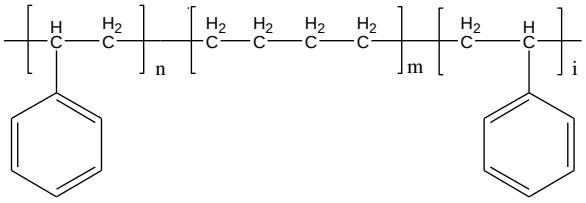

SEBS combines the plastic property of PS and elastic property of EB block. Usually, the degree of hydrogenation of butadiene is higher than 90%, which provides the excellent combination properties such as good thermal stability, resistance to aging and flexibility. Due to the particular structure of EB-compatible aliphatic segments which is well miscible with the non-polar PP domains, and S-chain segments which exhibit strong affinity with PC, SEBS with both compatibilizing and toughening effect was applied to modify PP/PC blend in this study for obtaining the materials with high impact toughness and balanced tensile strength.

4.2 Effect of SEBS on mechanical properties of PP/PC blends

Generally, modification of a polymeric material seldom results in the improvement of both strength and toughness simultaneously. As expected, SEBS as a rubber inevitably brings noticeable reduction in tensile strength to the blends as shown in Fig 4.2, but its compatibilizing effect and satisfying results in toughness modification are also remarkable due to its particular structure with affinity to both PP and PC.

There is a clear dependence of strength and toughness on the composition of the blends in Fig. 4.1-4.3. Compared with neat PP, mechanical properties including notched charpy impact strength, tensile strength and elongation at break of PP/PC binary blend decrease due to the bad compatibility between PP and PC. The notched charpy impact strength and the elongation at break of the PP based blends improve remarkably as the content of SEBS increases for the same content of PC, although the tensile strength decreases at the same time. SEBS takes both roles of compatibilizer and elasticizer. Firstly, it disperses at the interface between PP and PC as an effective compatibilizer; when the concentration of SEBS is more than the critical value, SEBS phase separates out and forms

the microzone of its own which is very important for the improvement of toughness of PP [63].

For a certain content of SEBS, the addition of PC leads to the decrease of elongation at break. The tensile strength decreases first, and it begins to rise at about 15 wt% of PC, which is more obvious in the blends with low loadings of SEBS. On the other hand, the notched charpy impact strength of the blends is improved as the content of PC increases for the same content of SEBS, especially at high content of SEBS, and it declines to a low value when the content of PC reaches about 30wt% since the higher content of PC increases the extent of phase separation. PP with 25 wt% SEBS and 20 wt% PC can reach 21 MPa of tensile strength and 70 KJ/m^2 of impact strength, respectively.

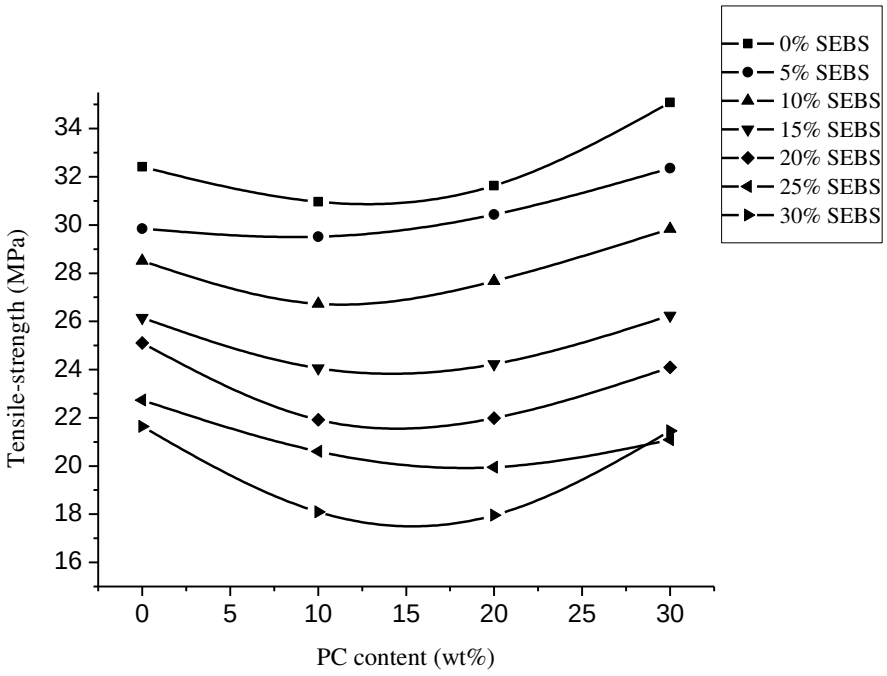

Fig.4.1 The tensile strength of PP/PC/SEBS ternary blends

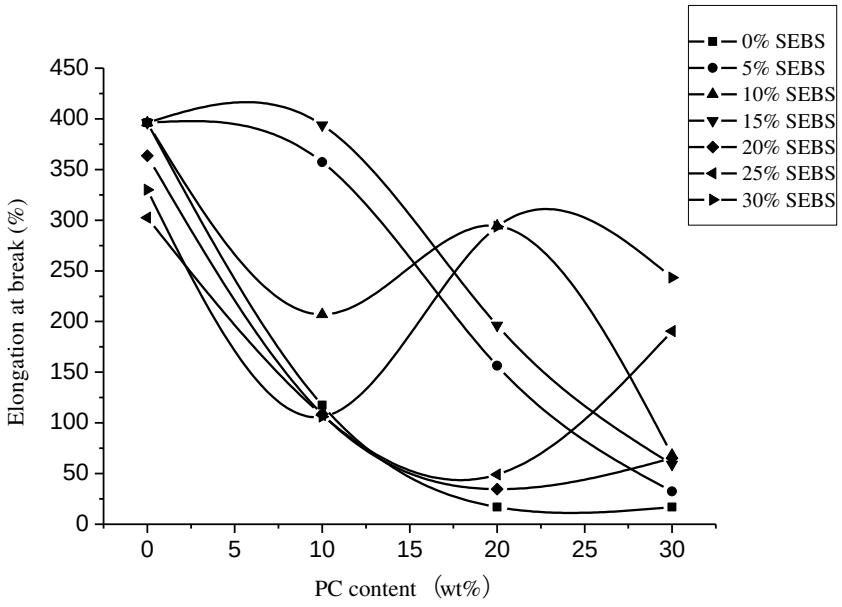

Fig.4.2 The elongation at break of PP/PC/SEBS ternary blends

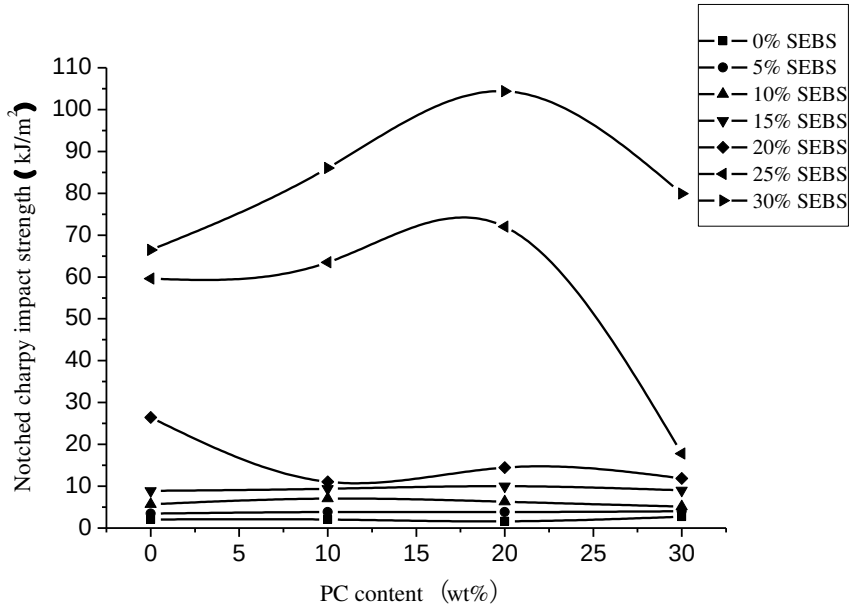

Fig.4.3 The notched charpy impact strength of PP/PC/SEBS ternary blends

4.3 Effect of SEBS on dynamic mechanical properties of PP/PC blends

The DMA curves of PP and PP based blends were represented in Fig. 4.4. For comparison purpose, the DMA curve of PC was also plotted. The well separated T_g peaks of neat PP and neat PC indicate the obvious phase separation between them. The maximum absorption peaks of loss modulus of PP and PC in PP/PC binary blend almost stay in the

same place compared with neat PP and neat PC. However, by addition of SEBS, all peaks of PP shift to higher temperatures while the peaks of PC shift to lower temperatures, which suggest the immiscible system becomes miscible because of the enhanced interaction between PP and PC phase. The compatibilizing effect is further strengthened by addition of PP-g-BPA in PP/PC/SEBS system.

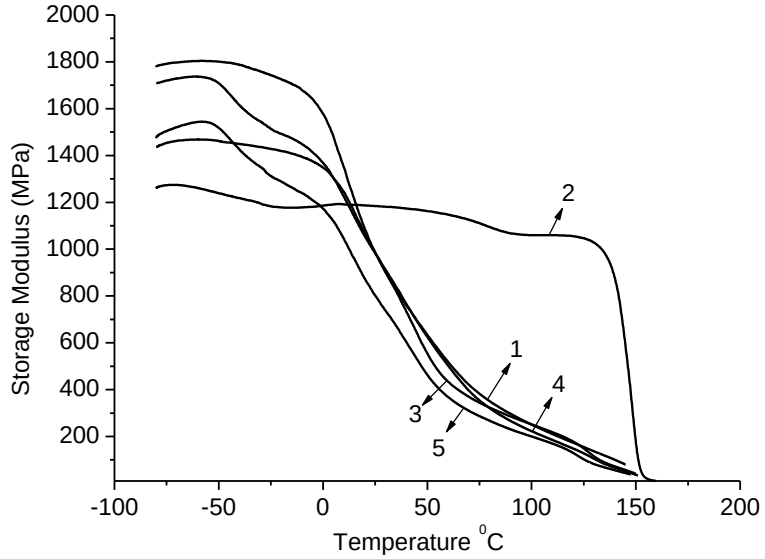

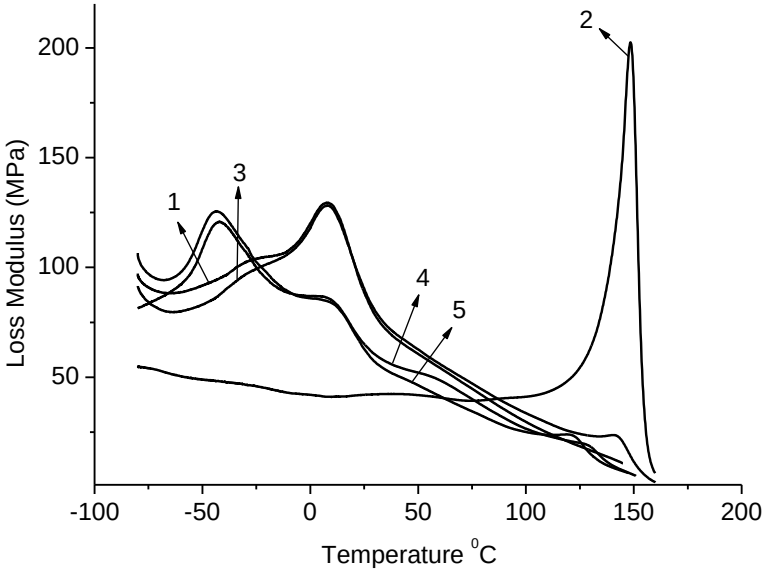

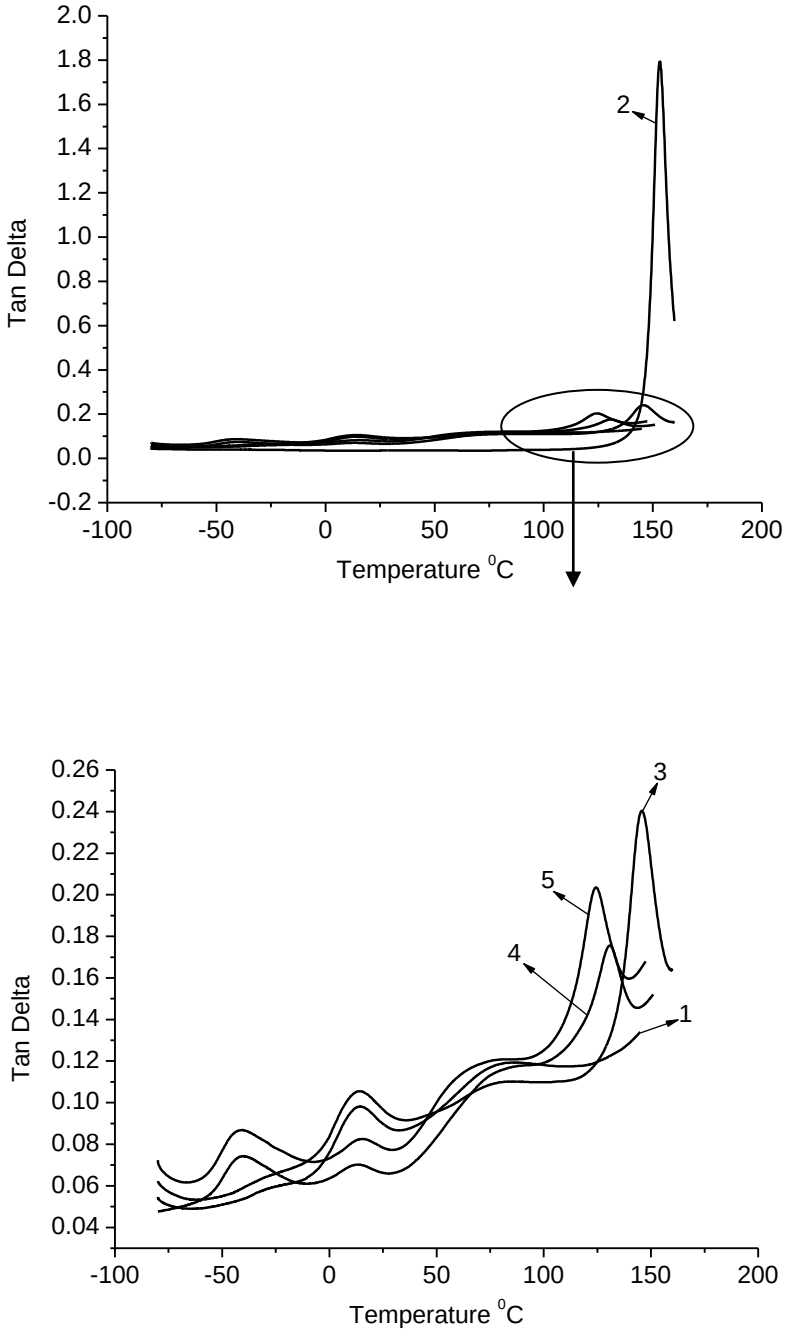

Fig.4.4 DMA curves of (1) PP; (2) PC (3) PP/PC (85/15); (4) PP/PC/SEBS (70/15/15); (5) PP/PC/PP-g-BPA/SEBS (55/15/15/15) blends.

Table 4.1 DMA data of PP based blends.

Sample	PP	PC	PP/PC (85/15)	PP/PC/SEBS (70/15/15)	PP/PC/PP-g-BPA/SEBS (55/15/15/15)
T_g °C (Loss modulus)	7.8	149.0	7.8/142.9	8.5/126.3/-41.9	13.2/118.2/-42.0
T_g °C (Tan delta)	13.5	152.7	13.6/146.3	15.0/130.7/-40.6	17.6/124.8/-40.1

4.4 Effect of SEBS on crystalline properties of PP/PC blends

Compared with PP/PC binary blend, addition of SEBS leads to a slight fall in melting temperature, which is ascribed to the more uniformly distributed PC in PP matrix and amorphous component of SEBS both increase the imperfections of the blend.

The major differences in thermal behavior of the PP based blends occurred during the DSC cooling scan period as shown in Fig.4.5 and Table 4.3. In PP/PC binary blend, the solidification of PC particles dispersing in the PP melt easily results in the heterogeneous nucleation, which significantly increases the exothermic peak temperature (T_{peak}) of the crystallization of PP. The T_{peak} of a binary PP/PC blend displayed 8℃ higher than that of neat PP. The nucleation effect of PC is reduced in the PP/PC/SEBS ternary blend, because of the appearance of the special molecular structure of PC encapsulated by SEBS, which reduces the direct interfacial contact between PP and PC. In addition, a slight improvement of T_{peak} is observed by addition of PP-g-BPA in PP/PC/SEBS ternary blend.

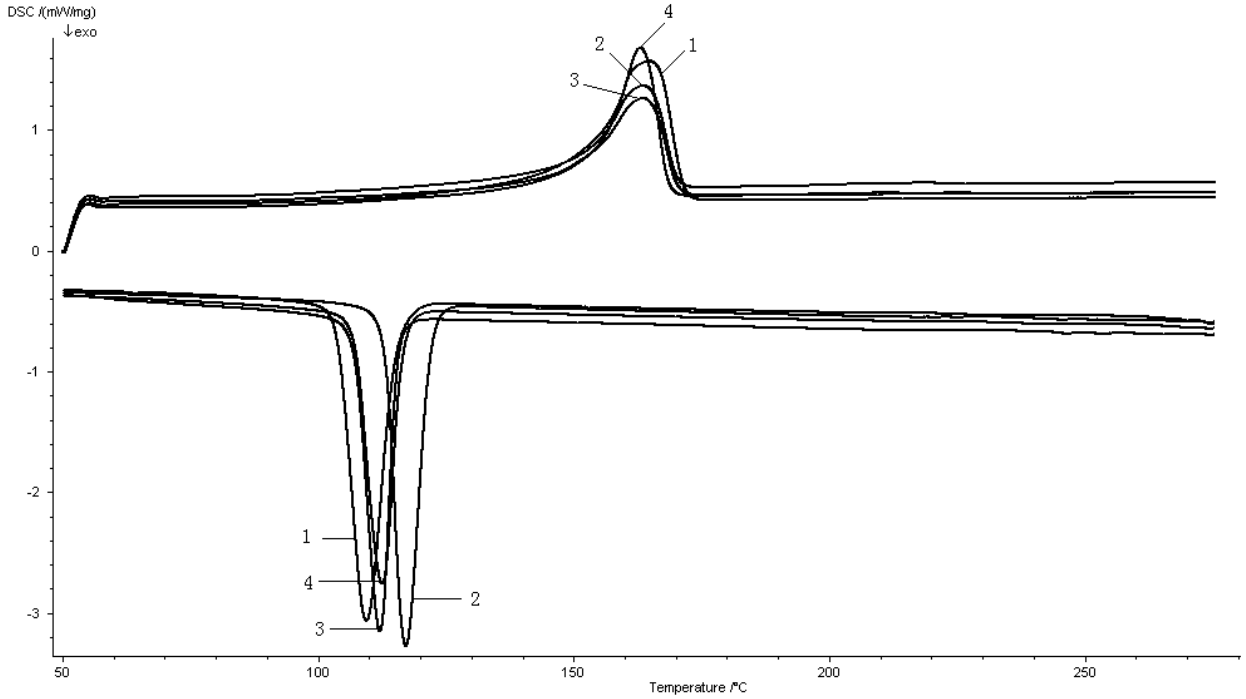

Fig.4.5 DSC curves of (1) PP; (2) PP/PC (85/15); (3) PP/PC/SEBS (70/15/15); (4) PP/PC/PP-g-BPA/SEBS (55/15/15/15) blends.

Table 4.2 DSC results for PP based blends.

Sample	T_m (℃)	T_{cOnset} (℃)	T_{cPeak} (℃)	T_{cEnd} (℃)	T_m-T_{cPeak} (℃)	$\triangle W_c$ (50%,℃)	$\triangle H_c$ (J/g)	X_c (%)
PP	163.6	103.9	109.6	115.5	54.0	6.6	120.8	57.8
PP/PC (85/15)	164.5	113.2	117.3	122.3	47.2	5.3	100.6	48.1
PP/PC/SEBS (70/15/15)	163.8	107.3	112.2	115.7	51.6	5.0	87.5	41.9
PP/PC/PP-g-BPA/SEBS (55/15/15/15)	163.5	108.3	112.7	116.7	50.8	5.7	87.7	41.9

4.4 Effect of SEBS on morphologies of PP/PC blends

As shown in Fig 4.6, the residual holes are etched phase of SEBS. Addition of SEBS not only leads to the much finer and more uniformly dispersed phase domain size of PC, but also results in the encapsulated structure of PC by SEBS. The formation of boundary layer is beneficial to the improvement of the interfacial adhesion, which finally enhances the mechanical properties of the blends. Particle size of PC further decreases by addition of PP-g-BPA in PP/PC/SEBS system.

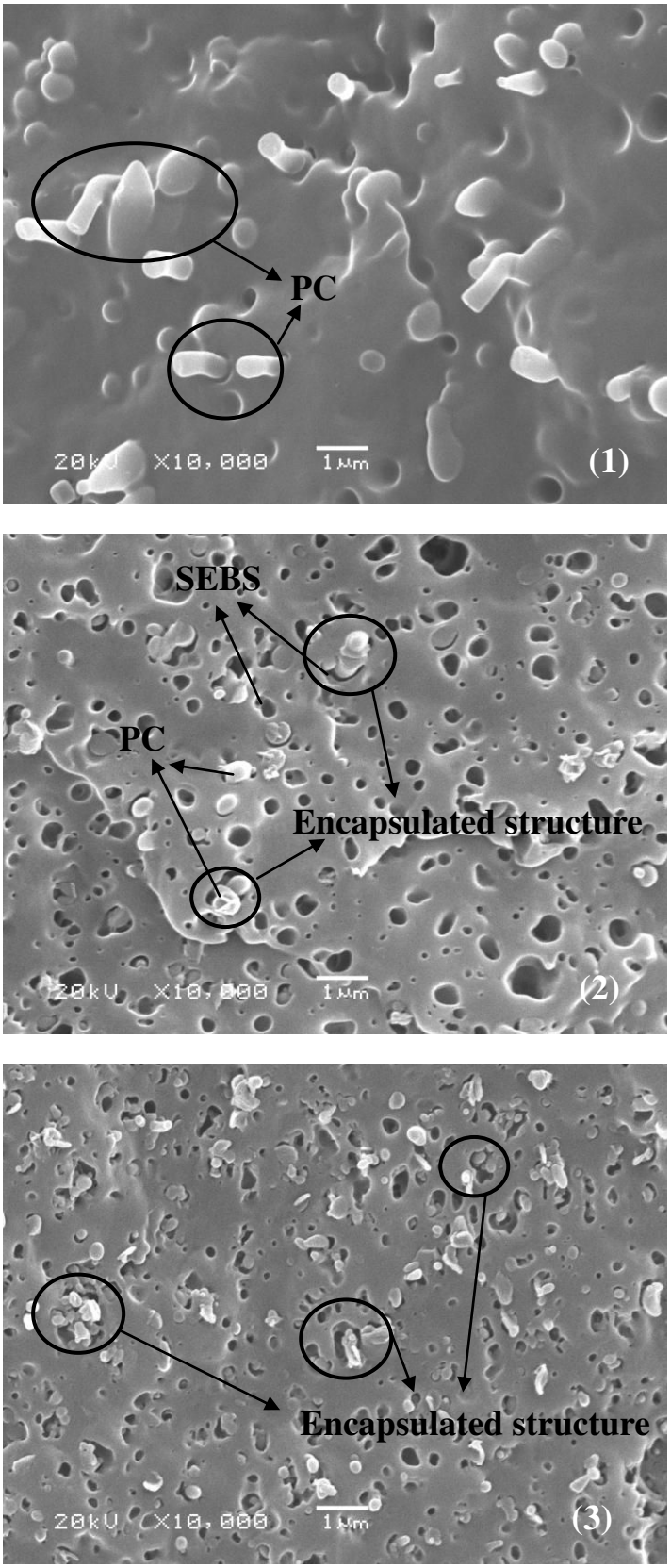

Fig.4.6 SEM images and the diameter distribution of PP and PP based blends (×10000)
(1) PP/PC (85/15); (2) PP/PC/SEBS (70/15/15); (3) PP/PC/ PP-g-BPA/SEBS (55/15/15/15)

4.5 Toughening mechanism of PP/PC/SEBS blends

4.5.1 Analysis of impact fracture surfaces

As shown in Fig. 4.7, PC in skin layer deforms into stick shape because of the high shearing force during injection processing. The crack propagated easily across the section and left smooth impact fracture surfaces and much sharp split in PP/PC binary blend. Increasing the magnification, it can be concluded that PC particles with smooth surface were almost directly pulled out of the matrix during impact process due to the weak interaction between PP and PC. By addition of 10wt% SEBS, the surface of blend also represents the typical brittle fracture, but there are obvious deformation and fracture surface of PC. Further increasing the content of SEBS, the blend represents tough fracture. The whole fracture surface is fully covered with the regularly distant striation. PP and PC phase can't be separated even at a high magnification.

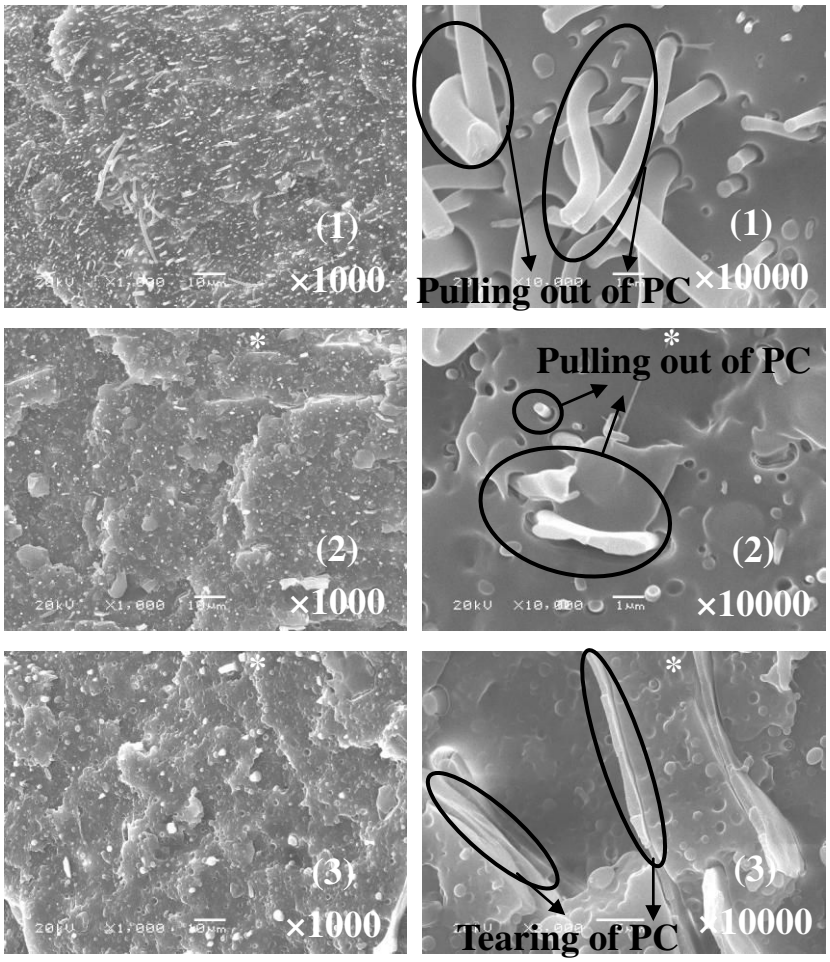

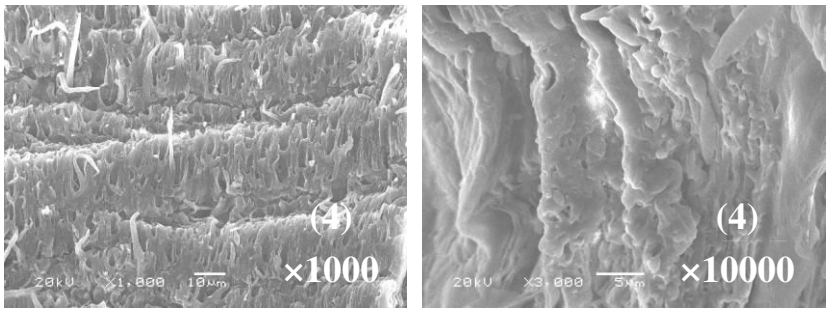

Fig.4.7 SEM images of impact fracturing skin layer of PP blends
(1) PP/PC (85/15); (2) PP/PC/SEBS (75/15/10); (3) PP/PC/SEBS (65/15/20); (4) PP/PC/SEBS (55/15/30)

Morphology evolution in the core layer with the increase of concentration of SEBS is similar with the skin layer, except the initial shape of PC. Spherical PC particles off the matrix easily before compatibilizing, and leaves sharp split in the fracture surface. By addition of 10wt% SEBS, the surface of blend also represents the typical brittle fracture, but there are obvious deformation and fracture surface of PC. Further increasing the content of SEBS till 30wt%, the blend represents tough fracture.

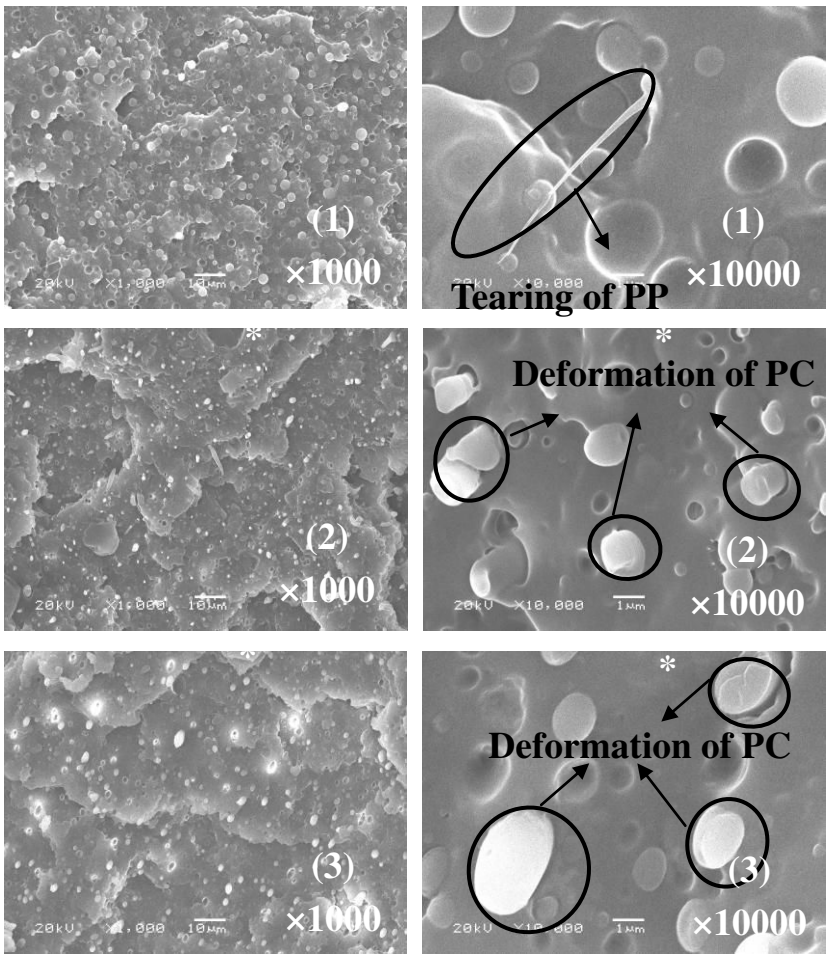

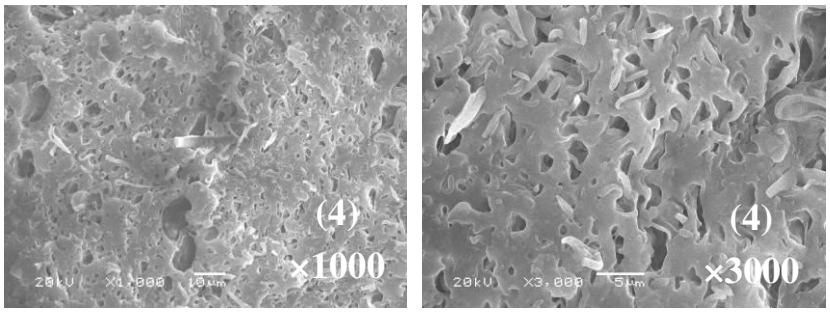

Fig.4.8 SEM images of impact fracturing core layer of PP blends
(1) PP/PC (85/15); (2) PP/PC/SEBS (75/15/10); (3) PP/PC/SEBS (65/15/20); (4) PP/PC/SEBS (55/15/30)

4.5.2 Analysis of fracture toughness

SEM images of fracture surfaces of PP based blends prepared according to the method of ASTM E813-87 is shown in Fig. 4.9. Propagated-crack of sample develops with the improved falling distance of loading point, namely, the increasing loading time. Compared with PP/PC binary system, the propagated-crack of PP/PC/SEBS ternary blend is less with the same loading time, which indicates that the SEBS toughened blend has a much higher crack propagation resistance.

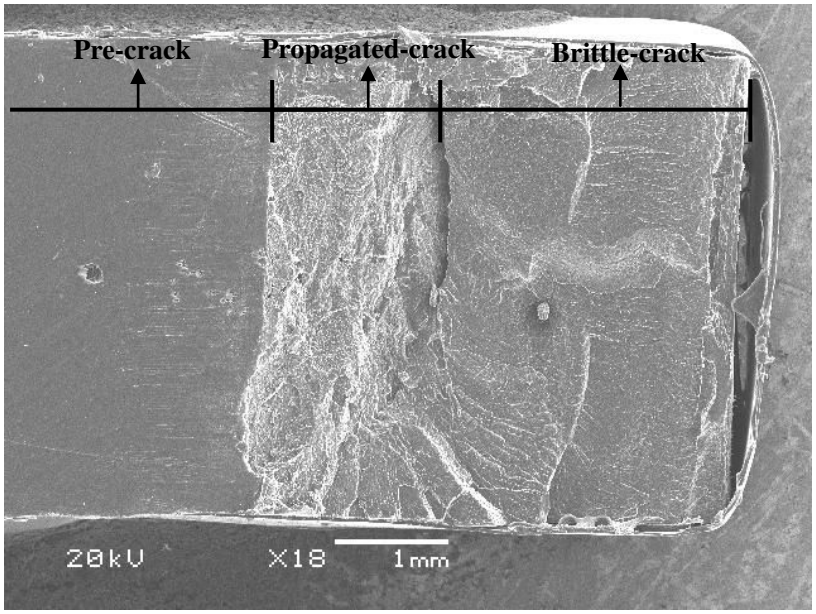

(1) PP/PC（85/15）falling 2mm off

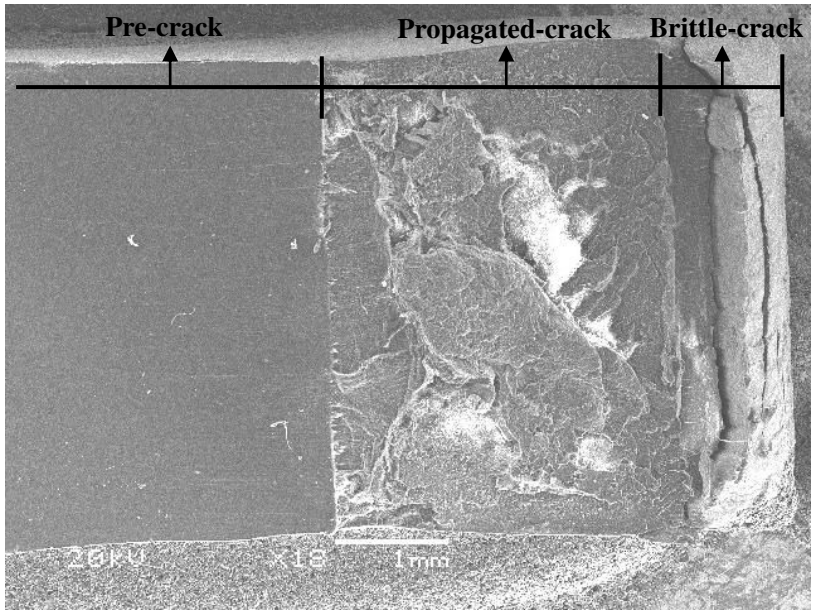

(2) PP/PC（85/15）falling 5mm off

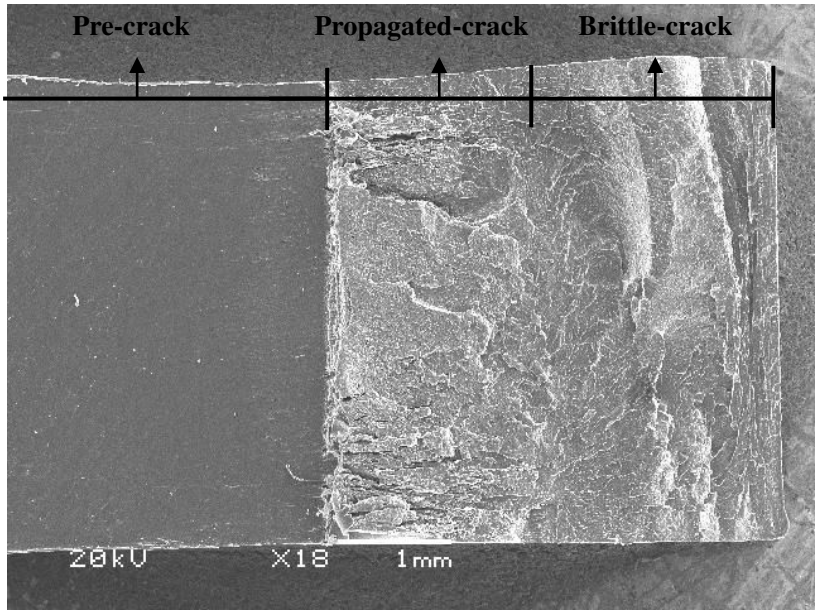

(3) PP/PC/SEBS（55/15/30）falling 5mm off

Fig.4.9 The shape of typical propagated crack of PP blends (×18)

The J-R curves with blunting line for PP based blends are plotted in Fig. 4.10. J_{IC} values of all specimens calculated from the intersection of J-R curves and blunting lines are listed in Table 4.3. $J \geq J_{IC}$, specimen experiences an unstable type of crack growth. The J_{IC} of PP/PC blend is relatively low, and after a certain amount of stable crack propagation, crack instability occurs abruptly in this binary system. On the other hand, due to the enhanced J_{IC}, PP/PC/SEBS could experience comparatively longer stable crack propagation, indicating

the utilization of SEBS has greatly improved the fracture toughness of PP/PC blend.

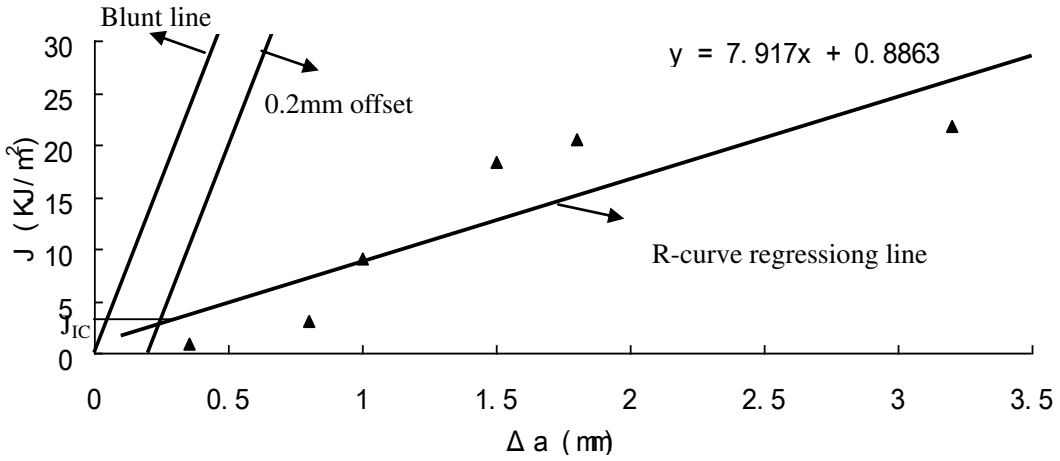

(1) PP/PC（85/15）

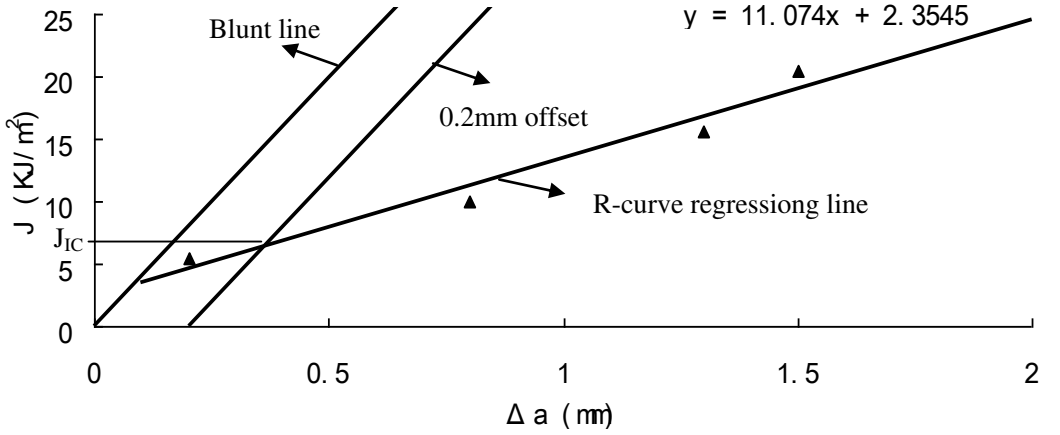

(2) PP/PC/SEBS（55/15/30）

Fig.4.10 J-values versus crack growth for PP based blends

Tab.4.3 J_{Ic} of PLA/TPU blends

Sample	σ_y （MPa）	E（MPa）	J_{Ic} （KJ/m^2）
PP/PC=85/15	33.14	3351	2.8
PP/PC/SEBS=55/15/30	19.80	1337	6.3

Note：σ_y-tensile yield strength，E-young's modulus

The concept of tearing modulus (E_m) is also used to describe the stability of crack propagation, and it can be calculated as the following equation:

$$Em = E \times (dJ/d\Delta a)/\sigma_y^2 \quad (4.1)$$

Where σ_y is the yield stress, E is the young's modulus.

E_m of PP/PC and PP/PC/SEBS blends is calculated to be 24.16 and 37.8 respectively, indicating SEBS improves not only the crack initiation resistance but also crack propagation resistance.

The dissipation of impact energy of the blends mentioned above is probably summarized as the following factors: first, the isolated SEBS particles play a significant role in either arresting the cracks or at least reducing their propagation rate; secondly, the improved adhesion between PP and PC avoids early decohesion, and is later capable of cavitation; thirdly, energy contribution from the fracture of PC.

4.6 Conclusion

Due to the particular structure with EB-compatible aliphatic segments which is well miscible with the non-polar PP domains, and S-chain segments which exhibit strong affinity with PC because of the similar molecular structure, SEBS with both compatibilizing and toughening effect was applied to modify PP. Certain content of PC can improve both notched impact strength and tensile strength of blends, but too high content of PC led to serious phase separation. High content of SEBS represented more obvious compatibilizing effect but decreased the efficiency of forming cavity due to the accumulation of molecules. PP blended with 25 wt% SEBS and 20 wt% PC can reach 21 MPa of tensile strength and 70 KJ/m^2 of impact strength respectively. By addition of SEBS, the two T_gs of PP and PC phase shifting inside of their respective original T_g suggested partial miscibility of the two polymers. Besides, crystallinity, crystallizing point and melting point decreased due to the formation of the encapsulated structure of PC by SEBS. Addition of PP-g-BPA into PP/PC/SEBS blend further enhanced the compatibilizing effect and heterogeneous nucleation of PC. Compared with PP/PC blend, much more finely dispersed PC phase can be observed after adding SEBS，the interface became diffusing and some of PC particles are encapsulated by SEBS which reduced the contact between PP and PC。Addition of PP-g-BPA into PP/PC/SEBS blend further decreased the size of PC particles and improved the dispersion.

The evolutions in skin and core layer of blends with the increasing of SEBS are similar except the initial shape. PC in skin layer deformed into stick shape because of the high shearing force during injection processing, and PC in core layer mainly existed in spherical

shape. The impact fracture surfaces of PP/PC binary blend represented typical brittle fracture and PC particles were almost directly pulled out under impact. With increasing SEBS content, the surface changed from mosaic fracture into mixture of mosaic and striation, finally total striation, and the interaction between PP and PC was enhanced during the evolution. Both J_{IC} and E_m were improved in PP/PC/SEBS blend compared with PP/PC blend, indicating that SEBS improved not only the crack initiation resistance but also crack propagation resistance.

Chapter 5 Preparation and study of structure and properties of PP/PC/POE blend

5.1 Introduction

Recently, interests have been focused on the use of ethylene-octene copolymer (POE) which is the most potential elastomer as toughness modifier of PP [64-65], because of its high speed of dispersion in polyolefine matrix.

POE was applied to toughen PP/PC blend and styrene-ethylene-propylene-styrene block polymer (SEPS) with as high as 60wt% content of PS block was applied as the compatibilizer for PP/PC/POE blend in this research. EP-aliphatic block is well miscible with the non-polar PP and POE domains, and S-chain segments exhibit strong affinity with PC because of the similar molecular structure. The molecular structure of SEPS is shown as follow:

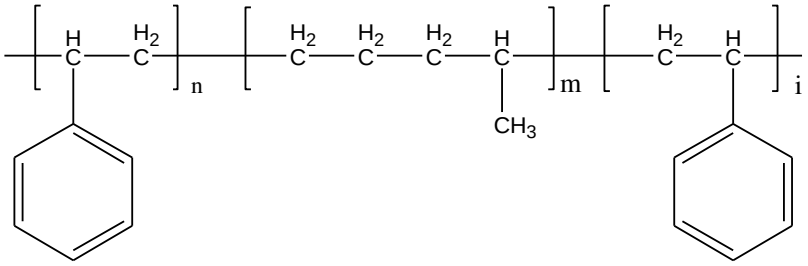

High viscosity ratio of PC/PP leads to the poor dispersion of PC in the PP matrix. The method of secondary processing by pre-blending of PC and SEPS can reduce the apparent viscosity of PC effectively and leads to favorable matched viscosity of the blend.

EVA with similar ester group with PC and aliphatic chain with PP and POE was further selected to compatibilize PP/PC blend. The molecular structure of EVA is shown as follow:

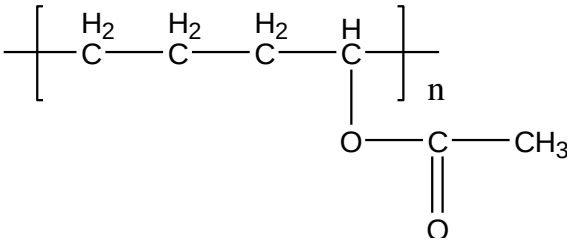

5.2 Study of structure and properties of PP/PC/POE/SEPS blend

5.2.1 Effect of SEPS on mechanical properties of PP/PC/POE blend

The tensile strength and notched charpy impact strength of PP/PC/POE blends as the function of the content of the compatibilizer (SEPS) are summarized in Fig. 5.1. The impact strength of PP/PC/POE ternary blends increases significantly with the increase of the content of POE from 10wt% to 20wt%, but the tensile strength of the samples is impaired substantially. Compared with PP/PC/POE ternary blend, the impact strength of SEPS compatibilized systems is significantly improved, while all the samples retained relatively high values of tensile strength, which is more pronounced at high content of POE. When 5 wt% SEPS was added to PP/PC/POE blends (20 wt% POE), the impact strength of the blends was enhanced from 24 KJ/m^2 to 43 KJ/m^2 with little drop in the tensile strength (Less than 1Mpa).

The mechanical behavior of a blend is determined by the contribution of each component, as well as by the blend morphology and the interfacial adhesion. POE may cause deformation or form microvoid which can absorb large amount of energy during being impacted [66]. The toughness improvement of compatibilized blends also indicates the compatibilizing effect of SEPS is remarkable due to its particular structure which represents strong affinity with non-polar PP, olefinic rubber POE, and PC. The use of SEPS decreases the interfacial tension and increases the chain entanglement within the interphase. PC particles are easy to yield and generate phenomenon of cold draw, which further improve the mechanical properties of blends. Therefore, the toughness and stiffness of these blends are in good balance.

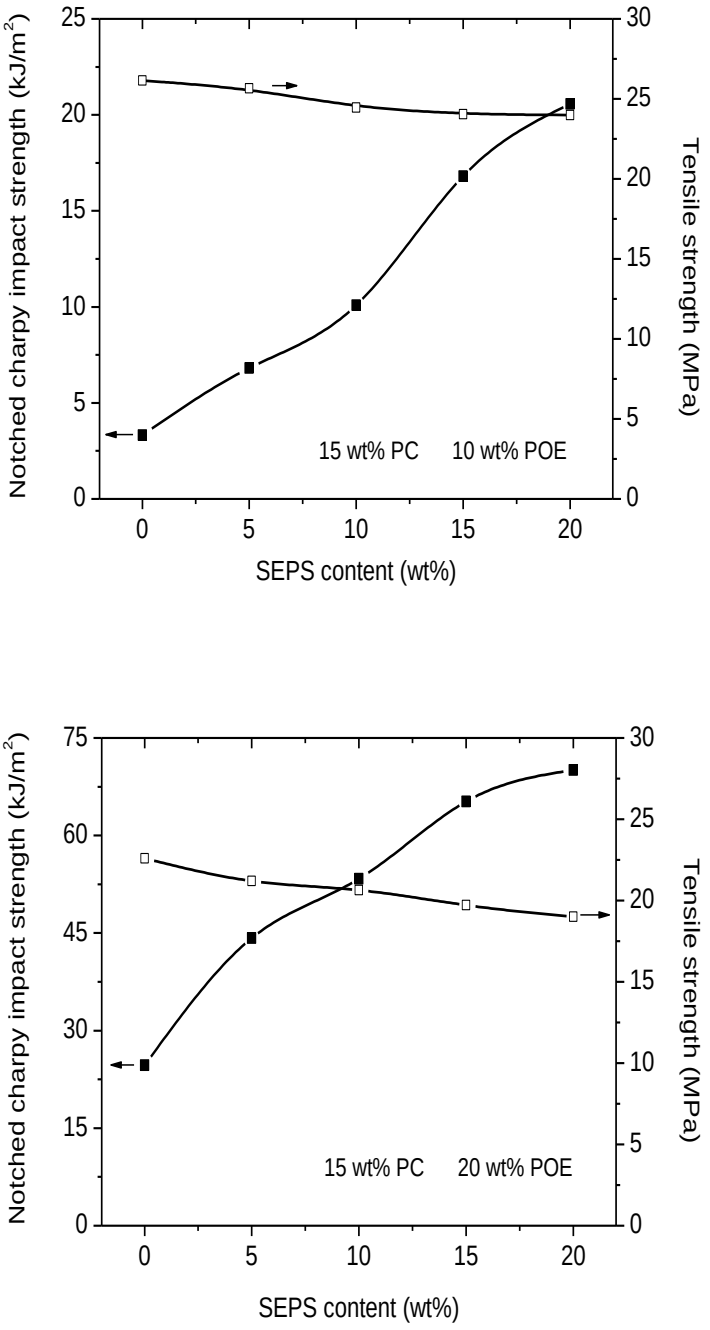

Fig.5.1 The notched charpy impact strength and tensile strength of PP/PC/POE/SEPS blends

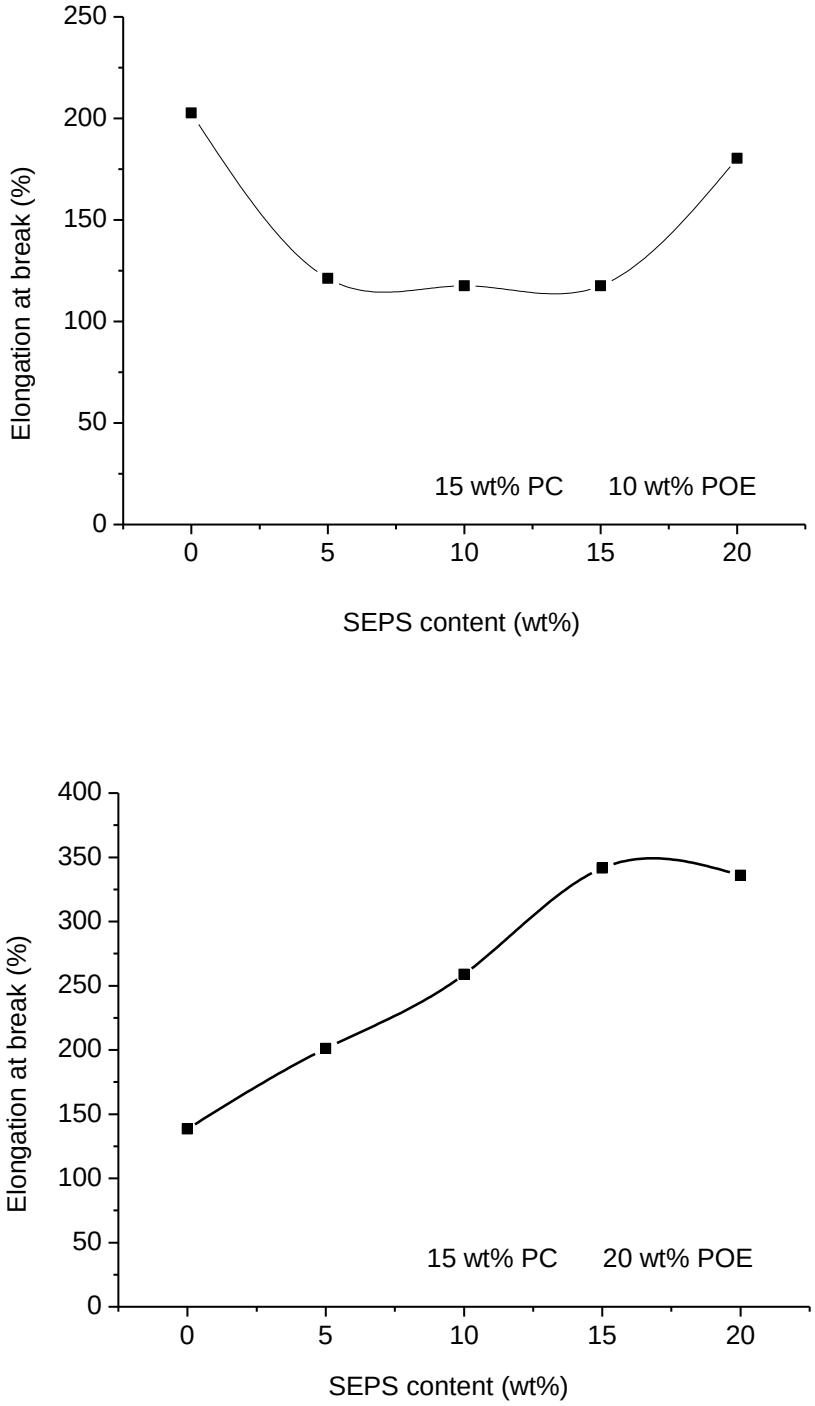

Fig.5.2 The elongation at break of PP/PC/POE/SEPS blends

Based on the conclusion mentioned above and the mechanical properties of PP/PC/Compatibilizer blends as shown in Table 5.1, it can be concluded that although it is a kind of SBS block polymer, SEPS with 60 wt% styrene selected in this work provides this compatibilizer relatively high stiffness and weak toughness. When 25 wt% SEPS is added

into PP/PC blends, the impact strength of the blends only rise to 4.97 KJ/m^2, and the enhancement of elongation at break which is sensitive to the load transfer between phase is also slight. It can be demonstrated that SEPS can't toughen PP as elastomer but effectively compatibilize PP/PC/POE ternary system, then improve toughness and maintain modulus of PP based blends.

Table 5.1 The mechanical properties of PP/PC/SEPS blends.

Sample	Notched charpy impact strength (KJ/m^2)	Tensile strength (MPa)	Elongation at break (%)
PP/PC/SEPS:85/15/0	2.34	33.07	97.4
PP/PC/SEPS:80/15/5	2.53	32.38	104.0
PP/PC/SEPS:70/15/15	3.98	30.84	157.4
PP/PC/SEPS:60/15/25	4.97	30.60	147.1

5.2.2 Effect of SEPS on dynamic mechanical properties of PP/PC/POE blend

Fig. 5.3 is a composite plot of temperature dependence of the storage modulus, loss modulus and loss tanδ of the component polymers in the selected blends. The storage modulus is directly related to the elastic response of the tested material and tanδ is intimately associated with the chain relaxation that takes place [67]. All the storage modulus - temperature curves experience a gradual decline in storage modulus with increase in temperature from -100°C to 160°C. The addition of POE leads to a reduction in storage modulus obviously, and when more content of POE added, there was more reduction in modulus. The loss modulus and loss tanδ reveal more clearly the corresponding transition temperatures and the width of transition zones. In PP/PC/POE ternary system, the glass transition of POE occurs at -50°C to -20°C with a peak at about -40°C. There exists a β–transition of PP at -10°C to 35°C with a peak at about 14°C and a α-relaxation peak around 90°C. The glass transition peak of PC is noted at around 145°C in the heating cycle. These well separated transitions are indicative of immiscibility of the component polymers. The most interesting observation in Fig. 5.3 is the appearance of a new transition peak around 100°C by addition of SEPS in PP/PC/POE blends. The peak temperature of the new transition is a little lower than that of neat SEPS (107°C). More SEPS added, broader and stronger transition is noticed in this region and the transition shifts to higher temperature in the meantime, in other words, more close to the transition temperature of SEPS.

Generally, glass transition shifts in the blends can be explained based on the physical interactions between the components [68]. The observed shift in glass transition values of PP, POE and PC in these compatibilized blends is not expected as such variations are normally

observed in partially or fully miscible blends. However, the data of DMA clearly show that the compatibilizing effect of SEPS is carried out by the movement of PP, PC or POE molecules into the phase of SEPS. SEPS is the key component in this new domain and polymers in this new domain are miscible to each other.

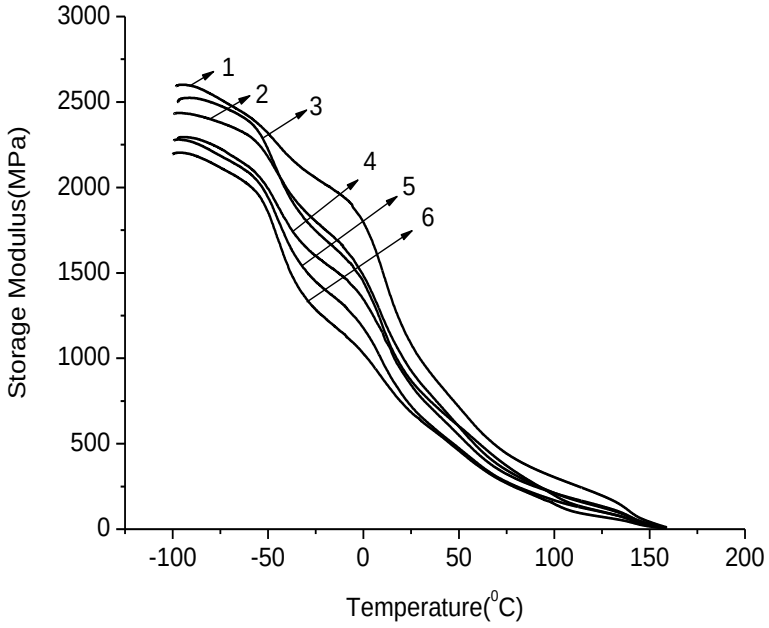

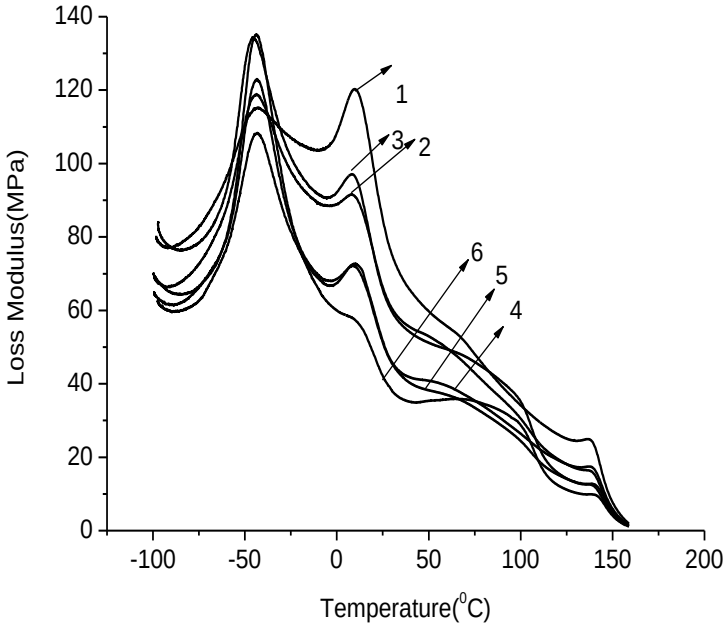

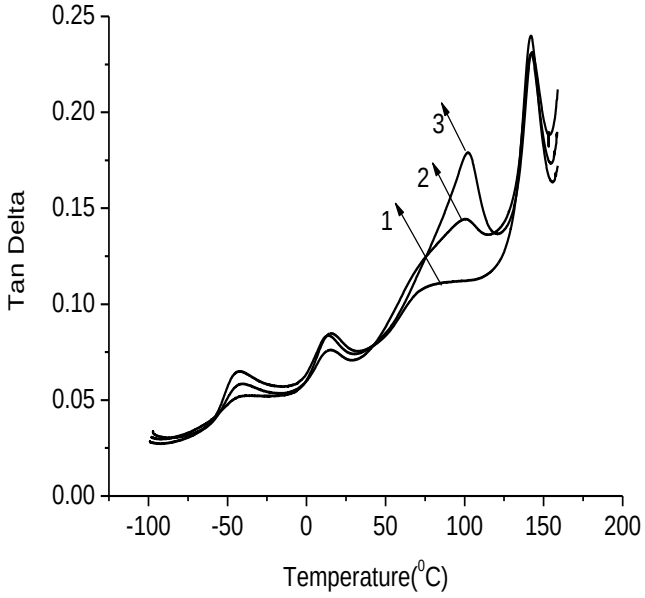

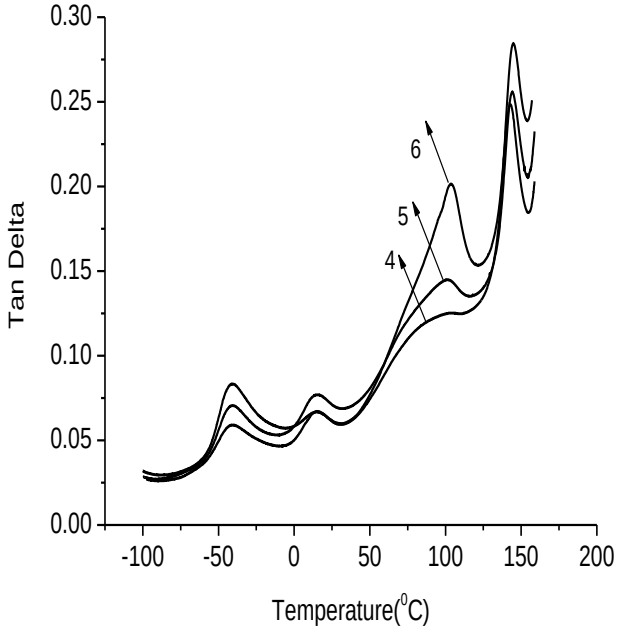

Fig.5.3 DMA curves of PP blends 1：PP/PC/POE/SEPS (75/15/10/0); 2: PP/PC/POE/SEPS (65/15/10/10); 3: PP/PC/POE/SEPS (55/15/10/20); 4: PP/PC/POE/SEPS (65/15/20/0); 5: PP/PC/POE/SEPS (55/15/20/10); 6: PP/PC/POE/SEPS (45/15/20/20).

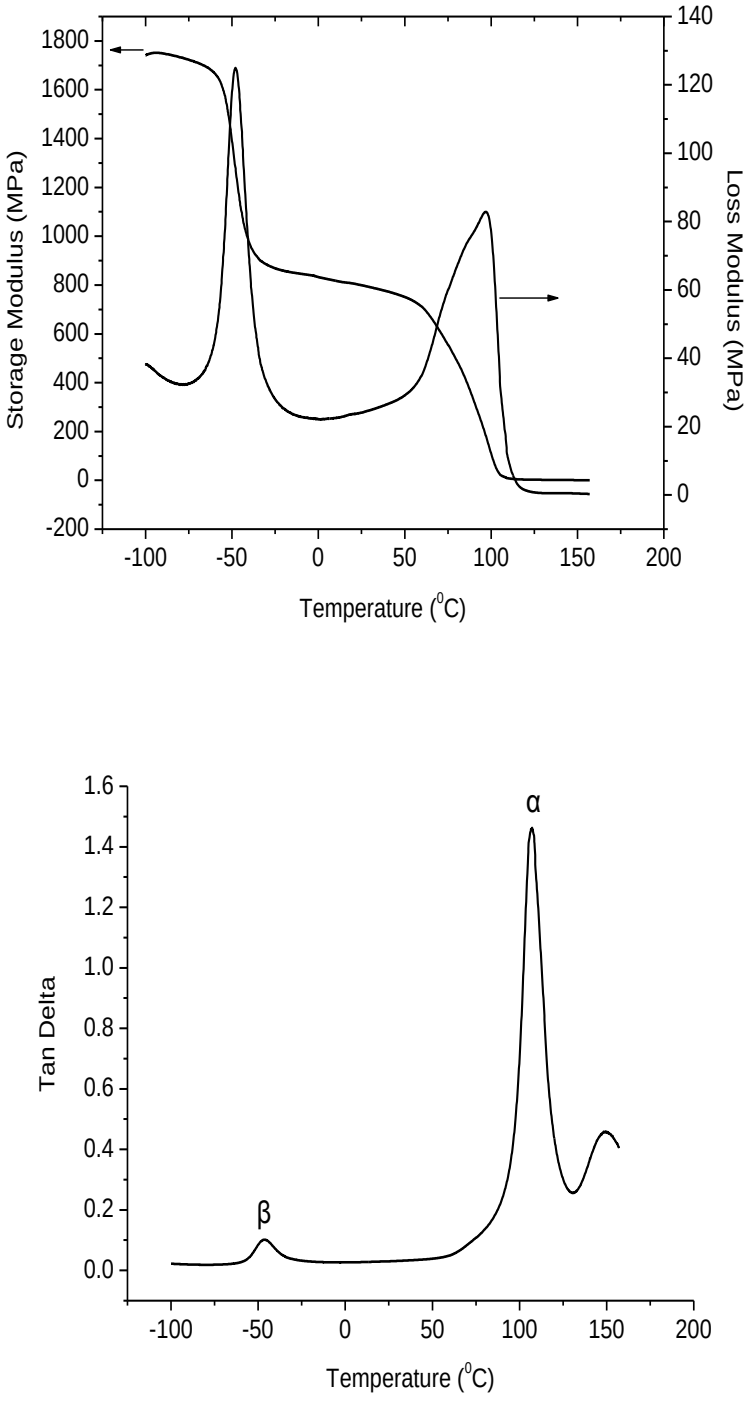

Fig.5.4 DMA curves of SEPS

Table 5.2 DMA data (from Tan delta) of PP based blends.

Sample	T_g (PC)	T_g (SEPS)	T_g (PP)	T_g (POE)
PP/PC/POE/SEPS (75/15/10/0)	141.7	/	15.1	-42.1
PP/PC/POE/SEPS (75/15/10/10)	141.7	100.2	14.0	-41.7
PP/PC/POE/SEPS(75/15/10/20)	142.9	101.7	13.2	-41.3
PP/PC/POE/SEPS (75/15/20/0)	142.5	/	15.5	-41.7
PP/PC/POE/SEPS (75/15/20/10)	144.0	100.9	15.9	-41.3
PP/PC/POE/SEPS (75/15/20/20)	144.9	104.0	16.3	-41.1
SEPS	/	107.1	/	/

5.2.3 Effect of SEPS on crystalline properties of PP/PC/POE blend

Nonisothermal crystallization is important because it's close to the practical situation during process [69]. The major differences in thermal behavior for different PP based blends also occurred during the DSC cooling scan period, as shown in Fig. 5.5 and Table 5.3. For PP/PC/POE ternary blends, the solidification of PC particles dispersing in the PP melt easily results in heterogeneous nucleation, which significantly increases the crystallization peaks of PP (T_{peak}). On the other hand, the structure of PC encapsulated by SEPS reduces direct interfacial contact between PP and PC particles and weakens the effect of heterogeneous nucleation at the same time. The latter effect is more obvious during the crystallization process of these PP based blends, so T_{peak} of PP shift to lower temperatures with the addition of SEPS. More SEPS leads to further decrease in crystallization temperature compared with PP/PC blend. The compatibilized system also represents the broader crystalline half-peak width and lower crystalline enthalpy, indicating the reduction of the crystalline growth rate and crystallinity of the PP blends.

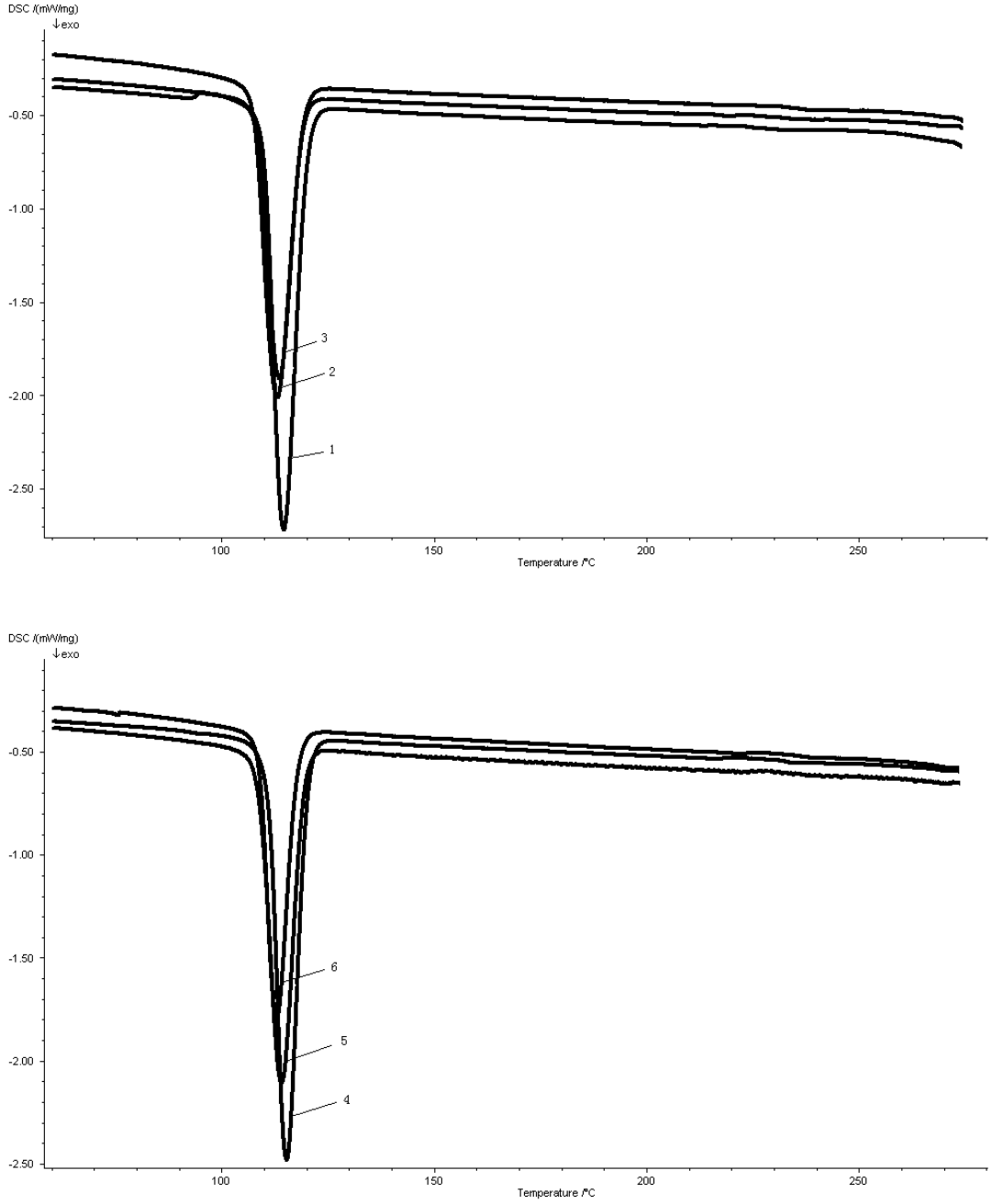

Fig.5.5 DSC curves of PP blends 1 ：PP/PC/POE/SEPS (75/15/10/0); 2 : PP/PC/POE/SEPS (65/15/10/10); 3:PP/PC/POE/SEPS (55/15/10/20)blends ； 4: PP/PC/POE/SEPS (65/15/20/0); 5: PP/PC/POE/SEPS (55/15/20/10); 6: PP/PC/POE/SEPS (45/15/20/20).

Table 5.3 Effect of SEPS on the crystallization parameters of PP based blends

Sample	T_{cOnset} (℃)	T_{cPeak} (℃)	T_{cEnd} (℃)	$\triangle W_c$ (50%, ℃)
PP/PC/POE/SEPS (75/15/10/0)	110.1	114.7	120.2	5.9
PP/PC/POE/SEPS (65/15/10/10)	107.7	113.1	119.3	6.9
PP/PC/POE/SEPS (55/15/10/20)	108.6	113.6	119.1	6.3
PP/PC/POE/SEPS (65/15/20/0)	111.2	115.4	120.4	5.4
PP/PC/POE/SEPS (55/15/20/10)	108.9	114.2	119.5	6.2
PP/PC/POE/SEPS (45/15/20/20)	109.0	113.0	118.0	5.3

Notes: T_m: melting point. T_{cOnset}, the onset crystallization temperature. T_{cPeak}, the crystallization peak temperature. T_{cEnd}, the end crystallization temperature. T_m-T_{cPeak}: the degree of supercooling.$\triangle W_c$, the crystalline half-peak width. X_c, the degree of crystallinity. $\triangle H_c$, the crystalline enthalpy

Fig. 5.6 shows the XRD scans of PP and PP/PC/POE blends with increasing content of the compatibilizer. The detailed analysis of neat PP is given in Table 5.4. The typical crystalline form for isotactic PP is α-form with a characteristic diffraction peak at about 18.6° corresponding to the 130 plane diffraction as observed. Core layer of PP displays a prominent increase in the intensity at lower 2θ values when compared with skin layer of PP. This clearly reflects that the shearing force during injection is a very important factor affecting crystallization of polymer. A strong influence of blending PP with PC/POE on the behavior of conversion of material from a crystalline to the amorphous state is clearly seen in Fig. 5.6 When the compatibilizer SEPS was added in the blends, the intensity of characteristic peaks of skin and core layer slightly increased and broadened, indicating the improved mixability of PP matrix and amorphous PC.

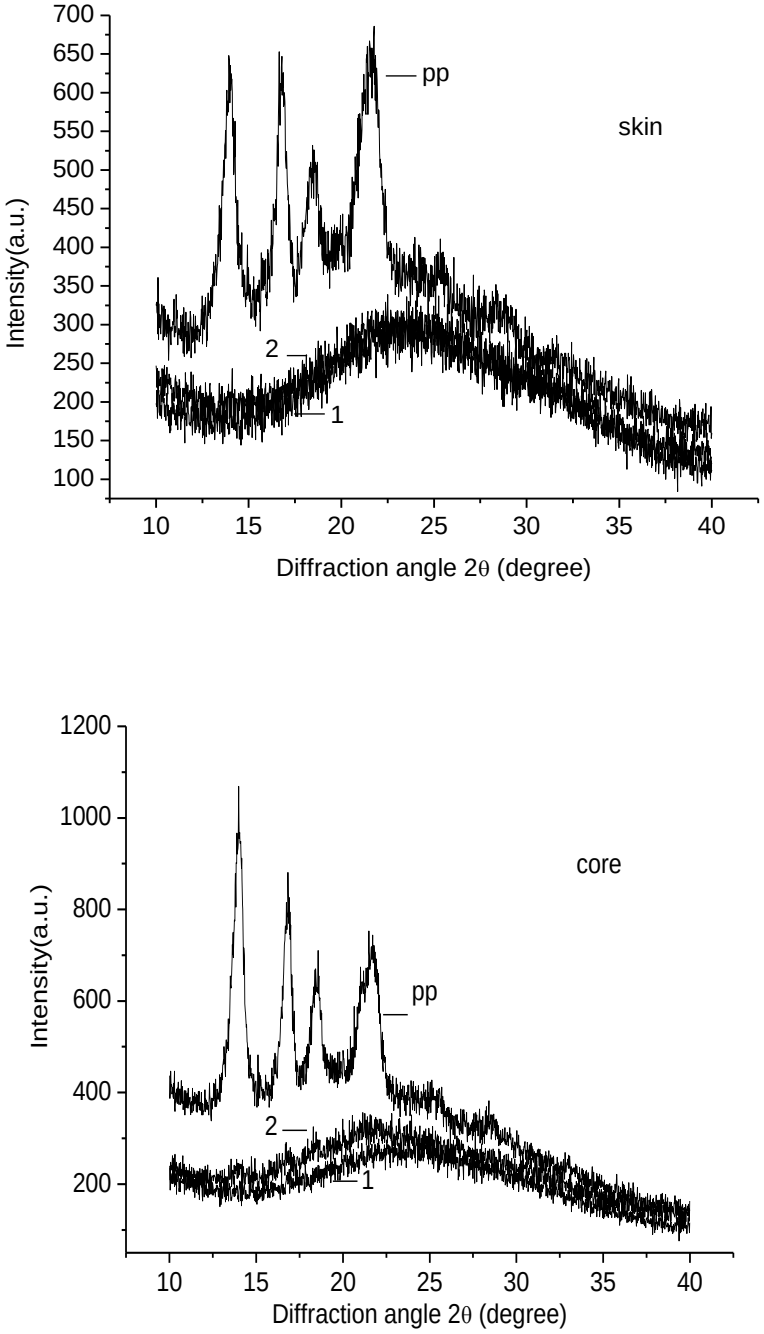

Fig.5.6 XRD patterns of PP and PP based blends
1: PP/PC/POE/SEPS (65/15/20/0); 2: PP/PC/POE/SEPS (65/15/20/20)

Table 5.4 XRD analysis of PP

d-spacing (nm)	Angle (2θ)	Relative Intensity (%)	Tip Width (2θ)
		Skin layer	
6.32	14.00	87.62	0.32
5.63	15.72	17.76	0.12
5.31	16.68	84.82	0.20
5.25	16.88	87.00	0.16
4.79	18.52	63.43	0.56
4.10	21.64	100	0.96
3.51	25.35	32.56	0.48
3.14	28.73	19.11	1.28
		Core layer	
6.31	14.01	100	0.44
5.26	16.85	76.22	0.24
4.83	18.36	45.59	0.28
4.78	18.56	52.16	0.16
4.23	21.00	50.40	0.24
4.10	21.66	64.69	0.56
3.50	25.41	18.80	0.96
3.13	28.52	15.54	0.32
2.72	32.93	7.16	0.48

5.2.4 Effect of SEPS on morphologies of PP/PC/POE blend

Mechanical strength is often related to the morphology, domain size, and size homogeneity of the polyblends and it is believed that interaction between two phases is one of the key factors deciding the degree of dispersion [70]. When the rigid PC particles are added in PP/POE blends, and depending on the location of PC, three types of microstructures may form: “separate” dispersion structure, where the PC particles reside in the matrix and not coated with POE; Encapsulation or core-shell structure, where PC particles partition preferentially in the dispersed phase POE; Mixture of the former two. A separated microstructure, wherein the rigid particles partitions favourably in the PP matrix, without affecting the elastomer phase, is desirable for optimum reinforcement of blends. As shown in Fig. 5.7, SEM images of etched skin layer of PP based blends clearly reveals the morphologies of the uncompatibilized and compatibilized blending systems at the magnification of 5000. In the skin layer of the blends, most PC particles (bright particles) localize exclusively in the PP matrix phase and formed the desired separated microstructure without affecting the POE phase, because PC particles will be effectively forced out from high viscosity of POE and eventually agglomerate together in PP matrix or SEPS domains

under the shear force. The dark holes and slots formed by shear stress during injection moulding represent the etched POE particles and SEPS phase. PC particles are non-uniformly distributed over the skin layer of the blends and smooth interface between PP and PC is observed for the blends with 10wt% and 20wt% POE, as shown in Fig. 5.7 (1) and (4). It reveals a poor adhesion between phases in absence of the compatibilizer agent (SEPS), as demonstrated by the fracture developing along the interface. Moreover, very small amount of the dark holes and slots can be observed for the blends with low content of POE, indicating that there appears little POE in the skin layer of the blends in this case. The addition of SEPS leads to a decreasing and much more homogeneous size of the dispersed PC particles in the skin layer of the blends, and large amount of dark holes and slots representing the POE and SEPS phase can be observed clearly.

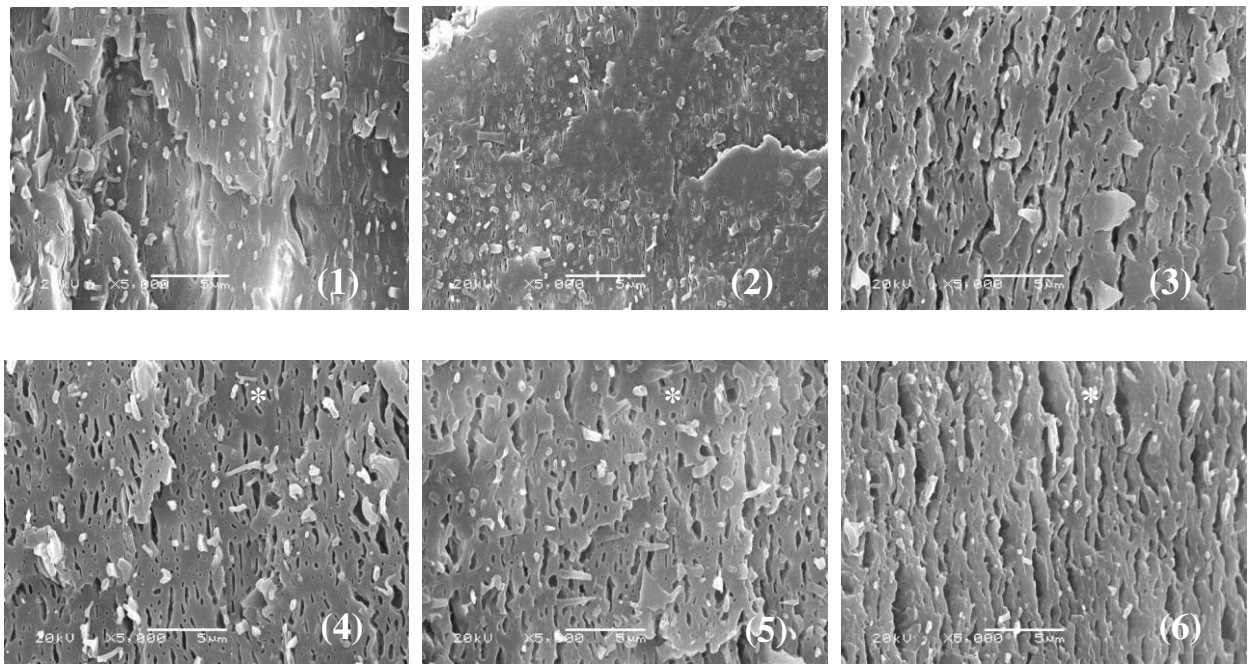

Fig.5.7 SEM images of etched skin layer of PP blends (×5000)
(1) PP/PC/POE (75/15/10); (2) PP/PC/POE/SEPS (65/15/10/10); (3) PP/PC/POE/SEPS (55/15/10/20); (4) PP/PC/POE (65/15/20); (5) PP/PC/POE/SEPS (55/15/20/10); (6) PP/PC/POE/SEPS (45/15/20/20)

As shown in Fig. 5.8 (1) and (4), in the core layer, the ternary PP/PC/POE blends exhibit very big spherical-shaped domains which may be formed by PC. The residue holes in polyblends are formed by the etched POE phase. It can be easily concluded that PC and POE phase dispersed in the PP matrix respectively, namely, forming the “separate” dispersion structure as in the skin layer. Smooth and clean interface between PP and PC results in the great interfacial tension and weak adhesion between PP and PC. As expected, the addition of SEPS results in decreasing and much more homogeneous size of the

dispersed PC phase, which change to rod-like in shape in the mean time and the extent is enhanced with the increase of the content of SEPS. Some of PC phase are encapsulated by SEPS as shown in Fig. 5.8 (3) and (6). On the other hand, the addition of SEPS not only leads to the much finer phase domain size, but also brings the structure of PC encapsulated by SEPS, indicating the decrease of interfacial tension and enhancement of adhesion between PP and PC, which is beneficial to the improvement of the mechanical properties of the blends. With 20wt% POE and 20% SEPS loading, the morphologies of the blend are coral-like in the perpendicular plane, close to the co-continuous phase morphology. It is reasonable to believe that this kind of phase structure of the PP based blends explains, to some extent, why the material can keep a good balanced rigidity and toughness.

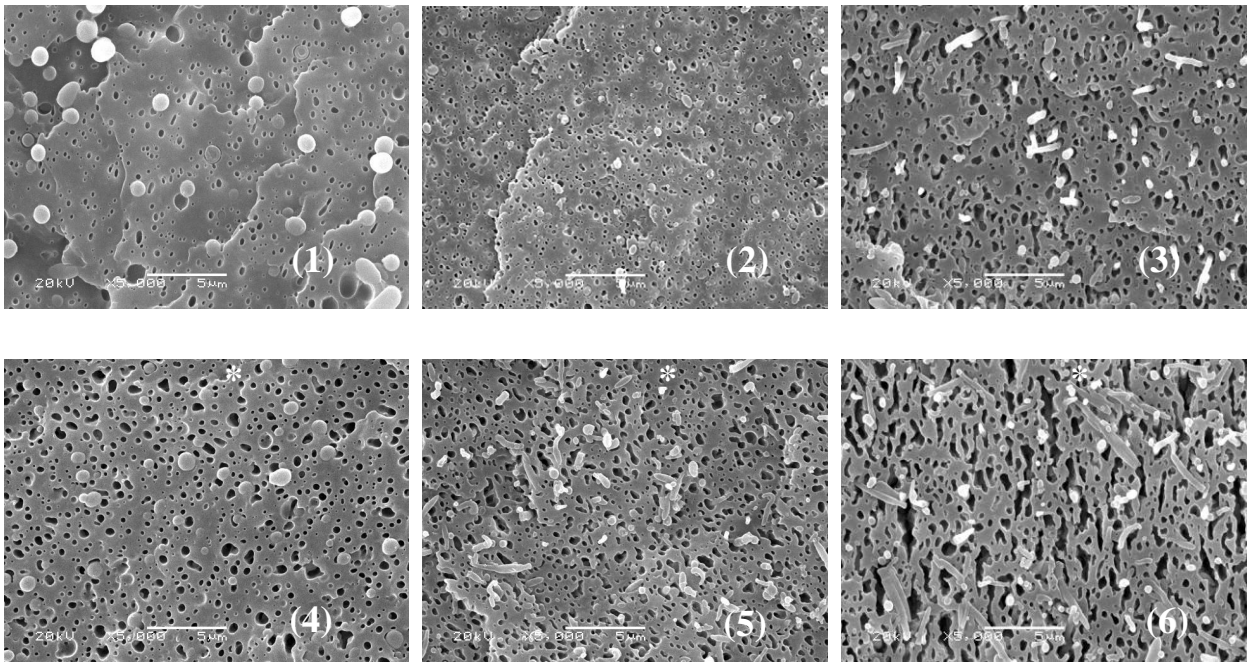

Fig.5.8 SEM images of etched core layer of PP blends (×5000)
(1) PP/PC/POE (75/15/10); (2) PP/PC/POE/SEPS (65/15/10/10); (3) PP/PC/POE/SEPS (55/15/10/20); (4) PP/PC/POE (65/15/20); (5) PP/PC/POE/SEPS (55/15/20/10); (6) PP/PC/POE/SEPS (45/15/20/20)

5.2.5 Effect of viscosity ratio on structure and properties of PP/PC/POE blend

The main mechanism governing phase morphology development in immiscible polymer blends is believed to be the result of both droplet break-up and coalescence. It is well known that droplet break-up is dependent on the viscosity ratio of the dispersion/matrix phase, the matrix viscosity and the shear rate experienced during blending. Dispersed domains under shear flow will break-up as long as the shear forces applied by the flow field can overcome the interfacial forces. High viscosity ratios, namely, the low viscous matrix often acts as a lubricant for the dispersed phase and reduces the droplet break-up. Low viscosity ratios and

low viscous dispersed phase lead to obvious deformation also without break-up.

The melt flow characteristics of PP, PC, POE, SEPS and the pre-blends determined by capillary rheology are shown in Fig. 5.9 as the relationship of viscosity vs. shear rate. All the samples are non-Newtonian fluids and present shear-thinning behavior, and SEPS has the smallest viscosity while PC has the greatest. By varying the order of mixing, and the amount of SEPS in PC/SEPS pre-blends, it becomes possible to obtain viscosity ratios much close to the condition of favorable viscosity ratio (≈1) [71-77]. It can be seen that the apparent viscosity of PC drops obviously even at a low concentration of SEPS. Continue to increase the concentration of SEPS leads to further decreasing of apparent viscosity of PC. Even though the viscosity of the PP is significantly lower than that of the PC, in most of the studied shear rate range, the shear viscosity behavior of the PC/SEPS pre-blend is much close to that of the neat PP, which facilitates the break-up of the droplet of PC.

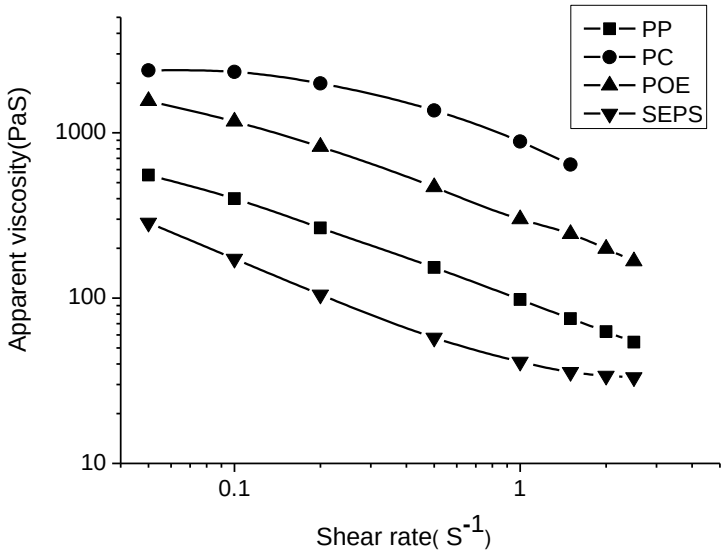

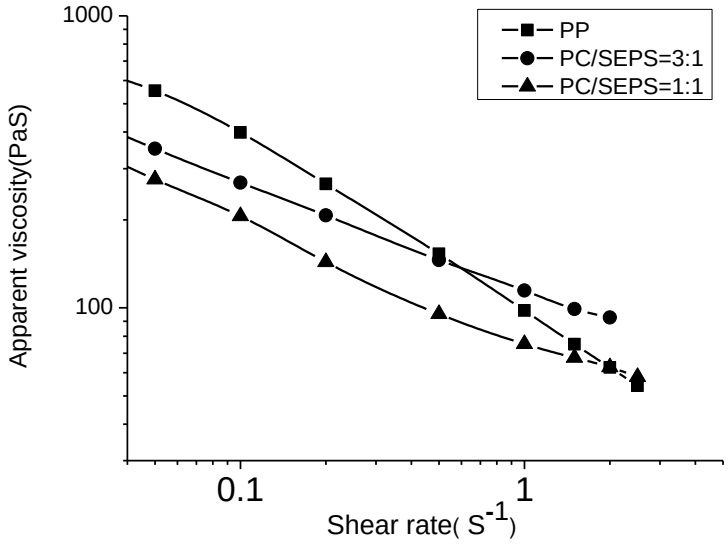

Fig.5.9 The relationship between shear rate and apparent viscosity of each component of the PP blends

Table 5.5 displayed the notched charpy impact strength and tensile strength of the blends prepared by different blending process. The method of secondary processing by pre-blending of PP and PC leads to better mechanical properties of PP based blends.

Table.5.5 The notched charpy impact strength and tensile strength of PP/PC/POE/SEPS blends

Sample	Notched Impact strength (kJ/m^2)	Tensile strength (Mpa)
PP/PC/SEPS=85/15/5	4.81	31.1
PP/(PC/SEPS)=85/(15/5)	6.47	29.53
PP/PC/SEPS=85/15/15	5.10	31.02
PP/(PC/SEPS)=85/(15/15)	6.02	29.59
PP/POE/PC/SEPS=70/15/15/5	29.84	24.70
PP/POE/(PC/SEPS)=70/15/(15/5)	33.22	24.12
PP/POE/PC/SEPS=70/15/15/15	51.60	23.29
PP/POE/(PC/SEPS)=70/15/(15/15)	55.07	23.41

As shown in Fig. 5.10, surfaces occupied by more PC particles are obtained after etching the phase of SEPS and POE, indicating pre-blending of PC and SEPS increases the encapsulated structure of PC by SEPS.

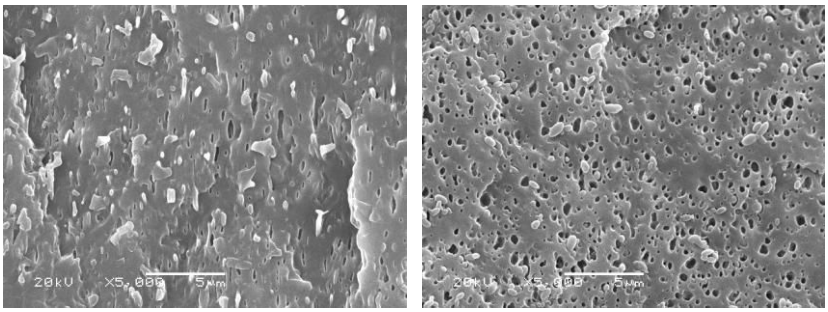

Skin layer　　Core layer

(1) One-time processing　　PP/PC/POE/SEPS (65/15/10/10)

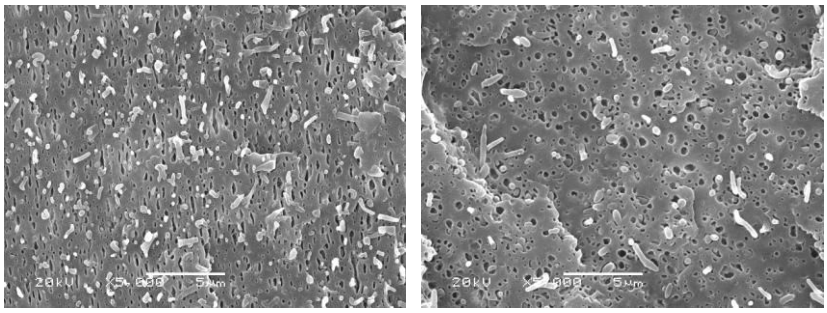

Skin layer　　Core layer

(2) Two-time processing　　PP/PC/POE/SEPS (65/15/10/10)

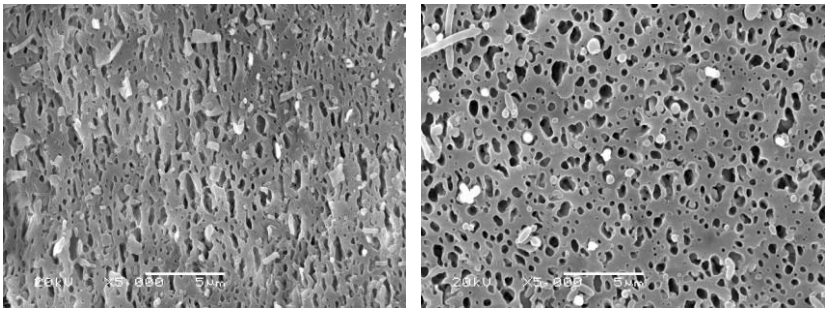

Skin layer　　Core layer

(3) One-time processing　　PP/PC/POE/SEPS (55/15/20/10)

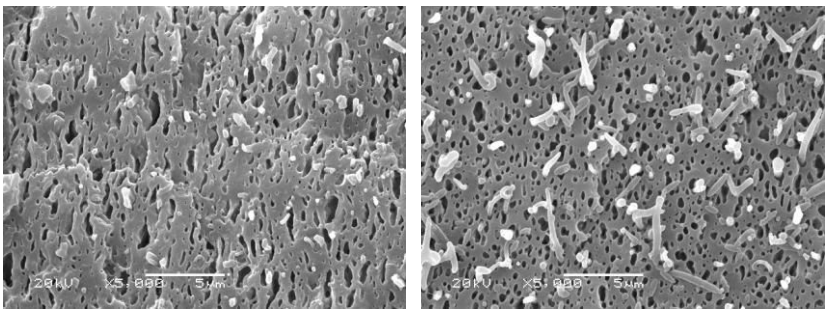

Skin layer　　Core layer

(4) Two-time processing　　PP/PC/POE/SEPS (55/15/20/10)

Fig. 5.10 SEM images of etched PP blends prepared through varying processing techniques (×5000)

5.2.6 Toughening mechanism of PP/PC/POE/SEPS blend

Toughening mechanism in rubber-modified single-phase polymers has been well established [78-81]. According to the framework of Wu's theory [82-83], for polymer/rubber blend, a sharp brittle-ductile transition (BDT) occurs at a critical interparticle distance [84-96], described by:

$$ID_c = [\frac{A}{\sigma_y \varepsilon_Y} + d^3]^{\frac{1}{3}} - d \qquad (5.1)$$

Where d is the average dispersed particle diameter, A is a parameter related to the strain energy. Li [97] reported that ID_c of PP/rubber system is 0.15μm.

In order to study the effect of interparticle distance on BDT, it is necessary to determine the ID values of PP/rubber blends, which can be determined from:

$$ID = d[(\frac{\pi}{6V_r})^{\frac{1}{3}} - 1] \qquad (5.2)$$

Where V_r is the rubber volume fraction, d is the rubber particle diameter. The volume fraction V_r of the rubber can be given by:

$$V_r = \frac{W_f \rho_m}{W_f \rho_m + (1 - W_f)\rho_f} \qquad (5.3)$$

Where W_f, ρ_f and ρ_m refer to the weight fraction of the rubber, density of rubber and density of matrix, respectively. On the base of SEM images shown in Fig 5. 11 and Eqs 5.1-5.3, the average diameter of POE particles, volume fraction V_r of POE and ID value for PP/PC/POE blends are listed in Table 5.6.

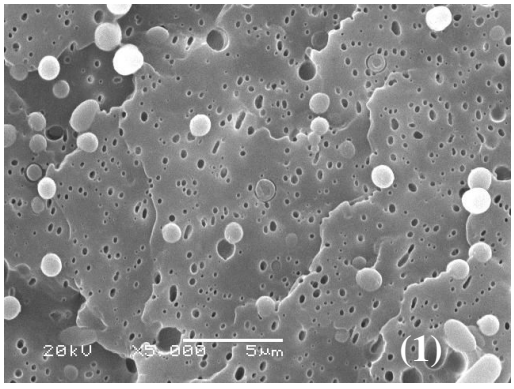

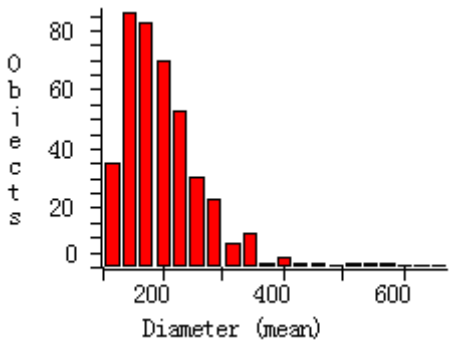

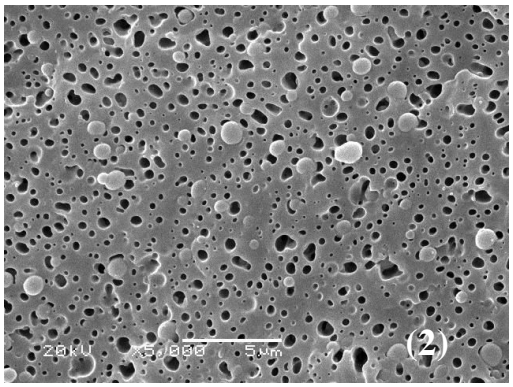

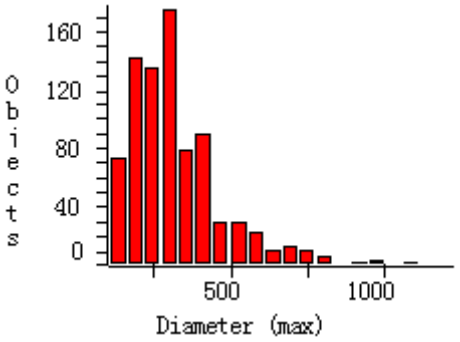

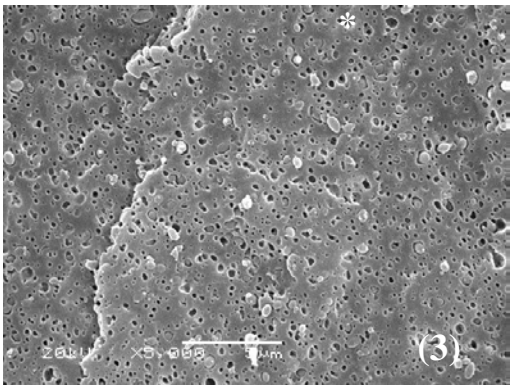

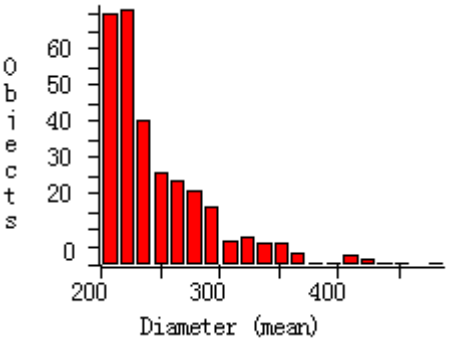

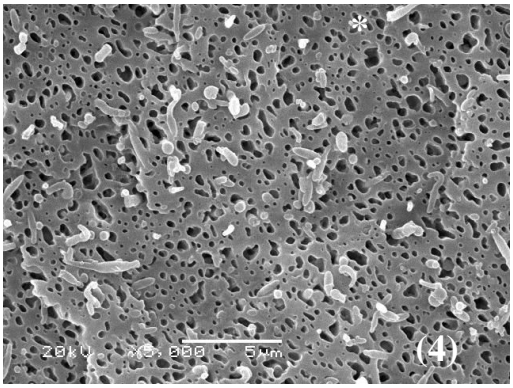

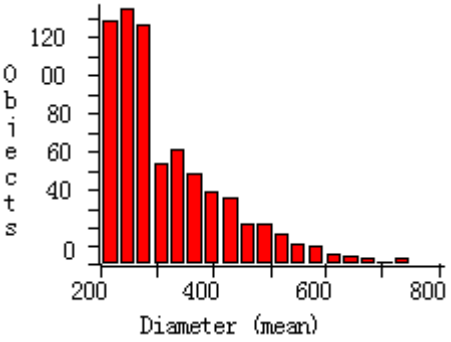

Fig.5.11 SEM images and the diameter distribution of PP and PP based blends (×5000)
(1) PP/PC/POE (75/15/10); (2) PP/PC/POE (65/15/20);
(3) PP/PC/POE/SEPS (65/15/10/10); (4) PP/PC/POE/SEPS (55/15/20/10)

Before compatibilization, ID of the blend with 10wt% POE is more than 0.15μm, namely, the material fails in a brittle manner. With the increasing of concentration of POE, ID value of the blend with 20wt% POE is decreases to 0.13μm, which indicates the continuum percolation of stress volume around elastomer particles would occur. The matrix yielding would propagate and through the entire matrix, and then the blend would be tough. The BDT of this system happens earlier after compatibilization. Further insight into the results of phase morphology discussed above, in PP/PC/POE/Compatibilizer blends,

dispersed POE particle size is obviously decreased and effectively reduces the interparticle distance. Besides, the stress field around PC particles can interfere or overlap with those around POE particles when POE particles are close to rigid particles after compatibilization. In this case, the stress fields around PC particles seem to serve as a bridge between two neighboring elastomer particles. Therefore, the synergic effect of these two factors is believed to result in the observed increase of impact strength in the compatibilized blends.

Table.5.6 Average POE particle diameter and ID value of PP/PC/POE blends

Sample	Vr (%)	d (μm)	ID (μm)
PP/PC/POE=75/15/10	10.4	0.23	0.16
PP/PC/POE=65/15/20	20.7	0.37	0.13
PP/PC/POE/SEPS=65/15/10/10	20.7	0.25	0.09
PP/PC/POE/SEPS=55/15/20/10	31.0	0.33	0.06

The morphology of the impact fracture surfaces of the skin and core layer of PP based blends as shown in Fig. 5.12 and 5.13 provides a better understanding of the toughening mechanism. The cavitation of isolated elastomer particles and SEPS interlayers represents the main mechanisms of damage and volume dilatation for polymer blends. Deformation damage is essentially controlled by elastomer cavitation and interfacial debonding. In addition, rod-like geometry of PC particles improves somehow the impact resistance thank to its favorable orientation perpendicular to the crack propagation direction.

Before compatibilization, the crack propagated easily across the section and left smooth fracture surfaces and much sharp split as shown in Fig. 5.12 (1), (4) and Fig. 5.13 (1), (4), namely, the material presents brittle fracture (mosaic), indicating the comparatively low interfacial adhesion which is markedly destroyed when the specimen is subjected to being impacted. For blending with a small amount of SEPS, enhanced interlayer and appearance of rod-like dispersed PC phase result in the decreasing of sharp split and the increasing of roughness. The fracture surfaces change from irregular mosaic to the mix of mosaic and striation. Further increase of the content of SEPS, the character of tough fracture presents much more obvious, and the fracture surface is fully covered with the regularly distant striation as shown in Fig. 5.12 (6) and Fig. 5.13 (6), in agreement with the results of the mechanical properties.

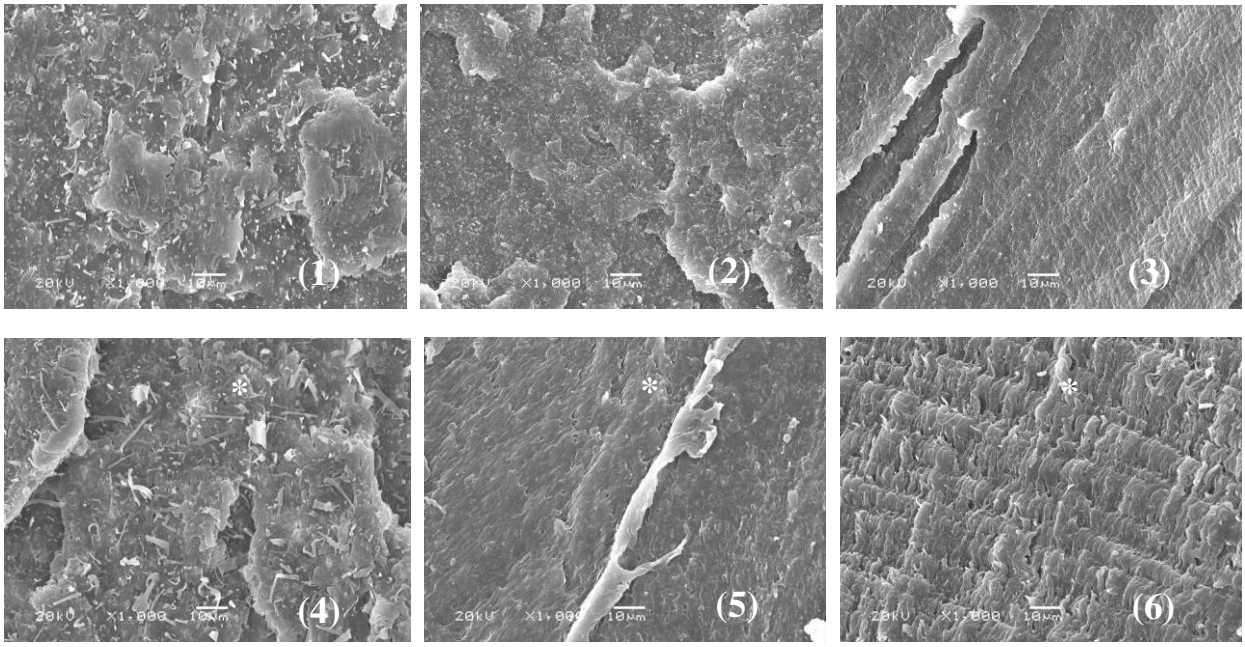

Fig.5.12 SEM images of impact fracturing skin layer of PP blends (×1000)
(1) PP/PC/POE (75/15/10); (2) PP/PC/POE/SEPS (65/15/10/10); (3) PP/PC/POE/SEPS (55/15/10/20);
(4) PP/PC/POE (65/15/20); (5) PP/PC/POE/SEPS (55/15/20/10); (6) PP/PC/POE/SEPS (45/15/20/20)

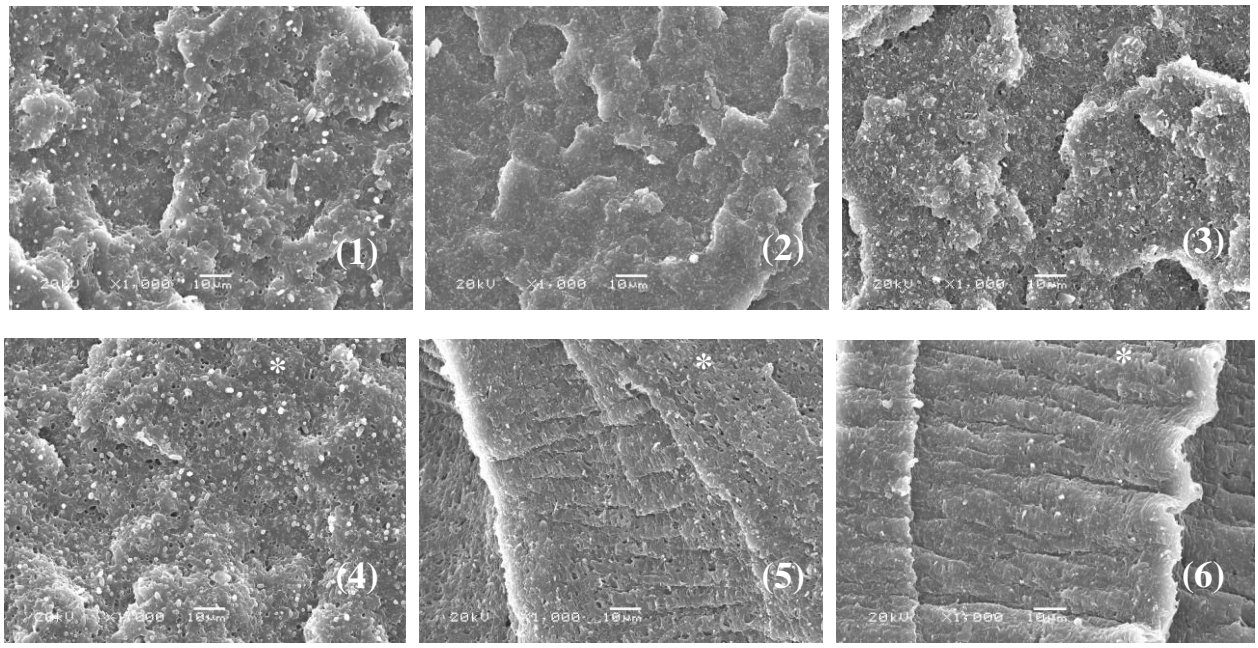

Fig.5.13 SEM images of impact fracturing core layer of PP blends (×1000)
(1) PP/PC/POE (75/15/10); (2) PP/PC/POE/SEPS (65/15/10/10); (3) PP/PC/POE/SEPS (55/15/10/20);
(4) PP/PC/POE (65/15/20); (5) PP/PC/POE/SEPS (55/15/20/10); (6) PP/PC/POE/SEPS (45/15/20/20)

Fig. 5.14 presents the schematic diagram of fracture mechanism of PP based blends. PC particles in the PP/PC binary system are easy to off the matrix due to the weak interaction between PP and PC. However, large plastic deformation of PC particles occurs

in the compatibilized system due to the enhanced interaction and static stress generated from the different Poisson ration between PP and PC. In the first situation, the properties of matrix almost determine the properties of the blend. In the second situation, cold draw of PC generates and PC particles are broken with PP matrix, which is benefit to the improvement of mechanical properties of PP based blends.

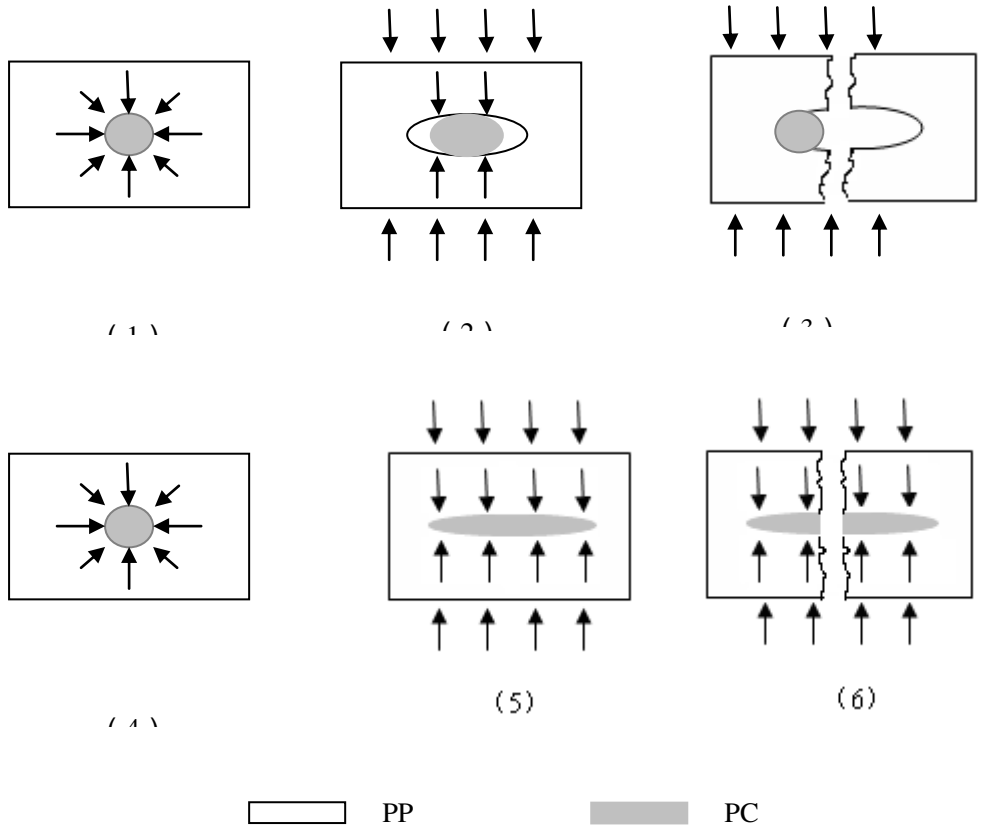

Fig.5.14 The breaking model of PP/PC blend and compatibilized blend

5.3 Compatibilizing effect of EVA/SEPS on PP/PC blend

5.3.1 Effect of EVA/SEPS on mechanical properties of PP/PC blend

EVA with similar ester group with PC and aliphatic chain miscible with PP was further selected to compatibilize PP/PC blend. The tensile strength, notched charpy impact strength and elongation at break of PP based blends are summarized in Table 5.7. The impact strength and elongation at break of PP based blends with different ratio of PP/PC increase by addition of 5wt% SEPS, while the tensile strength of materials maintains at a high level or even improves. Addition of 5wt% EVA in PP/PC blend improves the impact strength and elongation at break of blends, while decreases the tensile strength slightly. Compared with the single compatibilizer, EVA/SEPS compound compatibilizer improved

the elongation at break of blend obviously.

Table 5.7 Mechanical properties of PP and PP based blends

Sample	Impact strength (kJ/m^2)	Tensile strength (Mpa)	Elongation at break (%)
PP/PC=80/20	1.68	30.72	23.2
PP/PC/SEPS=80/20/5	4.37	31.04	41.4
PP/PC/EVA=80/20/5	3.08	29.83	52.9
PP/PC/EVA/SEPS=80/20/5/5	3.67	29.20	66.1
PP/PC=50/50	6.70	37.75	6.7
PP/PC/SEPS=50/50/5	8.74	38.40	22.7
PP/PC/EVA=50/50/5	8.54	36.67	9.86
PP/PC/EVA/SEPS=50/50/5/5	9.72	36.51	74.6
PP/PC=20/80	39.14	48.06	29.7
PP/PC/SEPS=20/80/5	58.06	47.48	154.1
PP/PC/EVA=20/80/5	45.57	45.87	52.7
PP/PC/EVA/SEPS=20/80/5/5	48.44	45.80	361.7

5.3.2 Effect of EVA/SEPS on morphologies of PP/PC blend

Addition of EVA or compound compatibilizer (EVA/SEPS) leads to a decreasing and much more homogeneous size of PC particles as shown in Fig. 5.15.

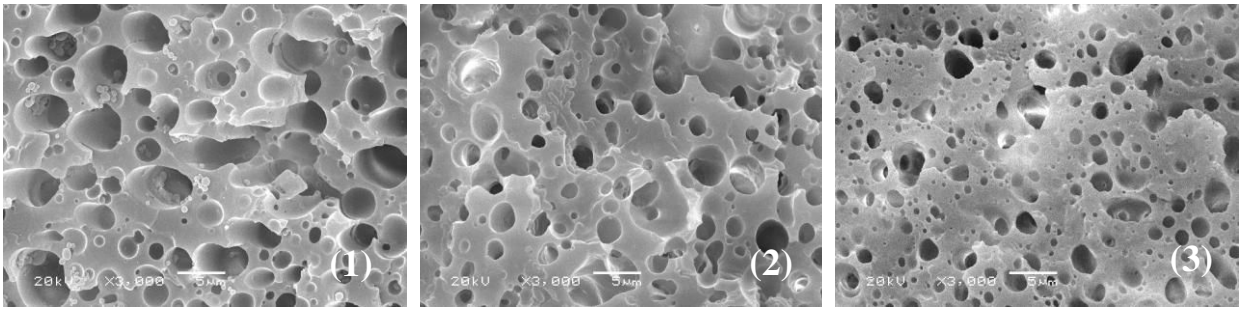

Core layer

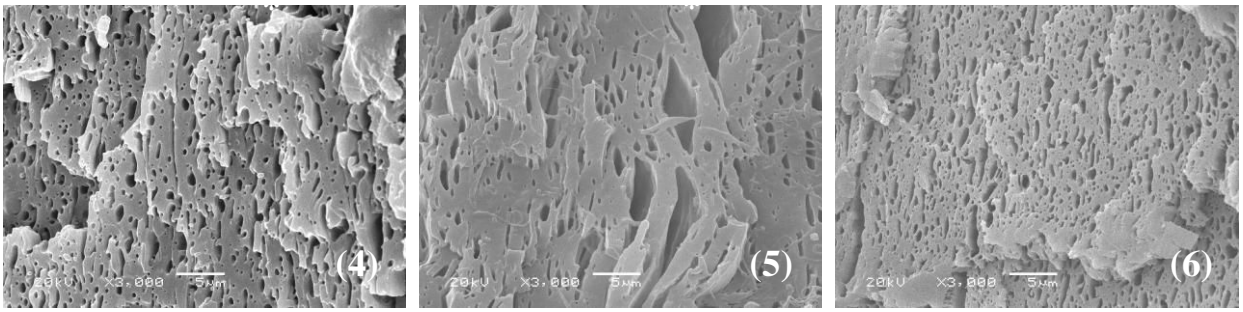

Skin layer

Fig.5.15 SEM images of etched PC based blends (×3000)
(1) PP/PC (50/50); (2) PP/PC/EVA (50/50/5); (3) PP/PC/EVA/SEPS (50/50/5/5);
(4) PP/PC (50/50); (5) PP/PC/EVA (50/50/5); (6) PP/PC/EVA/SEPS (50/50/5/5)

5.3.3 Effect of EVA/SEPS on impact feature surface of PP/PC blend

As shown in Fig. 5.16, effects of EVA and EVA/SEPS on the morphologies of PP/PC blend couldn't be observed in the core layer of fracture surface with a low magnification. Increasing the magnification to 1500, it can be seen that PC particles are pulled out from matrix directly in the binary system. By addition of EVA, there are obvious fracture surfaces of PC. Addition of EVA/SEPA even makes the fracture surfaces of PC almost at the same level as PP. In the skin layer, by addition of EVA/SEPS, tough fracture surface can be observed even in the low magnification. Further increasing the magnification, we find out that PC particles are pulled out of matrix with smooth surface before compatibilizing. PC and PP deformed together during the impact process because of the strong interaction in the EVA/SEPS compatibilized system, and it's difficult to separate two phases.

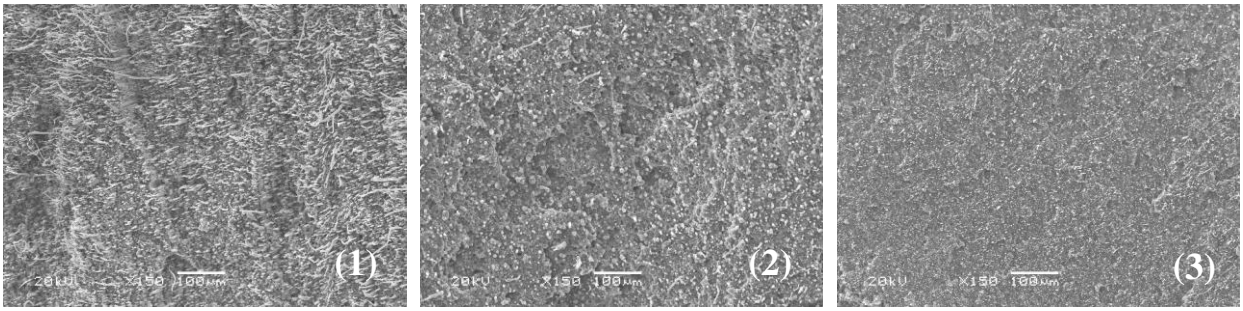

Core layer ×150

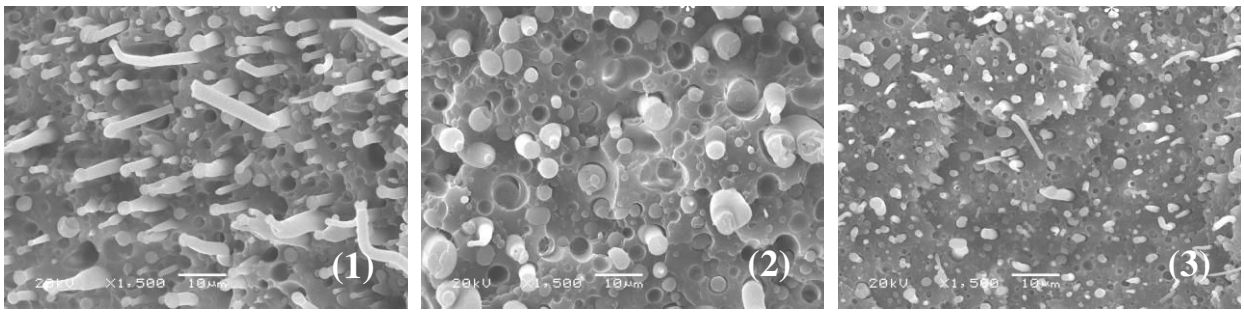

Core layer ×1500

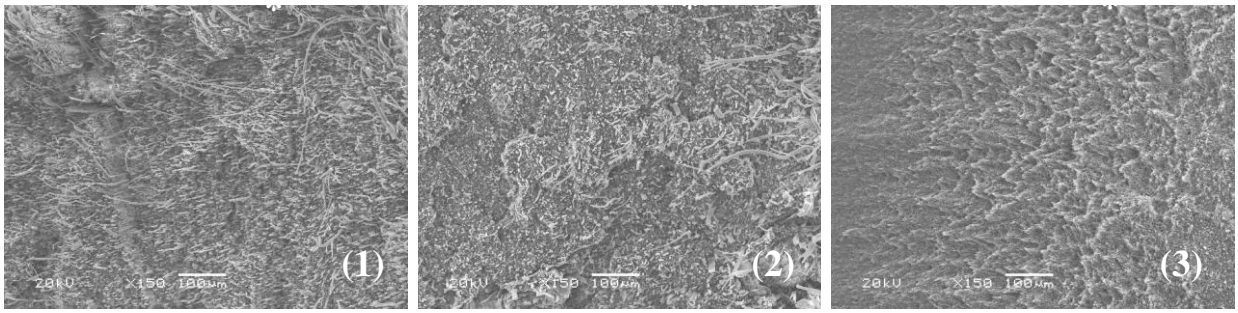

Skin layer ×150

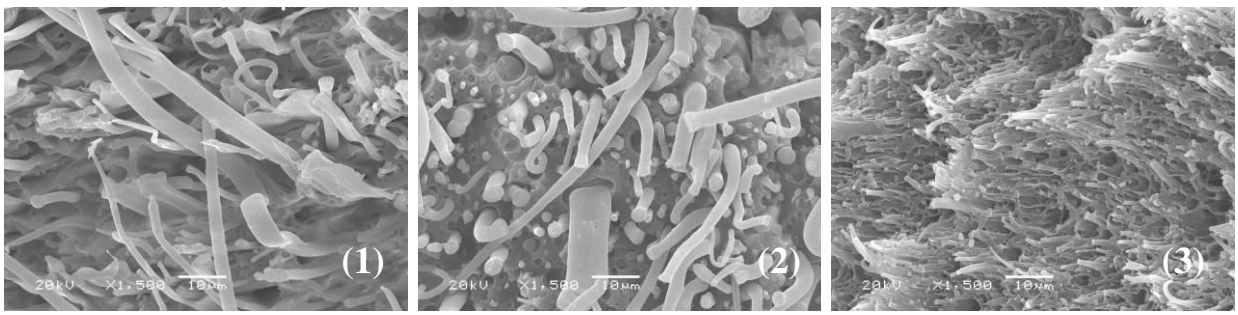

Skin layer ×1500

Fig.5.16 SEM images of impact fracturing surface of PP blends.
(1) PP/PC (50/50); (2) PP/PC/EVA (50/50/5); (3) PP/PC/EVA/SEPS (50/50/5/5);

5.4 Conclusion

POE was applied to toughen PP/PC, and SEPS with as high as 60wt%content of PS block was applied as the compatibilizer of PP/PC/POE in chapter 5. The compatibilized PP based blends represented remarkable improvement in impact strength and balanced tensile

strength. SEPS can't toughen PP but showed a remarkable compatibilizing effect. A new absorption peak of blend appeared in the DMA curve by addition of SEPS, and the peak temperature of the new transition was a little lower than that of neat SEPS. More SEPS added, more close to the transition temperature of SEPS, and the transition temperature of other components of the blend was slightly affected, which showed that the compatibilizing effect was achieved by PP/PC phase moving into SEPS compatibilizing phase during blending. By addition of SEPS, crystallizing point of blends increased, crystal size decreased, the interface became diffusing, melting range became wider and the crystallinity decreased. The method of secondary processing by pre-blending of PP and PC can reduce the apparent viscosity of PC and led to matched viscosity of each component in the blend and more encapsulated structure, and further improved mechanical properties of the blends.

Without compatibilizing, the content of POE was low in the skin layer of blend, and PC particles with big size non-uniformly dispersed in the matrix. In the core layer, etched POE left big cavities. PC particles with spherical shape and big size had weak interaction with PP. Morphologies of blends showed a decreasing and much more homogeneous size of dispersed PC and POE particles through addition of SEPS. The content of POE became high in the skin layer of blend, spherical particles changed into stick shaped particles, and the number of the encapsulated structure of PC by SEPS increased. Co-continuous structure appeared with the high concentration of PC and SEBS. In the lower loading of POE blend, the interval distance (ID) between rubber particles was bigger than the critical value of ID (ID_c) and the system presented brittle fracture. Brittle-tough transition occurred with increasing of POE which reduced the interval distance, and the transition occurred earlier by addition of SEPS. The impact fracture surfaces of the skin and core layer of PP/PC binary blend represent typical mosaic shape, and then it changed into mixture of mosaic and striation, finally totally covered with striation with increasing SEPS.

EVA with similar ester group with PC and aliphatic chain with PP was further selected to compatibilize PP/PC blend. EVA/SEPS compound compatibilizer improved the elongation at break of blend obviously. A decreasing and much more homogeneous size of dispersed PC and POE particles through addition of EVA/SEPS was observed in the morphology of blends. The strong interface bonding made the fracture of PP and PC at the same time which contributed to the toughness of blends.

Chapter 6 Molecular simulation on relationship between composition and microscopic structure of PP/PC blend

6.1 Introduction

With the development of the hardware and software, molecular simulations become the most important tools to predict blend compatibility of polymers and structure-property relationship of polyblends. In this study, the blend compatibility of PP with PC was studied over the whole range of composition allowed by the atomistic and mesoscopic simulation methods. Simulation results were further supported by mechanical properties of blends. From the mesoscopic simulation, effects of compatibilizer SEBS on morphologies of PP/PC blend were constructed, which showed the trends similar to those experimentally measured by SEM in Chapter 4.

6.2 Molecular dynamic simulations of PP/PC blend

The results of molecular dynamic simulations on PP/PC blend were used to investigate Flory-Huggins interactions between PP and PC at the molecular level, but due to space limitations of data storage of computer, simulations couldn't be performed using the actual size of polymer. The size of the macromolecule used in the simulations is important to calculate thermodynamic parameters of interest and, hence, it would be appropriate to understand what minimum molecular size is sufficient to represent the real polymer chain.

To determine this minimum size, solubility parameters of PP and PC at different repeating units, namely, different molecular weight were computed up to a point when increasing the polymer molecular weight won't change the value of the solubility parameters. As displayed in Fig 6.1, the solubility parameters of PP levels off as the number of repeating units of PP increases more than 30. For PC, the minimum number of repeating units is 10. Data of corresponding molecular weight and solubility parameters are given in Table 6.1.

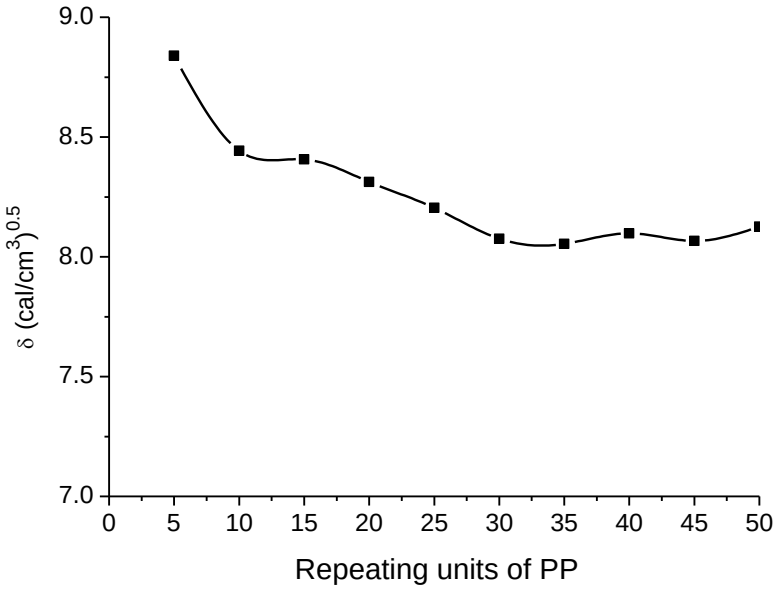

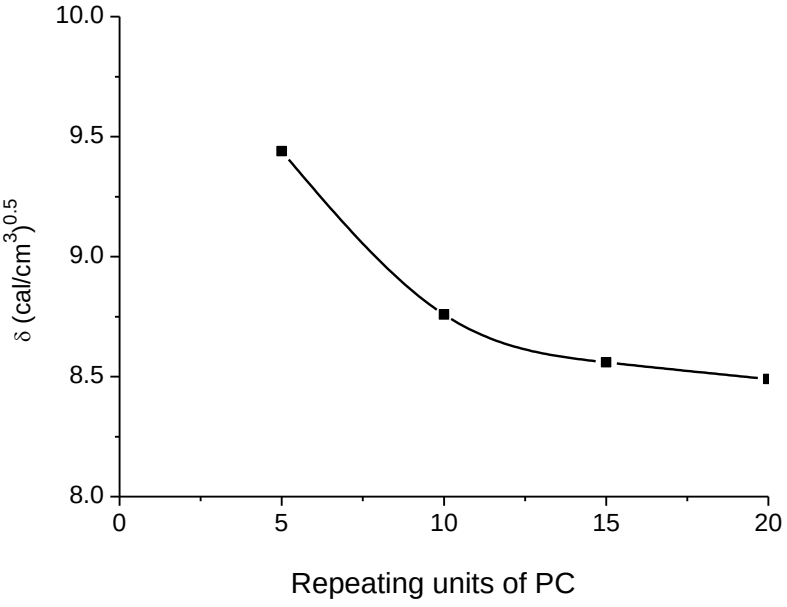

Fig.6.1 Dependence of solubility parameters (δ) of PP and PC on the number of repeating units

Table 6.1 Solubility parameters of PP and PC

Polymer	Repeating Units	Molecular Weight	Solubility Parameters $(cal/cm^3)^{0.5}$
PP	30	1260	8.07
PC	10	2540	8.76

The detailed model construction procedure of PP/PC blends is established by different

ratios of the number of chains of PP to the number of chains of PC in the unit simulation cell. The number of chains per unit cell, composition, and density are summarized in Table 6.2.

Table 6.2 Simulation details of PP/PC blends

Number of chains per unit cell	Composition (wt% PC)	Density (g/cm^3)	Molar volumn (cm^3/mol)
1 PP chain	0	0.9	1400
1 PC chain	100	1.2	2116
9 PP chain, 1 PC chain	18	0.93	1492
7 PP chain, 3 PC chain	46	0.99	1661
5 PP chain, 5 PC chain	69	1.05	1810
3 PP chain, 7 PC chain	82	1.11	1942
1 PP chain, 9 PC chain	95	1.17	2062

A typical snapshot unit cell for the PP/PC=54/46 (weight ratio) blend is shown in Fig 6.2 which contains 2900 atoms. The carbon atoms are gray, hydrogen, white, and oxygen, red. The original configuration must be minimized after construction because of the high level of energy.

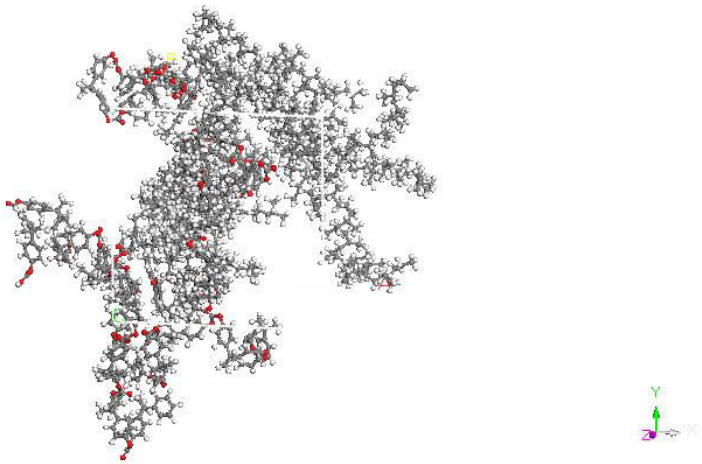

Fig.6.2 Snapshot of the amorphous unit cell for a 54:46 blend of PP/PC

Flory-Huggins interaction parameter χ is given by:

$$\chi = \frac{z\Delta E_{mix}}{RT} \tag{6.1}$$

Where z is a coordination number, the value of which for the cubic lattice model is taken as 6, R is the molar gas constant (8.314J/mol•K), and T is the temperature in Kelvin,

at which simulation was performed. The energy of mixing, ΔE_{mix}, needed to compute χ was caiculated as:

$$\Delta E_{mix} = \phi_A (\frac{E_{coh}}{V})_A + \phi_B (\frac{E_{coh}}{V})_B - (\frac{E_{coh}}{V})_{mix} \quad (6.3)$$

Where subscripts A, B, and mix represent CED values of PP, PC, and their blend, respectively. Φ_A and Φ_B represent the volume fractions of PP and PC, respectively. To understand whether PP and PC are miscible or immiscible, the critical value of χ is also calculated by the following equation:

$$(\chi_{AB})_{critical} = \frac{1}{2}(\frac{1}{\sqrt{m_A}} + \frac{1}{\sqrt{m_B}})^2 \quad (6.4)$$

Where m_A and m_B are the degree of polymerization of A and B. Blends are miscible if $\chi < \chi_{critical}$. If χ is slightly greater than $\chi_{critical}$, the blends are partially miscible. If χ is considerably greater than $\chi_{critical}$, then the component polymers are totally immiscible. As shown in Fig. 6.3, $\chi_{critical}$ is 0.1244, which is indeed the line of demarcation for the blend to be treated as miscible, and PP/PC blends are immiscible in the whole range of weight fraction of PC. Further insight into the figure, it can be concluded the blend with 5% PP is in comparatively better compatibility.

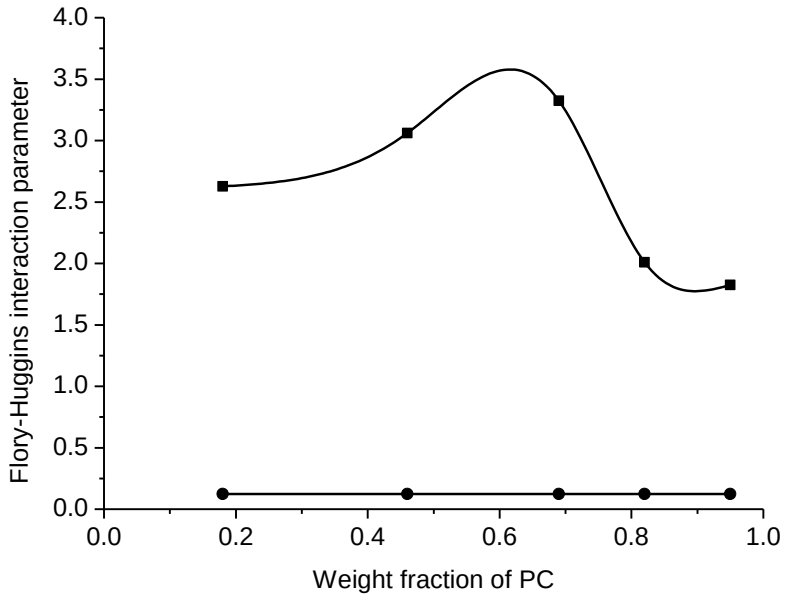

Fig.6.3 Flory-Huggins interaction parameters versus weight fraction of PP

The structure factor S(q,t) which effected by the crystal structure could be calculated through the X-ray, visible light or neutron scattering. q is the scattering vector equal to $(4\pi/\lambda)\sin(\theta/2)$, where λ and θ are the wavelength of light and scattering angle respectively, at regular time intervals [98]. Intensity can be plotted versus q as shown in Fig. 6.4 for PP/PC blends with different weight ratio. It is observed that the intensity of blends is higher for more immiscible systems (PP/PC=82/18; PP/PC=54/46; PP/PC=31/69) and lower for less immiscible systems (PP/PC=18/82; PP/PC=5/95). It is also observed that the maximum peak is moved toward bigger q with the increase of concentration of PC, which indicates lower peaks at the beginning due to thermal fluctuations.

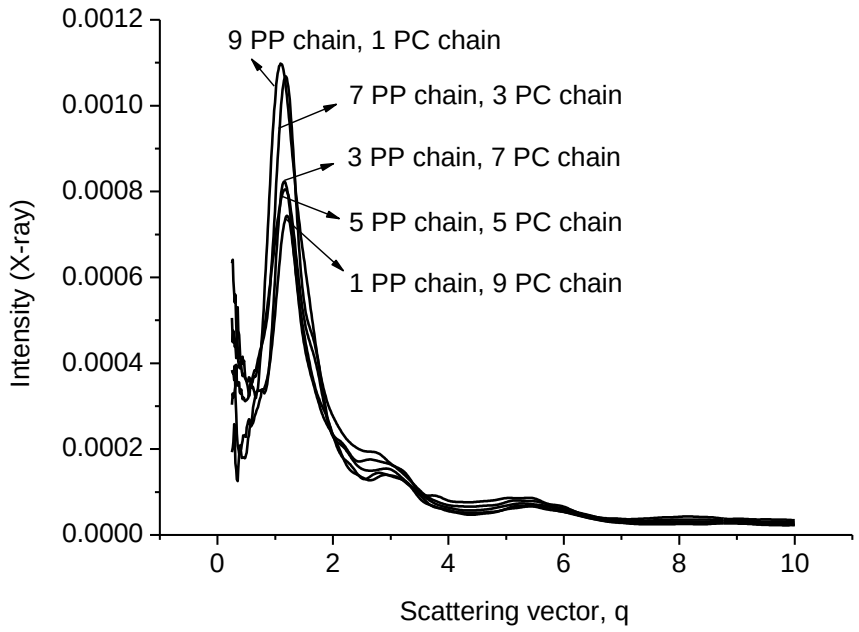

Fig.6.4 Intensity versus scattering vector plots for PP/PC blends

6.3 Mesoscopic dynamic simulations of PP/PC blend

The polymer chain lengths could be determined from the degree of polymerization and characteristic ratios of the polymers. The expression for Mesodyn chain length (N_{meso}) is given by:

$$N_{Meso} = \frac{M_p}{M_m C_n} \tag{6.5}$$

Where M_p is the polymer molecular weight, M_m is the monomer molecular weight, and C_n is the characteristic ratio ($(C_n)_{PP}$=6.9 , $(C_n)_{PC}$=2.4) [99]. The Mesodyn input parameter is related to the Flory-Huggins interaction parameter χ_{ij} through the equation:

$$\upsilon^{-1} \in_{ij} = \chi_{ij} RT \tag{6.6}$$

Where the χ_{ij} is taken from the atomistic simulation carried out for each blend at each composition, R is the molar gas constant, and T is taken to be 298K. To analyze the effects of composition of blend on its mesoscopic morphology, PP/PC binary blend with different weight ratio were investigated in detail. Fig 6.5 shows the morphologies of the blends and the corresponding iso-density surfaces of PC after 1×10^3 time steps Mesodyn simulation from random initial configuration. PC particles disperse in the PP matrix as spherical shape at a lower loading of PC. As the concentration of PC increases to 46%, phase size of PC increases and bicontinuous phase appears. At 69% concentration of PC, the bicontinuous phase of blend is more perfect. When the concentration of PC reaches at 82%, reversal of phase happens, and PP disperses in PC matrix as spherical shape. As the concentration of PC increases to 95%, phase size of PP particles decreases.

Compared with the results of mechanical properties tests shown in Fig 6.6, the appearance of co-continuous structure obtained from simulation corresponded to the transition point of impact strength and tensile strength. Before transition, the mechanical properties of blends depend on the properties of matrix PP because of the bad compatibility between PP and PC. After transition, the mechanical properties of blends depend on the properties of matrix PC, hence, the impact strength and tensile strength enhance obviously.

During the simulation step, free energy asymptotically approaches a stable value as the system attains dynamic equilibrium. However, the free energy density is not routinely calculated for real systems, and its direct comparison with experimental data is not possible. Even though, the evolution of free energy is a good measure of the stability of a system. The free energy density of blends decreases with the increase of simulation steps, and finally reaches at a stable stage. The systems of PP/PC=82/18 and PP/PC=5/95 experience a longer time to reach the equilibrium state, namely, a slower separation process. The systems of PP/PC=54/46、PP/PC=31/69 and PP/PC=18/82 with stronger immiscibility show the faster separation process.

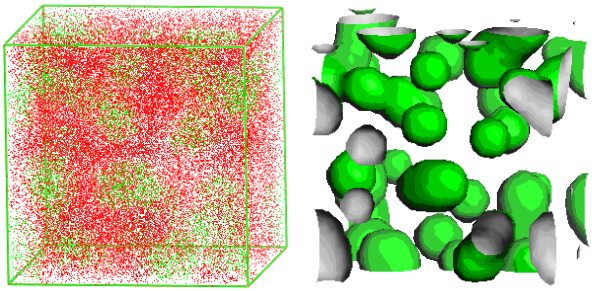

9 PP chain, 1 PC chain
PP/PC=82/18

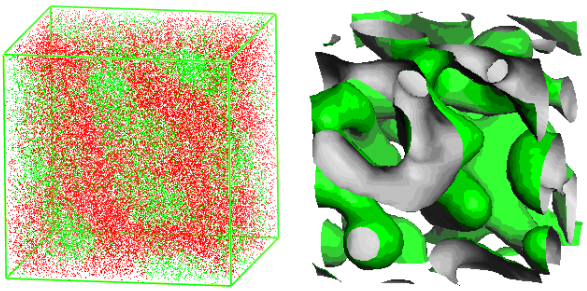

7 PP chain, 3 PC chain
PP/PC=54/46

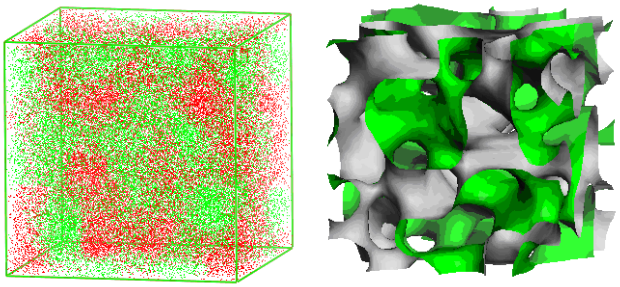

5 PP chain, 5 PC chain
PP/PC=31/69

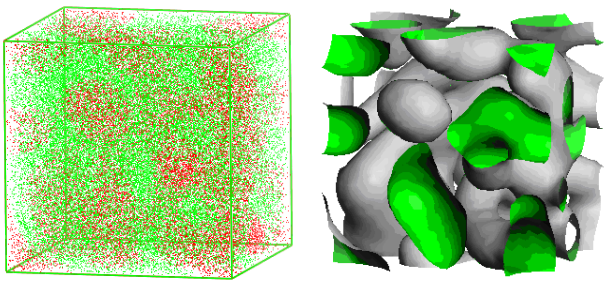

3 PP chain, 7 PC chain
PP/PC=18/82

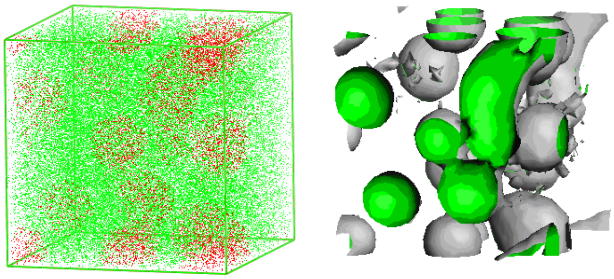

1 PP chain, 9 PC chain
PP/PC=5/95

Fig.6.5 Morphology of PP/PC blends (left) and iso-density surface of PC (right)
after 1×10^3 steps simulation from random initial configuration
The red and green beads represent PP and PC respectively

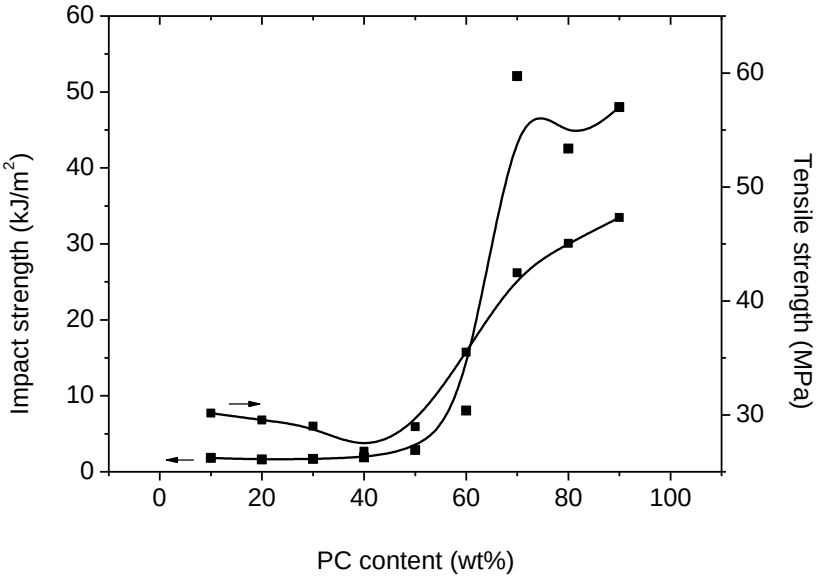

Fig.6.6 Impact strength and tensile strength of PP/PC binary blends

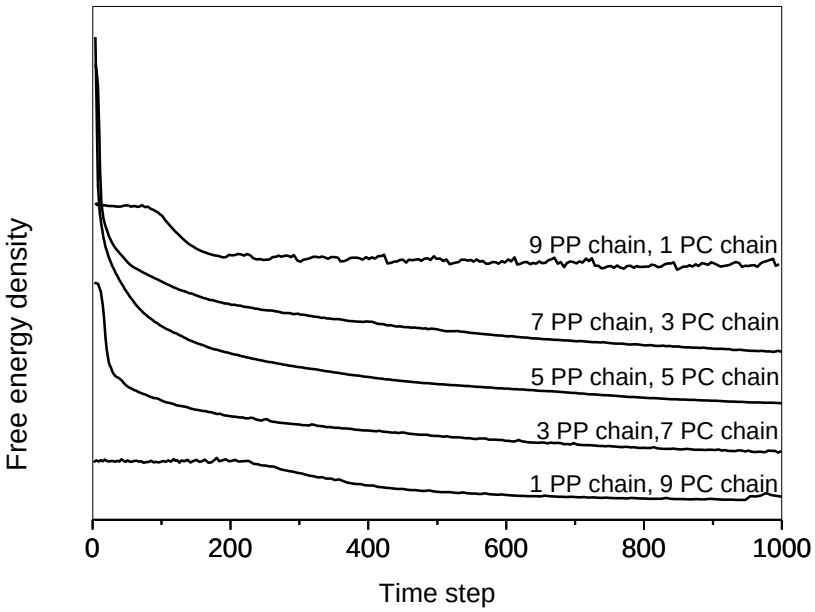

Fig.6.7 Plot of free energy density versus time step for PP/PC blends

The order parameter, P_i, defined as the volume average of difference between local density squared and the overall density squared, is given by the following integral:

$$P_i = \frac{1}{V}\int_v [\eta_i^2(r) - \eta_i^2]dr \qquad (6.7)$$

Where η_i is dimensionless density (volume fraction) for species i. As shown in Fig. 6.8,

the systems of PP/PC=54/46、PP/PC=31/69 and PP/PC=18/82 with larger value of order parameters indicates the strong phase segregation, more immiscibility and the faster separation process. The systems of PP/PC=82/18 and PP/PC=5/95 have the comparatively better compatibility and slower separation process, which is consistent with the results of free energy density.

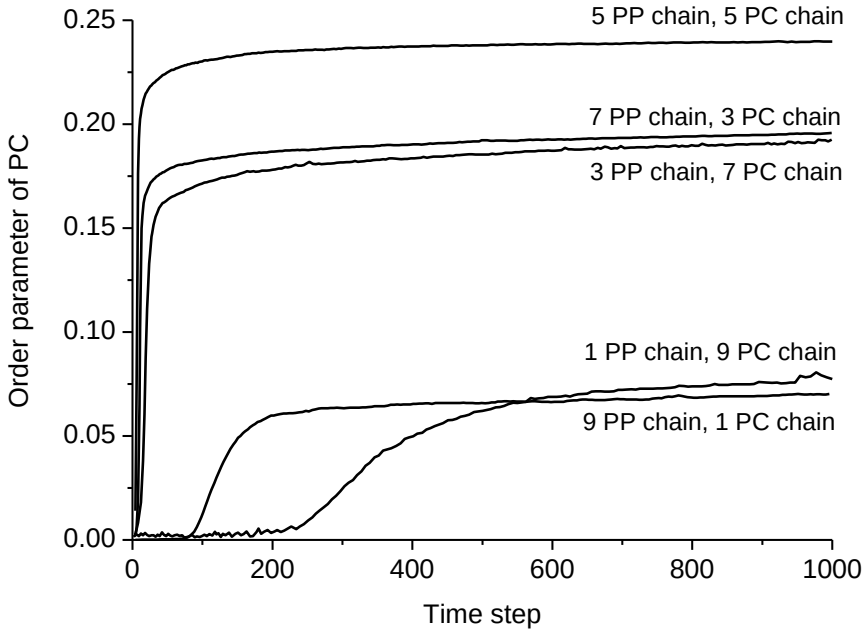

Fig.6.8 Mesophase order parameter of PC versus time step

The time evolution of the morphologies of PP/PC=54/46 blend was investigated as an example, and snapshots of the morphologies in the evolution process are shown in Fig. 6.9. The bicontinuous phase is developed from homogeneous initial configuration after 1×10^3 of simulation steps. With increasing of simulation steps, PC phase continues to grow and coarsen till 1×10^4 of simulation steps. Morphologies of blend finally developed into double-lamellar structure after 5×10^4 of simulation steps.

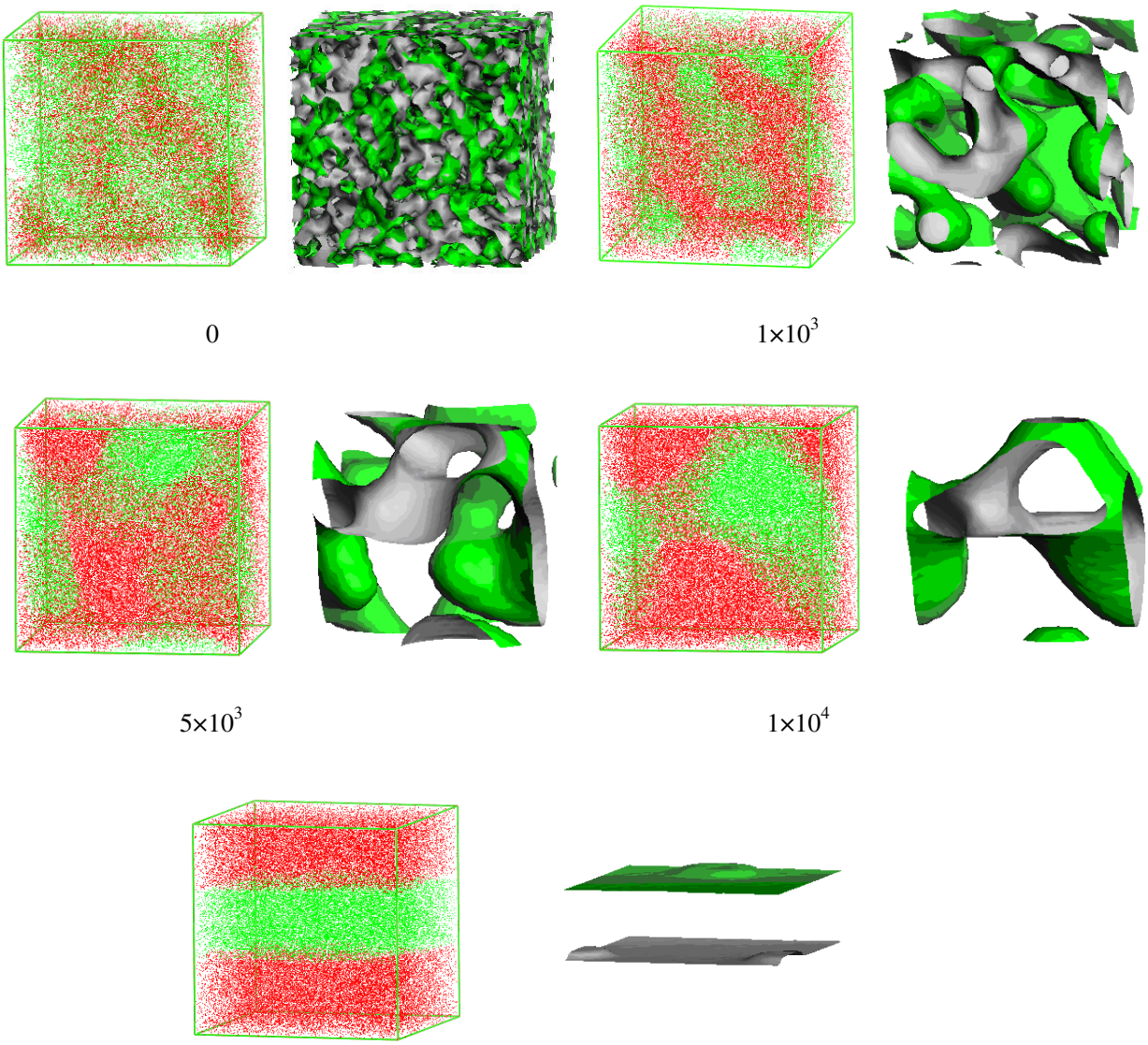

Fig.6.9 Time evolution of morphology of PP/PC=54/46 blends (left) and iso-density surface of PC (right) from random initial configuration
The red and green beads represent PP and PC respectively

6.4 Dynamic simulation of effect of SEBS on morphologies of PP/PC blend

SEBS is a triblock copolymer with polystyrene extremes and a copolymer of ethylene and butylene in the interior. The blocks are incompatible and phase separation is known to occur. The length of the individual blocks in SEBS varies from sample to sample, and we will assume block lengths at our convenience (N_{Meso}(PS)=10 ; N_{Meso}(EB)=10). The solubility parameters can be used to derive Flory-Huggins interaction values using:

$$\chi = \frac{V_{ref}(\delta_i - \delta_j)^2}{RT} \tag{6.8}$$

Where V_{ref} is a reference volume, taken to be the molar volume of one of the monomers (actually the mean volume of the two monomers). The calculated parameters used in the simulation are listed in Table 6.4.

Table 6.3 Simulation details of PP/PC/SEBS blends

Polymer	Van krecelen Solubility parameters $(J/cm^3)^{1/2}$	Molar Volume (cm^3/mol)
PP	16.06	49.04
PC	19.40	211.92
PS	19.52	96.98
EB	16.49	48.89

Table 6.4 χ_{ij}RT between Polymer i and j

Species	PP	PC	PS	EB
PP	0	1.456	0.867	0
PC	1.445	0	0	1.104
PS	0.867	0	0	0.661
EB	0	1.104	0.661	0

Take morphology evolution of PP/PC=54/46 blend as an example. Addition of SEBS slows down the separation of PP/PC blend. Bicontinuous phase is developed from homogeneous initial configuration after 1×10^3 of simulation steps. With increasing of simulation steps, PC phase continues to grow and coarsen till 1×10^4 of simulation steps. Morphologies of blend finally developed into a imperfect double-lamellar structure after 5×10^4 of simulation steps. The compatibilizer prefers to locate in the interface of PP and PC, and the structure of PC encapsulated by SEBS is consistent with the results of SEM images discussed in chapter 4.

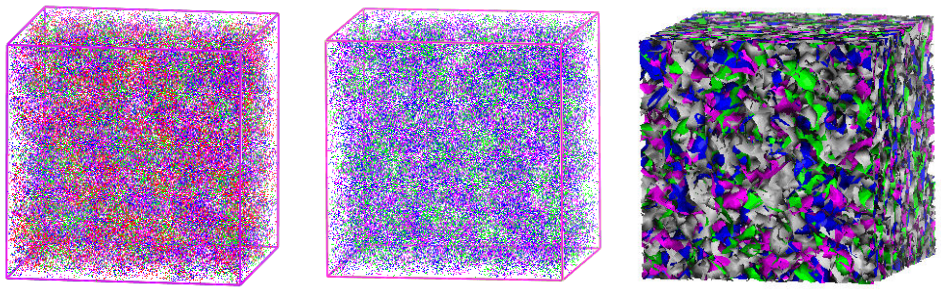

0

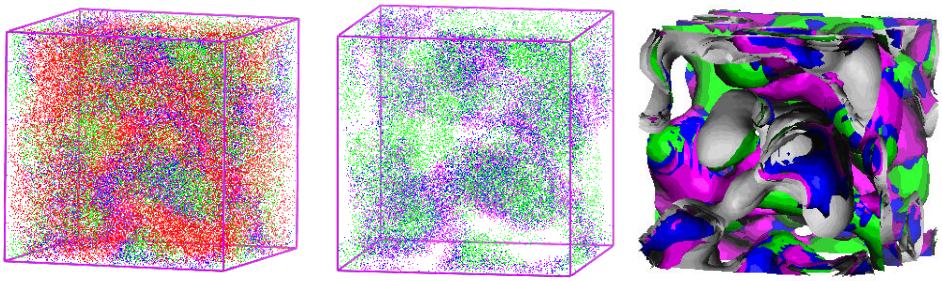

1×10^{3}

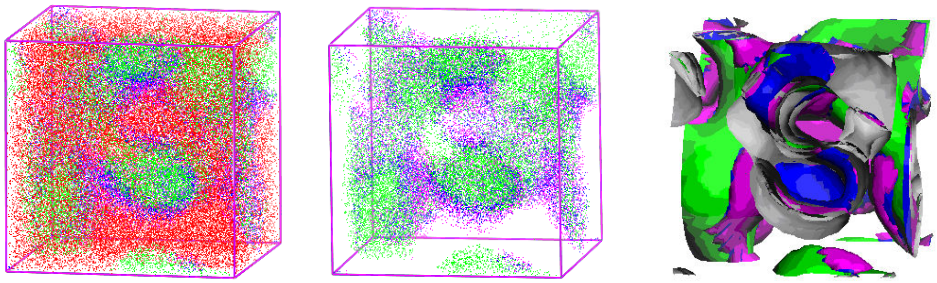

5×10^{3}

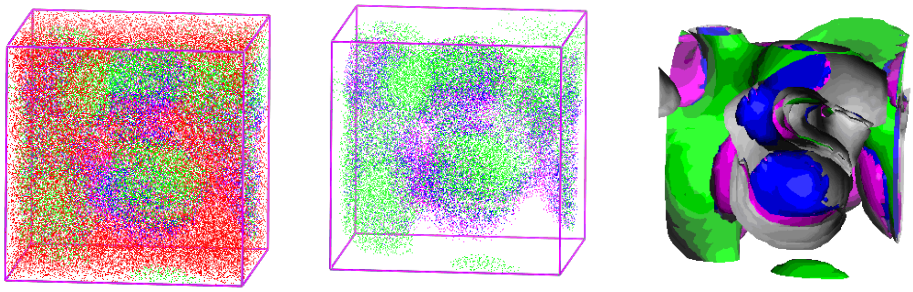

1×10^{4}

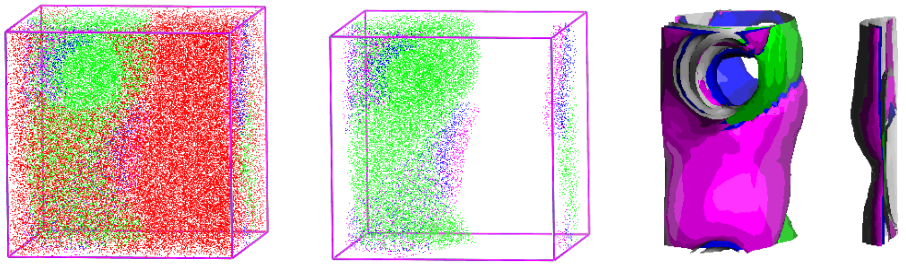

5×10^4

Fig.6.10 Time evolution of morphology of PP/PC/SEBS blends (left、middle) and iso-density surface of PC and SEBS (right)from random initial configuration
The red, green, blue and pink beads represent PP, PC, PS block and EB block respectively

Varying the content of PS block in SEBS from 36% to 63% (N_{Meso}(PS)=10, N_{Meso}(EB)=10 to N_{Meso}(PS)=10, N_{Meso}(EB)=30) has little effect on the morphology of blend.

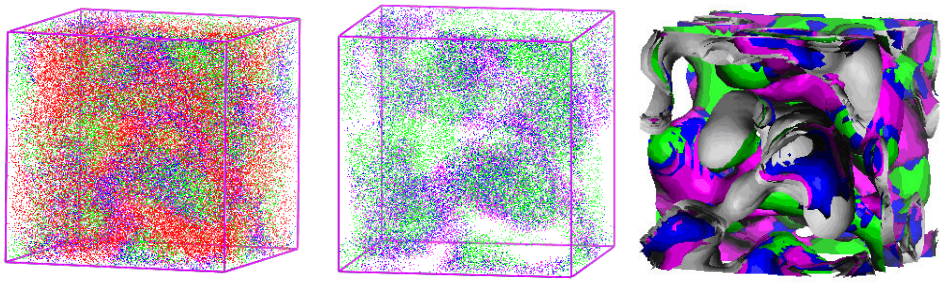

N_{Meso}(PS)=10； N_{Meso}(EB)=10

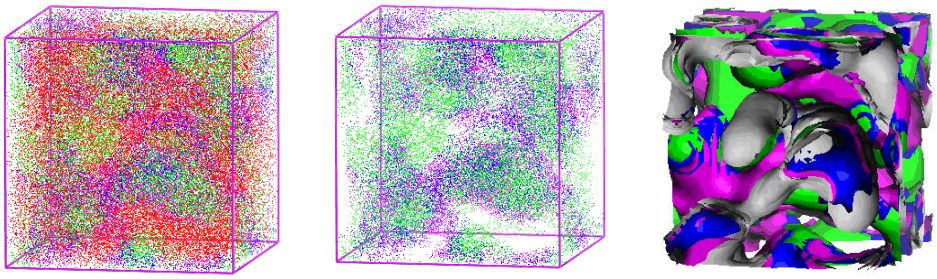

N_{Meso}(PS)=10； N_{Meso}(EB)=30

Fig.6.11 Morphology of PP/PC/SEBS blends (left、middle) and iso-density surface of PC and SEBS (right) after 1×10^3 steps simulation from random initial configuration
The red, green, blue and pink beads represent PP, PC, PS block and EB block respectively

The evolution of free energy and order parameter of compatibilized blends are shown in Fig. 6.12 and 6.13 respectively. Two systems with different content of PS block in SEBS have similar trends of evolution.

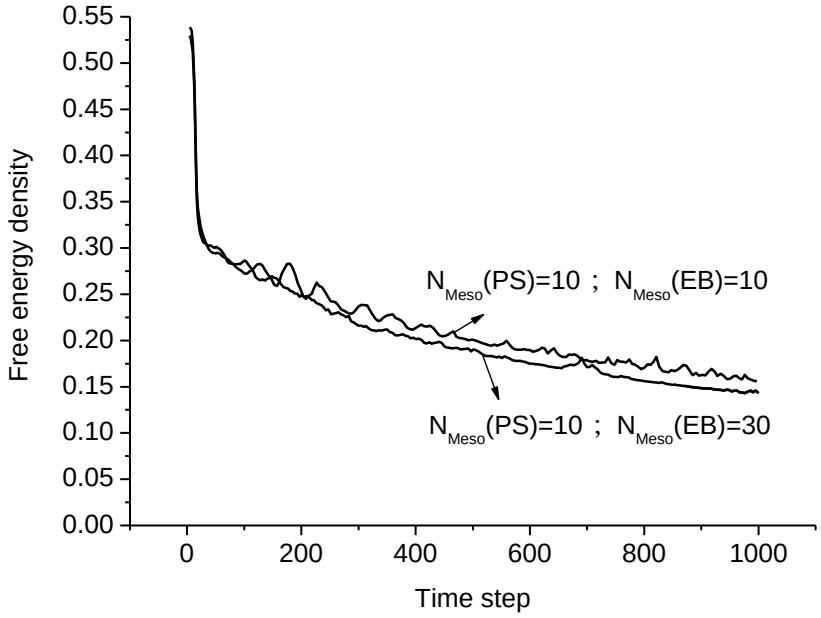

Fig.6.12 Plot of free energy density versus time step for PP/PC/SEBS blends

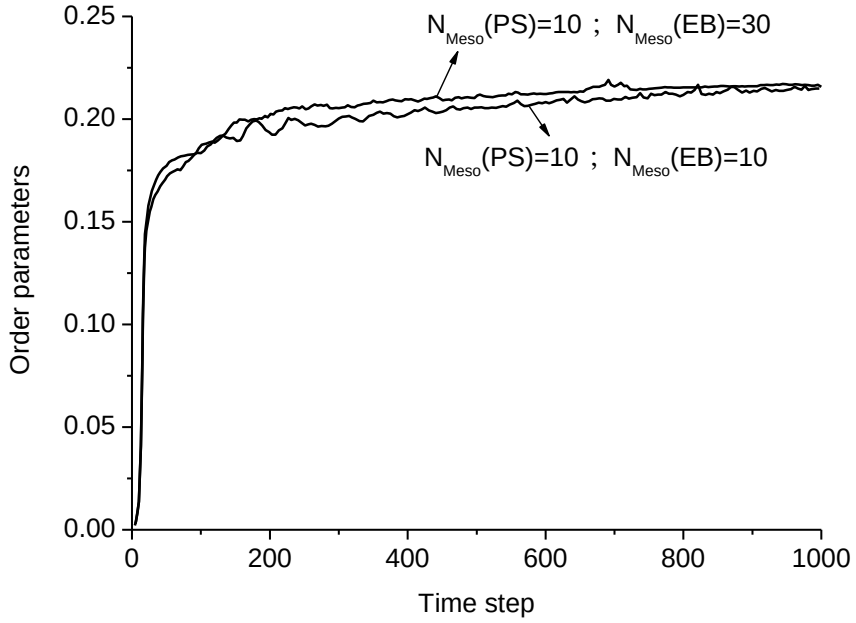

Fig.6.13 Mesophase order parameter of PC versus time step

6.5 Conclusion

Both molecular dynamics and mesodyn theories have been used to simulate the formation and evolution of morphology of PP/PC blends. Flory-Huggins interaction parameters between PP and PC with different weight ratio were always higher than the critical value, indicating poor compatibility between the two polymers. Integral structure factor of blend wasn't equal to zero, which indicated phase separations occurred in all the blend systems. PC as particles existed in PP matrix when the concentration of PC was low. Co-continuous structure appeared with the increase of PC concentration. Phase reversion occurred with further increasing PC, and PP as particles existed in the PC matrix. The size of PP reduced a bit when the concentration of PC continued to increase. Compared with the results of mechanical properties tests, the appearance of co-continuous structure obtained from simulation corresponded to the enhanced impact strength. The free energy density of blends decreased with the increase of simulation steps, and finally drove to a stable stage. The systems of PP/PC=82/18 and PP/PC=5/95 reached the equilibrium state after a longer time. The systems of PP/PC=54/46、PP/PC=31/69 and PP/PC=18/82 with larger value of order parameters showed the stronger immiscibility and the faster separation process. The systems of PP/PC=82/18 and PP/PC=5/95 had the comparatively better compatibility and slower separation process, which was consistent with the results of free energy density. Morphology of PP/PC=54/46 blend developed into double-lamellar structure after coarsening and growth of PC phase from homogeneous initial configuration of the blend with the increase of simulation steps. Addition of SEBS slowed down the separation of PP/PC blend. The compatibilizer existed in the interface of PP and PC, and encapsulated PC. Varying the content of PS block in SEBS had little effect on the morphology of blend.

Chapter 7 Conclusion

PP is one of the most widely used polymers. However, it exhibits low impact strength which limits its application potential greatly. Based on a so-called "rigid–rigid polymer toughening" concept, PC with high strength and toughness were blended to PP in this study, in order to improve the toughness of the latter while retaining as much as possible its rigidity. PC and PP are immiscible because of disparities in polarity and solubility parameters. Furthermore, high viscosity ratio of this polymer pair leads to the poor dispersion of PC in PP matrix. Therefore, it is very important to find an additive that act as an effective compatibilizer and reducing the viscosity of PC effectively.

Through molecular designing, PP are prepared by grafting different chemical components like BPA, GMA, St, 2A and HEDA. The composition, structure of grafted polymers and the grafting reaction were studied in terms of FTIR, GPC, degree of grafting and torque analysis. The mechanical properties, especially the tensile strength of PP based blends were improved with the use of these compatibilizers. PP/PC/PP-g-BPA ternary blend exhibited the best combination mechanical properties. With increasing PP-g-BPA, the T_g peaks of PP and PC shifting inside of their respective original T_g suggested partial miscibility of the two polymers. PC as the heterogeneous nucleator resulted in the reduction of nucleation potential barrier, increasing of crystallizing temperature, amount of crystals, and decreasing of crystallinity, crystal size and crystallization time. The heterogeneous nucleation effect of PC was enhanced by addition of PP-g-BPA. Spherical or stick shape of PC particles dispersed in the matrix in big size non-uniformly. The addition of PP-g-BPA or PP-g-HEDA resulted in decreasing and much more homogeneous size of the dispersed PC particles. The particle size was reduced to 289nm from 635nm by addition of PP-g-HEDA.

SEBS with both compatibilizing and toughening effect was applied to modify PP/PC blend. Certain content of PC can improve both notched impact strength and tensile strength of blends, but too high content of PC led to serious phase separation. High content of SEBS represented more obvious compatibilizing effect but decreased the efficiency of forming cavity due to the accumulation of molecules. PP blended with 25 wt% SEBS and 20 wt% PC can reach 21 MPa of tensile strength and 70 KJ/m^2 of impact strength respectively. By addition of SEBS, the two T_gs of PP and PC phase shifting inside of their respective original T_g suggested partial miscibility of the two polymers. Besides, crystallinity, crystallizing point and melting point decreased due to the formation of the encapsulated structure of PC by SEBS. Addition of PP-g-BPA into PP/PC/SEBS blend further enhanced

the compatibilizing effect and heterogeneous nucleation of PC. Compared with PP/PC blend, much more finely dispersed PC phase can be observed after adding SEBS , the interface became diffusing and some of PC particles are encapsulated by SEBS which reduced the contact between PP and PC. Addition of PP-g-BPA into PP/PC/SEBS blend further decreased the size of PC particles and improved the dispersion.

PC particles in skin layer deformed into stick shape because of the high shearing force during injection processing. With increasing SEBS content, the fracture surfaces of blends in the skin layer changed from mosaic fracture into mixture of mosaic and striation, finally total striation, and the interaction between PP and PC was enhanced during the evolution. The evolutions in core layer are similar with the process mentioned above except the initial shape which is spherulite in core layer. Both J_{IC} and E_m were improved in PP/PC/SEBS blend compared with PP/PC blend, indicating that SEBS improved not only the crack initiation resistance but also crack propagation resistance.

POE was applied to toughen PP/PC and SEPS with as high as 60wt% content of PS block was applied as the compatibilizer of PP/PC/POE blend. Addition of SEPS leads to remarkable improvement in impact strength and balanced tensile strength. The experimental results of DMA showed that the compatibilizing effect was achieved by PP, PC and POE phases moving into SEPS compatibilizing phase during blending. After compatibilizing, crystallizing point of blends increased, crystal size decreased, the interface became diffusing, melting range became wider and the crystallinity decreased. A pre-blending of SEPS and PC can reduce the apparent viscosity of PC and led to matched viscosity of each component in the blend and more encapsulated structure, and then further improved mechanical properties of the blends.

Without compatibilizing, the content of POE was low in the skin layer of blend, and PC particles with big size non-uniformly dispersed in the matrix. In the core layer, etched POE left big cavities. PC particles with spherical shape and big size had weak interaction with PP. Morphologies of blends showed a decreasing and much more homogeneous size of dispersed PC and POE particles through addition of SEPS. The content of POE became high in the skin layer of blend, spherical particles changed into stick shaped particles, and the number of the encapsulated structure of PC by SEPS increased. Co-continuous structure appeared with the high concentration of PC and SEBS. In the lower loading of POE blend, the interval distance (ID) between rubber particles was bigger than the critical value of ID (ID_c) and the system presented brittle fracture. Brittle-tough transition occurred with

increasing of POE which reduced the interval distance, and the transition occurred earlier by addition of SEPS. The impact fracture surfaces of the skin and core layer of PP/PC binary blend represent typical mosaic shape, and then it changed into mixture of mosaic and striation, finally totally covered with striation with increasing SEPS.

EVA with similar ester group with PC and aliphatic chain with PP was further selected to compatibilize PP/PC blend. EVA/SEPS compound compatibilizer improved the elongation at break of blend obviously. A decreasing and much more homogeneous size of dispersed PC and POE particles through addition of EVA/SEPS was observed in the morphology of blends. The strong interface bonding made the fracture of PP and PC at the same time which contributed to the toughness of blends.

Simulations based on molecular dynamics and mesodyn theories have been used to study the formation and morphology evolution of PP/PC blends. Flory-Huggins interaction parameters between PP and PC with different weight ratio were always higher than the critical value, indicating poor compatibility between the two polymers. Integral structure factor of blend wasn't equal to zero, which indicated phase separations occurred in all the blend systems. PC as particles existed in PP matrix when the concentration of PC was low. Co-continuous structure appeared with the increase of PC concentration. Phase reversion occurred with further increasing PC, and PP as particles existed in the PC matrix. The size of PP reduced a bit when the concentration of PC continued to increase. Compared with the results of mechanical properties tests, the appearance of co-continuous structure obtained from simulation corresponded to the enhanced impact strength. The free energy density of blends decreased with the increase of simulation steps, and finally drove to a stable stage. The systems of PP/PC=82/18 and PP/PC=5/95 reached the equilibrium state after a longer time. The systems of PP/PC=54/46、PP/PC=31/69 and PP/PC=18/82 with larger value of order parameters showed the stronger immiscibility and the faster separation process. The systems of PP/PC=82/18 and PP/PC=5/95 had the comparatively better compatibility and slower separation process, which was consistent with the results of free energy density. Morphology of PP/PC=54/46 blend developed into double-lamellar structure after coarsening and growth of PC phase from homogeneous initial configuration of the blend with the increase of simulation steps. Addition of SEBS slowed down the separation of PP/PC blend. The compatibilizer existed in the interface of PP and PC, and encapsulated PC. Varying the content of PS block in SEBS had little effect on the morphology of blend.

Acknowledgements

First and foremost I would like to express my best gratitude to my supervisors Prof. Guo-hua HU, and Prof. Lin YE. Their creative ideas of research, patient guidance and consistent encouragement push and inspire me to finish my PhD study. I also would like to express my great appreciation to Prof. Sandrine HOPPE and Prof. Huilin LI for providing much help and suggestions during my PhD study.

I am greatly thankful to my mates both in Chinese and French groups, Xiao-Wen ZHAO, Kai ZENG, Xian-Yu LI, Xiao-He LI, Lu GAN, Peng-Fei LIU, Jie WANG, Kai-Long WANG, Cai-Liang ZHANG, Yuan FANG, Christian PENU, Jean-Marie BOISSIERE, Sara RONASI, Ahmed BHRAN, who kindly helped me a lot during my PhD study. Thanks are also due to my friends Li ZHOU, Chun LIU, Ming XIAO, Si LIANG, Gui-Fang Shan, Man LUO, Xiao-Bo SONG, Tao-Tao FU and Jing-Xia LI who have great contributions to my wonderful life both in China and France.

This study couldn't been finished without the generous financial support from the National Basic Research Program of China (2005CB623800) and Program for Changjiang Scholars and Innovative Research Team in University (IRT0449).Thank China Scholarship Council for supporting my studying in France. Finally, I would like to express my great appreciation to my parents for their understanding and encouragement which support me to finish my PhD study.

References

[1] Srinivasan, K. R.; Gupta, A. K. J Appl Polym Sci 1994, 53, 1-17.

[2] Borggreve, R. J. M.; Gaymans, R. J.; Schuijer, J.; Ingen, H. J. F. Polymer 1987, 28, 1489-1496.

[3] Yang, H.; Zhang, X. Q.; Qu, C. Polymer 2007, 48, 860-869.

[4] Yang, J. H.; Zhang, Y.; Zhang, Y. X. Polymer 2003, 44, 5047-5052.

[5] Bai, S. L.; Wang, G. T.; Hiver, J. M.; Gsell, C. Polymer 2004, 45, 3063-3071.

[6] Chang, S. Q.; Xie, T. X.; Yang, G. S. J Appl Polym Sci 2006, 102, 5184-5190.

[7] Sung, Y. T.; Han, M. S.; Song, H. K.; Jung, J. W.; Lee, H. S.; Kum, C. K. Polymer 2006, 47, 4434-4439.

[8] Sahnoune, F.; Lopez, C. J. M.; Crespy, A. Polym Eng Sci 2003, 43, 647-660.

[9] Wilkinson, A. N.; Clemens, M. L.; Harding, V. M. Polymer 2004, 45, 5239-5249.

[10] Wei, G. X.; Sue, H. J.; Chu, J.; Huang, C.; Gong, K. Polymer 2000, 41, 2947-2960.

[11] Yang, H.; Zhang, Q.; Guo, M.; Wang, C.; Du, R. N.; Fu, Q. Polymer 2006, 47, 2106-2115.

[12] Zhang, L.; Li, C. Z.; Huang, R. J Polym Sci Part B: Polym Phys 2005, 43, 1113-1123.

[13] Fisher, I.; Siegmann, A.; Narkis, M. Polym Compos 2002, 23, 34-48.

[14] Lach, R.; Schneider, K.; Weidisch, R.; Janke, A.; Knoll, K. Eur Polym J 2005, 41, 383-392.

[15] Jannerfeldt, G.; Boogh, L.; Manson, J. A. E. J Polym Sci Part B: Polym Phys 1999, 37, 2069-2077.

[16] Machado, A. V.; Duin, M. V.; Covas, J. A. J Polym Sci Part A: Polym Chem 2000, 38, 3919-3932.

[17] Liu, X. H.; Wu, Q. J.; Berglund, L. A.; Fan, J. Q.; Qi, Z. N. Polymer 2001, 42, 8235-8239.

[18] Brandrup J. ; Immergut H. I.; Grulke E. A., Polymer Handbook, Weley, New York, 1999

[19] Retsos, H.; Anastasiadis, S. H.; Pispas, S.; Mays, J. W.; Hadjichristidis, N. Macromolecules 2004, 37: 524-537.

[20] Cigana, P.; Favis, B. D.; Jerome, R. Journal of Polymer Science Part B: Polymer Physics 1996, 34: 1691-1700.

[21] Edgecombe, B. D.; Stein, J. A.; Fréchet, J. M. J.; Xu, Z.; Kramer, E. J. Macromolecules 1998, 31: 1292-1304.

[22] Cigana, P.; Favis, B. D. Polymer 1998; 39: 3373-3378.

[23] Jannasch, P.; Hassander, H.; Wesslén, B. Journal of Polymer Science Part B: Polymer Physics 1996, 34: 1289.

[24] Hong, B. K.; Jo, W. H. Polymer 2004, 41: 2069-2079.

[25] Starý, Z.; Fortelný, I.; Kruliš, Z.; Šlouf, M. Journal of applied polymer science 2008, 107: 174-186.

[26] Kvist, L.; Bertilsson, H.; Meuller, P. Polymer Engineering and Science 1998, 38: 1303-1312.

[27] Adedeji, A.; Hudson, S. D.; Jamieson, A. M. Macromolecules 1996, 29: 2449-2456.

[28] Vranješ, N.; Lednický, F.; Kotek, J.; Baldrian, J.; Rek, V.; Fortelný, I. Journal of Applied Polymer

Science 2008, 108: 466-472.

[29] Matos, M.; Favis, B. D.; Lomellini, P. Polymer 1995, 36: 3899-3907.

[30] Lyatskaya, Y.; Gersappe, D.; Gross, N. A.; Balazs, A. C. Journal of Physical Chemistry 1996, 100: 1449-1458.

[31] Lyatskaya, Y.; Jacobson, S. H.; Balazs, A. C. Macromolecules 1996, 29: 1059-1061.

[32] Bourry, D.; Favis, B. D. Journal of Polymer Science Part B: Polymer Physics 1998, 36: 1889-1899.

[33] Chio, W. M.; Park, O. O.; Lim, J. G. Journal of Applied Polymer Science 2004, 91: 3618-3626

[34] Yin, J. H.; Mo, Z. S. Polymer Physics, Publish of science, Beijing, 2001.

[35] Qiu, Z. M.; Wang, J. H.; Zhang, S. B.; Ding, M. X. polymer 2006, 47, 8444.

[36] Theodorou, D. N.; Suter, U. W. Macromolecules 1985, 18, 1467.

[37] Meirovitch, H. J. Chem. Phys. 1983, 79, 502.

[38] Rigby, D.; Sun, H., Eichinger, B. E. Polym. Int. 1997, 44, 311.

[39] Fraaije, J. G. E. M.; van Vlimmeren, B. A. C.; Maurits, N. M.; Postma, M.; Evers, O. A.; Hoffman, C.; Altevogt, P.; Goldbeck-Wood, G. J. Chem. Phys. 1997, 106, 4260.

[40] Fan, C. F.; Cagin, T.; Chen, Z. M.; Smith, K. A. Macromolecules 1994, 27, 2383.

[41] Brandrup, J.; Immergut, H. I.; Grulke, E. A. Polymer Handbook, Weley, New York, 1999.

[42] Jung, C. H.; Choi, J. H.; Lim, Y. M.; Jeun, J. P.; An, S. J.; Kang, P. H.; Nho, Y. C. Macromolecular symposia 2007, 249-250(1), 573.

[43] L. Cui, Y. Zhang, Y. X. Zhang. J Polym Sci Part B: Polym Phys. 2006, 44(22), 3288-3303

[44] W. X. Zhong, X. Y. Qiao, K. Sun, G. D. Zhang, X. D. Chen. J. App. Polym. Sci 2006, 99(5), 2558-2564

[45] N. C. Liu, W. E. Baker. Adv. in Polym. Tech. 1992, 11(4), 249-262

[46] Q. Wei, D. Chionna, M. Pracella. Macromolecular Chemistry and physics 2005, 206(7), 777-786

[47]X. Y. Yao, X. Y. Tian, D. H. Xie, X. Zhang, K. Zheng, J. Xu, G. Z. Zhang, P. Cui. Polym. 2009, 50(5), 1251-1256

[48] J. P. Deng, L. F. Wang, L. Y. Liu, W. T. Yang. Progress in Polymer Science 2009, 34(2), 156-193

[49] J. J. Robin, C. Boyer, B. Boutevin, C. Loubat. Polym. 2008, 49(21), 4519-4528

[50] Kusmono, Z. A. Mohd Ishak, W. S. Chow, T. Takeichi, Rochmadi. Euro. Polym. J. 2008, 44(4), 1023-1039

[51] Y. C. Ahn, D. R. Paul. Polym. 2006, 47(8), 2830-2838

[52] Q. Shi, L. C. Zhu, C. L. Cai, J. H. Yin, G. Costa. Polym. 2006, 47, 1979-1986

[53] Q. W. Lu, C. W. Macosko, J. Horrion. J Polym Sci Part A: Polym Chem 2005, 43, 4217;

[54]Q. W. Lu, T. R. Hoye, C. W. Macosko. Polym Sci Part A: Polym Chem 2002, 40, 2310;

[55]G. Kaupp, J. Schmeyers, J. Boy. Tetrahedron 2000, 56, 6899;

[56] Q. W. Lu, C. W. Macosko. Polym 2004, 45, 1981;

[57] F. P. Tseng, J. J. Lin, C. R. Tseng, F. C. Chang. Polym. 2001, 42, 713

[58] Kelar K, Jurkowski B. Polymer 2000; 41(3): 1055-1062.

[59] G. C. N. Lee, J. R. Pridon. Polym Eng Sci 1969, 9, 360;

[60] Yin ZH, Zhang YJ, Zhang XM, Yin JH. Polymer 1998; 39(3): 547-551.

[61] Shi AF, Gong YB. Engineering plastic handbook. Shanghai science and technology press; 2003.

[62] Tseng FP, Lin JJ, Tseng CR, Chang FC. Polymer 2001; 42(2): 713-725.

[63] Matjaz D, Vojko M, Ivan S. Composites part A: applied science and manufacturing 2005; 36(9): 1282–1290.

[64] Yang, J. H.; Zhang, Y.; Zhang, Y. X. Polymer 2003, 44, 5047-5052.

[65] Bai, S. L.; Wang, G. T.; Hiver, J. M.; Gsell, C. Polymer 2004, 45, 3063-3071.

[66] Matjaz, D.; Vojko, M.; Ivan, S. Composites Part A: applied science and manufacturing 2005, 36, 1282

[67] Vivek, T.; Richard, L.; Thomas, N. Polymer 2006, 47, 5392.

[68] Wong, S. C.; Mai, Y. W. Polymer 2000, 41, 5471.

[69] Xie, M. J.; Li, H. L. European Polymer Journal 2007, 43, 3480.

[70] Yin, Z. H.; Zhang, X. M.; Zhang, Y. J.; Yin, J. H. J appl polym sci 1997, 63, 1857.

[71] Everaert, V.; Aerts, L.; Groeninckx, G. Polymer 1999, 40, 6627-6644.

[72] Taylor G. I., Proc. R. Soc. London A, 1932, 138, 41

[73] Taylor G. I., Proc. R. Soc. London A, 1934, 146, 501

[74] Chesters A. K., Chem. Eng. Res. Des., 1991, 69, 259

[75] Janssen J., Dynamics of liquid-liqiud mixing, Eindhoven, 1993

[76] Grace H. P., Chem. Eng. Com., 1982, 14, 225

[77] Serpe G., Jarrin J., Dawans F., Polym. Eng. and Sci., 1990, 30, 533

[78] Bucknall, C. B.; Heather, P.; Lazzeri, A. J Mater Sci 1982, 24, 1489.

[79] Yee, A. F.; Li, D.; Li, X. J Master Sci 1993, 28, 6392.

[80] Parker, D. S.; Sue, H.; Huang, J.; Yee, A. F. Polymer 1990, 31, 2267.

[81] Kinloch, A. J.; Shaw, S. J.; Hunston, D. L. Polymer 1983, 24, 1341.

[82] Margolina, A.; Wu, S. H. Polymer 1988, 29, 2170.

[83] Wu, S. H. J Appl Polym Sci 1988, 35, 549.

[84] Wu, S. H. Polymer 1990, 31, 971.

[85] Etelvino J. H., J. Am. Chem. Soc, 1976, 98, 6468

[86]Yang J., Zhang Y., Polym., 2003, 44, 5047

[87] Borggreve R. J. M., Gaymans R. J., Schujer J., Ingen Housz J. F., Polym., 1987, 28, 1489

[88] Borggreve R. J. M., Gaymans R. J., Schujer J., Polym., 1989, 30, 71

[89] Van Der Sanden M. C. M., De Kok J. M. M., Meijer H. E. H., Polym., 1994, 35, 2995

[90] Perkins W. G., Polym. Eng. Sci., 1999, 39, 2445

[91] Dijkstra K., Ter Laak J., Gaymans R. J., 1994, 35, 315

[92] Bartczak Z., Argon A. S., Cohen R. E., Weinberg M., Polym., 1999, 40, 2347

[93] Lin Z. H., Kwok K. W., Li R. K. Y., Choy C. L., Polym., 2002, 43, 2501

[94] Inberg J. P. F., Gaymans R. J., Polym., 2002, 43, 4197

[95] Arostegui A., Gaztelumendi M., Nazabal J., Polym., 2001, 42, 9565

[96] Arostegui A., Nazabal J., Polym., 2003, 44, 5227

[97] Li Q., Zheng W., Qi Z., Zhu X., Choy C., Sci. China B. 1992, 22, 236

[98] Debye, P. W. Ann. Phys. 1915, 46,809

[99] Brandrup J., Immergut H. I., Grulke E. A., Polymer Handbook, Wiley, New York, 1999

INSTITUT NATIONAL
POLYTECHNIQUE
DE LORRAINE

AUTORISATION DE SOUTENANCE DE THESE
DU DOCTORAT DE L'INSTITUT NATIONAL
POLYTECHNIQUE DE LORRAINE

o0o

VU LES RAPPORTS ETABLIS PAR :
Monsieur Yvan CHALAMET, Maître de Conférences, Université Jean Monnet, Saint-Etienne

Monsieur Yong JIN, Professeur, Chinese Academy of Sciences, Chengdu, Chine

Le Président de l'Institut National Polytechnique de Lorraine, autorise :

Madame DAI Shanshan

NANCY BRABOIS
2, AVENUE DE LA
FORET-DE-HAYE
BOITE POSTALE 3
F - 54501
VANDŒUVRE CEDEX

à soutenir devant un jury de l'INSTITUT NATIONAL POLYTECHNIQUE DE LORRAINE, une thèse intitulée :

« Elaboration et caractérisation de mélanges de polymères à base de polyprophylène et de polycarbonate à propriétés optimisées »

en vue de l'obtention du titre de :

DOCTEUR DE L'INSTITUT NATIONAL POLYTECHNIQUE DE LORRAINE

Spécialité : **« Génie des Procédés et des Produits »**

Fait à Vandoeuvre, le 03 mai 2010
Le Président de l'I.N.P.L.,
F. LAURENT

TEL. 33/03.83.59.59.59
FAX. 33/03.83.59.59.55

TITRE

Elaboration et caractérisation de mélanges de polymères à base de polypropylène et de polycarbonate à propriétés optimisées

RESUME

Le mélange de polymères offre une voie pratique et économique pour élaborer de nouveaux matériaux qui peuvent avoir des propriétés que chacun des polymères ne possède pas nécessairement. L'élaboration de mélanges de polymères à base de PP a souvent pour objet d'obtenir des matériaux avec une résistance au choc élevée, une rigidité suffisante et une processabilité adéquate. Le polycarbonate (PC) est mélangé avec le PP en raison de ses propriétés exceptionnelles (rigidité élevée et résistance au choc excellente) par rapport à d'autres polymères techniques.

Le PC se disperse mal dans le PP car ils sont immiscibles entre eux et leur rapport de viscosité très élevé. La clé pour obtenir des mélanges PP/PC avec une résistance au choc élevée et une rigidité suffisante consiste à les compatbiliser et à diminuer le rapport de viscosité de manière efficace. De nouveaux agents compatibilisants ont été développés pour renforcer les interactions entre le PC et le PP et contrôler la morphologie des mélanges. Les mélanges PP/PC obtenus ont une très résistance au choc et une rigidité suffisante. La performance des agents compatibilisants ainsi que les mécanismes d'amélioration de la résistance au choc ont été étudiés. L'évolution de la morphologie des mélanges PP/PC ainsi que la relation entre la composition et la microstructure ont été simulées avec l'aide des théories de dynamiques à l'échelle moléculaire et mésoscopique.

MOTS-CLES

Polypropylène, résistance au choc, procédé d'élaboration, agent compatibilisant.

TITLE

Preparation and characterization of polypropylene/polycarbonate blends with balanced properties

ABSTRACT

Polymer blending provides a practical and economic way of preparing new materials with combinations of properties not available in a single polymer. In order to improve the toughness of polypropylene while retaining its rigidity as much as possible, a new concept "rigid–rigid polymer toughening" was developed. Polycarbonate (PC) was selected to blend with PP in this study because of the advantages it provides over many other conventional engineering polymers in terms of high strength and toughness.

The key to obtaining materials with high toughness and balanced rigidity relies on effectively compatibilizing this polymer pair and reducing the viscosity ratio. In this study, novel compatibilizers for the PP/PC blend were prepared or chosen to promote interactions between PP and PC and control the morphology of the blend. Some of the compatibilizers took the role of both compatibilizer and toughener. The performance of compatibilizers and toughening mechanism of blends were studied in detail. The morphology evolution of PP/PC blends and the relationship between the composition and microstructure were simulated based on molecular dynamics and mesodyn theories.

KEY WORDS

Polypropylene, impact strength, processing, compatibilizer.